ABSTRACT

Title of Thesis: STRATEGIES FOR IMPROVED FIRE DETECTION RESPONSE TIMES IN AIRCRAFT CARGO COMPARTMENTS

Jennifer Marie Wood, Master of Science, 2020

Thesis Directed By: Dr. James A. Milke, Department Chair
Department of Fire Protection Engineering

Prompt fire detection in cargo compartments on board transport aircraft is an important safety feature. Concern has been expressed for the activation time of contemporary detection technologies installed on aircraft. This project will deliver a continuation of research on the issues that have been identified relative to fire detection improvements in cargo compartments on aircraft, with a particular emphasis on freighters. Gas sensors and dual wavelength detectors were demonstrated in a previous phase to be responsive to fires in the previous experiment program. Detectors placed inside a Unit Loading Device (ULD) responded quickly to the array of fire sources. Thus, a further exploration of these observations is conducted including wireless technology along with an analysis of the effects of leakage rates on fire signatures inside ULDs. One primary goal is to assess the differences in fire detection time for detectors located within ULD versus those located on the ceiling of the cargo compartment for fires which originate in a ULD. The results indicated the detector location with the shortest activation time is inside of the ULD.

Within the ULD, the wireless detector outperformed both air sampling detectors, however, the results could vary if threshold levels were more restrictive.

STRATEGIES FOR IMPROVED FIRE DETECTION RESPONSE TIMES IN AIRCRAFT CARGO COMPARTMENTS

by

Jennifer M. Wood

Thesis submitted to the Faculty of the Graduate School of the
University of Maryland, College Park, in partial fulfillment
of the requirements for the degree of
Master of Science
2020

Advisory Committee:
Professor James A. Milke, Ph.D., Committee Chair
Professor Peter B. Sunderland, Ph.D.
Robert I. Ochs, Ph.D.

Acknowledgements

I am extremely appreciative of all the support given throughout this project. First, I want to express my deepest gratitude to my academic advisor, Dr. Jim Milke, for his academic encouragement and support not only during this research project, but also over the course of my undergraduate academic experience. His ability to recognize a student's confusion or doubt and then explain the matter in a less intimidating way is one of the character traits I admire most about him. I would not have thought of starting this graduate program without his persuasion and reassurance. I must also give appreciation to Nicole Hollywood for advising me throughout the past five years. She is one of my favorite people in the Fire Protection Engineering Department and I sincerely want to thank her enough for her guidance.

Gratitude is given to the Fire Safety Branch of the Federal Aviation Administration for their physical and academic support for this research program. The entire team hosted me for 8 weeks during the summer of 2019 for all experimental testing. I cannot thank each one of the engineers and government contractors enough for their ability to help me at any point of my confusion. Appreciation is given to David Blake and Robert Ochs who have served as the Contracting Officer's Technical Representative for the project. Their advice and depth of knowledge especially helped with the direction of the project. A generous thanks to Robert who is on my committee as he has been supervising the project since my first day at the FAATC.

I would also like to recognize Dr. Peter Sunderland for being a valued member of my committee. As he was my first fire lab professor, I will always be impressed with his

wealth of expertise and friendliness. My understanding of fire protection expanded immensely with his teachings during my undergraduate career.

Xtralis and Space Age Electronics graciously provided equipment and resources. I would like to extend a huge thank you to Xtralis for their continued support and presence throughout all stages of testing. Peter Wynnyczuk provided major assistance throughout the entire experimental portion of this project. Khaleel Rehman served as the Xtralis program manager for this project, providing valuable resources that were critical to the execution of the experiments.

A special thank you to Emily James, Adam Lee, and Kelliann Lee for their consistent dedication this past year for converting and analyzing experimental data. I would also like to thank Adam Quiat for his help with my FDS understanding. Finally, I would like to extend an immense thank you to my family, friends, and roommates (especially Caitlin and Luke). Without their constant support, I would not be where I am today. Lastly, I would like to thank my mom and dad for motivating me to go into engineering and teaching me perseverance is the most important aspect of learning.

Table of Contents

List of Tables

List of Figures

List of Abbreviations

AC: Advisory Circular

ASD: Aspirating smoke detection

ASSD: Air Sampling Smoke Detector

ASGD: Air Sampling Gas Detector

CFD: Computational fluid dynamics

CO: Carbon monoxide

CO_2: Carbon dioxide

DAQ: Data Acquisition System

EMS: Very large eddy

FAA: Federal Aviation Administration

FAATC: Federal Aviation Administration Technical Center

FDS: Fire Dynamic Simulator

H_2: Hydrogen

HRR: Heat release rate

HRRPUV: Heat release rate per unit volume

IR: Infrared

LED: Light emitting diode

LLRM: Large Leakage Rate Model

MLR: Mass loss rate

MLRM: Medium Leakage Rate Model

NTSB: National Transportation Safety Board

O_2: Oxygen

OD: Optical density

PU: Polyurethane foam

Ppm: Parts per million

RH: Relative humidity

SAE: Space Age Electronics

SLRM: Small Leakage Rate Model

SMV: Smokeview

S-O-A: State of the art

TSO: Technical Standard Order

ULD: Unit load device

UMD: University of Maryland

UPS: United Parcel Service

VESDA: Very early smoke detection apparatus

VEA: VESDA-E (Addressable)

VEU: VESDA-E (Ultra-Wide Sensitivity)

Chapter 1: Introduction

One method of keeping humans and property safe in the presence of a fire is to design a detection system that can distinguish a fire in its earliest stages. For aircraft in flight, there is greater pressure to quickly detect a fire given the amount of time needed to respond. A review by Transport Canada of all known commercial aircraft fires, over a period of time, determined that on average there is as little as 18 minutes to successfully land (Moody, 2020). The detection system selected for aircraft must accurately activate to a fire to provide sufficient time for mitigation and extinguishment. To address the concern of fires on board aircraft, the Federal Aviation Administration (FAA) has set specific protocols that limit the time it takes for a detector to alarm once a fire begins, stating "the detection system must provide a visual indication to the flight crew within one minute after the start of a fire" (Title 14). Guidelines have also declared a Technical Standard Order (TSO) which accepts the Minimum Performance Standards to account for the large frequency of nuisance alarms from false fire sources such as water vapor and dust.

1.1 Motivation

The desire for fast fire detection inside of aircrafts has been a principle concern for the aircraft industry. More recently, the unease over fire detection activation times was heightened by the National Transportation Safety Board (NTSB) when an in-flight cargo compartment fire occurred on a United Parcel Service (UPS) aircraft in 2006 (Blake, 2009). The UPS flight was performing its routine task of delivering packages from Atlanta to Philadelphia when a smoke warning light turned on just after the crew received clearance to land the plane (Aviation Safety Network, 2020). After a runway mix up, the

aircraft was able to land with smoke escaping from it. The fire department was called, and the blaze was under control but only after the plane was completely damaged by the fire. The fire originated from an unknown source inside of the one of the cargo containers. The plane was also found to have inadequate certification test requirements for its smoke and fire detection systems and no on-board fire suppression method.

The encapsulation of cargo compartment containers with fire resistant barriers has elevated the concern of delayed detector activation times. The severity of a fire is extremely dependent on the time of detection as an early alarm can start the response of the aircraft crew to begin taking the correct mitigation steps before the fire is uncontrollable. However, if the cargo container is withholding the fire from breaching the cargo container, the aircraft detection system will most certainly be delayed and consequently the aircraft crew will be flying unknowing about the dangers growing inside of their airplane. The delayed activation and response of the crew will dramatically affect the efforts of safely landing the aircraft for an emergency landing.

To support the demand for more understanding in this field of aircraft fire safety, research was conducted to appreciate the challenge associated with effective cargo compartment fire detection strategies (Chin, 2019). A literature analysis was performed on a cargo compartments to compile descriptions and statistics connected with the response of cargo compartment fire detectors. The detection technologies examined were:

1. Ionization Smoke Detector
2. Photelectric Smoke Detector
3. Projected Beam Detectors
4. Aspirating Smoke Detector

5. Dual Wavelength Detection
6. Gas-Sensing Fire Detector
7. Video Detection
8. Spot Heat Detector
9. Line-Type Heat Detector
10. Radiant Energy Detector

The review included a comprehension of the nuisance alarm issue which was found to occur commonly in cargo compartments. Multiple cargo compartments and cargo containers were examined to understand the characteristics of cargo compartment environments.

The research conducted by Chin incorporated an experimental testing series to evaluate the detection ability of various modern-day fire detection system technologies. Initially performed at the University of Maryland (UMD), the first series of tests included a container which simulated a cargo compartment container but at a smaller scale. The goal was to recognize the best performing fire detection technologies and standardize the tests conducted for flaming and smoldering fires. The experiments were then carried to the Federal Aviation Administration Technical Center (FAATC) for testing in real aircraft cargo compartments and unit loading devices (ULDs). Various flaming and smoldering tests were conducted using several different fuels inside the ULD and then separately in the cargo compartment container to interpret the responsiveness of modern-day fire detection technology. Aspirating smoke detectors, gas analyzers, and dual-length smoke detection were utilized in the experiments as well as light obscuration meters and a standard photoelectric detector. The gas analyzers and dual wavelength sensors were

analyzed comprehensively to inspect if either technology had the ability to distinguish between nuisance sources and fire sources.

The research found the gas analyzers and dual wavelength detectors proved to respond well to fires, indicating they had the ability to work as technology equipped to deal with nuisance source prone environments. Testing of the modern-day detection technology demonstrated the aspirating smoke detectors correlated extremely well with the light obscuration levels. Wireless detectors were initially tested; however, they lacked the ability to transmit through aircraft walls. The research concluded that more tests comparing results between ULDs and cargo compartments should be performed and wireless detection technology should be further explored.

1.2 Problem Statement

In this study, a second phase of research was completed to deepen the understanding of cargo compartment fire detection technology. Determining a detector technology and location which could produce the shortest response time to a wide variety of fire sources was the primary focus of this research. This area of exploration provides a continuation of research on the problems that have been identified connected to improvements in cargo compartment fire detection, with a heavy level of importance on freighters. The first phase of research, conducted by Chin, demonstrated the abilities of gas sensing and dual wavelength technologies in ULDs and cargo compartments, separately. Thus, this second phase will delve into the detection technologies in a more realistic setting with the detection systems placed inside the ULD which will be positioned in the cargo compartment just as one would be in a real flight.

1.3 Scope of Work

A comprehensive review of past research and experimentation on fires in aircraft cargo compartment was conducted in Chapter 2. The research was divided into two tasks. Explained in Chapter 3, the first objective, similar to the experimental portion of Chin's work, was conducted at the FAATC to test realistic fire scenarios. As many cargo airplanes are shaped differently, the cargo containers that fit inside them must also be shapped uniquely, thus, there is an assortment of different dimensioned containers. Although the containers vary in size and shape, the most important aspect for them in this project was their leakage rate. This is a factor that affects the smoke transport when the fire source is blazing inside of the container. As testing was performed within a limited time frame, three unique ULD models were constructed to account for a variety of cargo compartment containers.

Investigating the contrasting smoke characteristics inside of the ULD and the cargo compartment was of interest for determining the best placement of a fire detection system. The instruments consisted of:

1. Light Obscuration Meters
2. Gas Analyzers
3. Blue & IR Wavelength Detector
4. Air Sampling Smoke Detectors (ASSD)
5. Air Sampling Gas Detectors (ASGD)
6. Wireless Detectors
7. Wired Detector
8. Video Cameras

The instruments were placed systematically throughout the testing area to measure the constrasting fire signatures in the different area of the cargo compartment and ULD. The tests were developed to simulate realistic fire scenarios, thus, the fire sources were selected based on their likelihood of existing inside of a cargo compartment and their presence in UL268 as fire sources that are currently used to certify smoke alarms (Smoke Detectors, 2016). All fire sources were tested three times, each in a different ULD leakage rate model. The data and comparison of the results can be found in Chapters 4 and 5, respectively. A description of the fire sources and the method used to conduct each experiment is included in Appendix A. The testing checklist completed before each test was performed and the data collection template are located in Appendix B. The compilation of all the data collected from the experimental testing is located in Appendix C.

The second task, descibed in Chapter 6, consisted of developing a computer simulation which could predict the results of the experiemental fires to provide a proof of concept of the programs ability. The computer simulation was modeled directly after the ULD and cargo compartment experimental set up. The FDS code created for the model can be found in Appendix D.

Chapter 2: Literature Review

This chapter will first describe the historical events that led to the heightened interest in aircraft fire detection and then explain the necessary characteristics needed in a fire source and fire detection system to meet current regulations. The section will later point out the high frequency of nuisance alarms inside of aircraft cargo compartments and then identify a multi-sensor detector that was developed to address the issue. An account of unique experiments will follow. There are three reports, the first explaining the effects of a loaded versus unloaded cargo compartment, the second demonstrating how the use of Unit Loading Devices (ULDs) can affect detector response time, and the third describing specific fire detectors may outperformed other more commonly used fire detectors. Computational Fluid Dynamic (CFD) modeling is lastly examined. The section of CFD modeling begins with a description of the model used and its simulation abilities and secondly in a report demonstrating the comparisons between experimental results and simulated results.

2.1 Brief History of Cargo Compartment Fires

Fire detection in airplane cargo compartments has been a source of concern of the Federal Aviation Administration (FAA) and National Transport Safety Board (NTSB) for decades. Apprehension increased after several grim airplane events ended in uncontrolled fires in cargo bays that caused accidents and fatalities (Workley, 1998). On August 19, 1980, a cargo compartment fire broke out on a Saudi Arabian airline plane due to an unknown source which resulted in all 301 passenger and crew members perishing in the accident (Hill, 2017). On November 28, 1987, a South African ‘combination’ airplane, carrying both passengers and cargo on the main deck of the aircraft, was traveling over

the Indian Ocean when a fire initiated in a cargo compartment and fatally crashed less than 20 minutes after the flight crew announced smoke was found (Federal Aviation Administration, South African Airways). After this crash, the FAA and independent authorities reacted to the inadequacy of reliance on Class B firefighting by requiring design and operational changes. Eventually this led to the reclassification of 'combination' aircraft compartments from Class C to Class F (Hill, 2017). On May 11, 1996, a Class D cargo compartment of a passenger aircraft took off near Miami, Florida (FAA Lessons Learned, 1996). The aircraft crashed while attempting to land due to an uncontrolled fire caused by the actuation of one or more chemical oxygen generators being improperly carried as cargo. Realizing there were many issues with current standards, the FAA set new regulations demanding fire detection and fire suppression systems inside existing and future airplane cargo compartments.

More recently, the NTSB called for more attention and research in cargo compartment fires after a United Parcel Service DC-8 aircraft caught fire in the cargo compartment on February 7, 2006 (NTSB 2006). The flight crew recalled smelling wood or cardboard burning, being especially strong towards the back of the cockpit and in the cargo compartment around 20 minutes before one of the crew members reported seeing smoke in the cargo compartment. The crew members safely landed the aircraft before the cockpit began to fill with smoke, however, the airplane was destroyed after landing along with the cargo on board the aircraft. Later investigations proved the fire was emanating from a cargo container inside the cargo compartment from an unknown ignition source. Further safety issues were discussed concerning inadequacies of smoke and fire detection

system test certification requirements and absence of on-board fire suppression systems prompting the investigation of slow detector response times.

As of 2017, 35% of the world's trade value was carried though air travel with future expectations that over the next 15 years freighters will increase the amount of goods they transport. The conditions inside of freighters work best for transporting higher value commodities that are time sensitive and economically perishable (World Air Cargo Forecast, 2017). The push for more efficient freighters is on the rise, thus, more cargo compartments are being packed full of unit loading devices (ULDs) for cost efficiency purposes. As more goods are being placed inside the ULDs, the likelihood of a fire originating inside of a ULD is likely to increase. ULDs, tightly sealed and manufactured out of fire-resistant materials, pose a threat to the response time of cargo compartment ceiling detectors as the ULD walls allow a fire to grow inside the container without any form of early detection (Chin , 2018). The fire intensity has the potential to be uncontrollable by the time the flames or smoke escapes the container, leading to unexpected dangerous landings and reduced firefighting time by the crew.

2.2 Characteristics of Fire Detection Systems and Fire Sources

A survey of fire detection technology was conducted by the FAA for evaluation and certification of their suitability in cargo compartments on airplanes (Cleary, 1999). The study determined that there were multiple, suitable goals for fire detection inside of cargo compartments: faster detection of real fire threats, improved nuisance source discrimination, enhanced reliability, and greater indication of hazard level. Enhanced fire detection is desired by all airlines, however, the constraints found from the research identified cost as a key player that inhibits innovational technology from entering aircraft

cargo compartments. Cost effective solutions are essential for new technology to be considered in the commercial business. In-flight testing can also present a time delay to new smoke detection technologies (Advisory Circular, 1994). Operational constraints also impact the implementation of successful fire detection such as temperature, pressure, humidity, and vibration conditions. The analysis suggested improving photelectric or ionization type detector behavior by applying advanced signal processing algorithms to inhibit nuisance alarms by reducing spurious signals that are not found in fire signatures in the sensing chamber. Using a multi-sensor detector was also prescribed as a potential solution after the survey was complete as this would better discriminate between nuisance and fire sources.

Comprehensive testing of smoke detector technologies for application in aircraft requires that fire sources be selected to provide a range of smoke conditions. In 2006, a report by David Blake was created to develop standardized fire sources for aircraft cargo compartments fire detection systems (Blake, 2006). A satisfactory fuel must release a plume of smoke and gases to eliminate any ambiguity of the fire's time of origin, generate all products of combustion expected from actual cargo fires, and have the ability to remotely activate from an unoccupied compartment. Chosen fire sources were based on their ability to generate quantifiable heat release rates, mass loss rates, and smoke and gas species production rates. The results from testing demonstrated the smoldering fire sources failed to generate a fire signature that would be useful in the development of multicriteria fire detectors with the potential of avoiding nuisance alarms.

Alternatively, use of smoldering sources or smoke generators can be advantageous when deliberating quantity of smoke, as less smoke is required by

smoldering fires to cause light scattering (Blake, 2006). While flaming fuel sources, such as flaming polyethylene (PU) foam, produce much smaller particle sizes when compared to the same fuel when smoldering (Fabian, 2007). The fire signature created by the flaming fires allowed for distinction between real fires and nuisance sources in smaller volume compartments (Blake, 2006). The findings additionally pointed out the smoke concentrations used in previous smoke certification tests do not create enough smoke to be detected in less than one minute.

A CFD model was also constructed to predict the smoke, gas, and heat transport inside of the cargo compartment. A comparison between experimental and simulation results found the experimental individual particle sizes of smoke from flaming fires were between 3 to 750 times smaller than predicted CFD particle sizes. The model also predicted the photoelectric smoke detectors would respond faster to the smoldering or artificial fires than the flaming fires due to the higher light scattering. Fire sources are described and chosen selectively from UL268 where these fuels have been tested directly for experimental conduct (Smoke Detectors, 2016).

Further research has been conducted on smoke generator testing as this removes the chances of hazardous testing environments (Emami, 2018). The machines use safe and nontoxic theatrical smoke to model realistic fire scenarios. Experimentation performed at the FAA provided insight that smoke characteristics can be easily altered depending on the fluid used in the smoke machine. A smoke machine using an oil-based fluid was found to create much smaller particle sizes than the smoke machine which used a water-based fluid. The results suggested the oil-based smoke machine was able to alarm the “false alarm resistant” detector while the water-based machine could not create a

nuisance alarm until the light obscuration levels were significantly higher than the oil-based machine.

2.3 Nuisance Alarm Frequency and New Detection Technology

The number of cargo compartment smoke detector alarm incidents on United States registered aircrafts over 26 years was reported to show the ratio of false alarms to real alarms has been steadily increasing (Blake, 2000). The data count, conducted by the FAA, revealed the growing false alarm rate is expected to accelerate as more aircraft are being supplied with smoke detectors. A statistical analysis estimated the ratio of false cargo compartment fire detector alarms to actual fire detector alarms had grown to 200 to 1 between the years 1995 to 2000.

To reduce the frequency of nuisance alarms, research into new technology started progressing in the airline industry. A fire signature is composed of gas particulate levels, gas concentration, and temperature fluctuations (Girdhira, 2008). Current smoke detectors in the airline industry most popularly use photoelectric and ionization technology inside their sensing chamber. However, these mechanisms solely rely on particulate levels meaning the chance of a false alarm occurring is greater because there is only one check. A multi-sensor smoke detector algorithm was developed by the FAA to account for more than one parameter in a fire signature to increase the level of confidence that a received alarm was due to a fire. The advanced fire detection system combined an ionization smoke detector, thermocouple, light obscuration meter, and a carbon monoxide (CO) and carbon dioxide (CO_2) gas probe. Numerous algorithms were generated to explore the most effective multisensory design that would produce the fastest response to fire while also decreasing the chance of a nuisance alarm. To define

the physical range of the multi-sensor detector and the enhanced algorithm, a Computational Fluid Dynamic (CFD) model was constructed. The simulated model and real fire tests correlated well, providing an average time difference of 2.57 seconds between the detector activation times. The multi-sensor detector was found to comply with the FAA rule which requires detection of a fire within one minute of its origin (Title 14). The new technology also achieved 100% nuisance immunity with a matching success rate while the standard tested photoelectric detector yielded a 66.7% success rate and the ionization detector provided a 73.3% success rate.

2.4 Effects of Cargo Compartment Load

The response of a smoke detector depends on the airflow and density of smoke and location of the detector. Smoke detection in cargo compartments was conducted in two different conditions: fully loaded and empty (Blake, 2009). Active containers which have controlled climate systems maintaining the container's temperature and humidity during flight were also studied to determine their effect on smoke detector response time in a cargo compartment. Testing at the FAA was performed by David Blake in a B-727 and B-747 aircraft supplied with ventilation and photoelectric smoke detection systems. The B-727 fully loaded cargo compartment was fitted with 8 AAY cargo containers and the B-747 was equipped with 10 AKE containers for the fully loaded label. The B-727 results proved the smoke detector response time was on average 20 seconds faster for the fully loaded cargo compartment compared to the empty compartment. Analysis proved the detection time was highly dependent on the detector's location inside of the cargo compartment. When intermittent detector alarms were ignored, the analysis proved the loaded compartment yielded faster detection times in 9 out of 10 positions. The B-747

results were more erratic necessitating more testing before conclusions could be verified. Ambient temperatures and outside windspeed had a higher than expected effect on the repeatability of the results. The tests pertaining to the active containers demonstrated these specific units do not have a consistent influence on smoke detection times under the airflow conditions tests meaning there was no pattern found from the use of fans versus no fans.

2.5 Cargo Container Effects on Detector Response Times

Cargo containers inside of cargo compartments can create major delays in smoke detection times when the fire detector system is located in the ceiling of the cargo compartment. Led by Tyler Wilks, testing was conducted to determine cargo compartment smoke detector response delays (Wilks, 2014). Investigations using an Aviator Smoke Generator inside of a DC-10 aircraft were conducted to find the settings needed to provide a response time of the cargo compartment smoke detector of less than one minute. The exact setting and location found to create consistent smoke densities was used again but in a second series of tests inside of a cargo container located in the cargo compartment.

Two types of AAY containers were used, one with two swing open doors constructed to contain a fire for 4 hours and a second with a pull-down door which created small gaps for smoke to escape. An AAY container is fit for narrow body freighter aircrafts. Traditionally constructed out of aluminum, the main deck container is 82 inches tall with an 88-inch by 125-inch footprint (Nordisk, 2018). The results showed the first container was sealed so tightly that even with an extremely high light obscuration reading inside the cargo container, the cargo compartment detector was unable to detect

any smoke particles. The second container which allowed for more air flow, created enough smoke in the exterior of the cargo container allowing for the cargo compartment smoke detector to alarm around 7 minutes and 35 seconds on average. When comparing the detection time without a cargo container to the detection time with the cargo container, the average detection delay time was 6 minutes and 37 seconds, demonstrating the use of cargo containers can negatively affect the smoke detector response times.

2.6 Fire Detector Performance Tests inside DC-10 Cargo Compartments

To address the performance of fire detection inside aircraft cargo compartments, guidelines were made by the FAA. Per Title 14 Code of Federal Regulations 25.858, the cargo compartments that require detection must meet the following:

> (a) The detection system must provide a visual indication to the flight crew within one minute after the start of a fire.
>
> (b) The system must be capable of detecting a fire at a temperature significantly below that at which the structural integrity of the airplane is substantially decreased.
>
> (c) There must be means to allow the crew to check in flight, the functioning of each fire detector circuit.
>
> (d) The effectiveness of the detection system must be shown for all approved operating configurations and conditions.

Advisory Circular (AC) 25-9A specifies that warnings should be provided by the smoke or fire detection system prior to the fire. The regulations also require the smoke detection tests must demonstrate the smoke detection system installed in the aircraft will respond to a smoldering fire generating a small amount of smoke. Taken directly from

the literature, the requirements are ambiguous with no quantitative restrictions with the exception of the 1-minute detection time rule. The current standards do not provide detail on what equates to a "small amount" which can lead to a lack of reproducible testing. The constraints also fail to require fire testing in a flaming mode of combustion despite a fire detector must be able to detect a flaming fire. Detectors placed in building applications must adhere to the requirements in UL268 which requires both flaming and smoldering testing in order to certify a detector. Thus, it is logical for aircraft detection testing to have the same testing conditions and rules. In regard to the one-minute detection time requirement, the arbitrary time should instead be determined based on the hazard level of the material.

An experimental investigation operated by Selena Chin at the Federal Aviation Technical Center (FAATC) found that ULDs present delays to the response times of fire alarms (Chin, 2019). Various testing was performed inside of a ULD, DC-10 cargo compartment, and 1 m^3 box at University of Maryland. Limited testing was conducted with the ULD inside of the cargo compartment. Thermocouple trees, light obscuration meters, and aspirating sampling detectors (ASDs) were used in each of the three experimental settings with the addition of dual wavelength detector (Blue and IR) and a wired photoelectric detector in the cargo compartment setting. Fire sources included heptane, polyurethane (PU) foam, suitcases, shredded paper, baled cotton, wood chips, and boiling water. Communication tests with wireless detectors found that they could not successfully transmit through the metal enclosures of a ULD to a wireless base station, thus they were deemed unfit for further testing.

In the fire tests, the ASD systems outperformed the wired detector, the blue and IR wavelength detector strongly mimicked the light obscuration meter, and the gas concentration correlated well to the optical density. The above average performance of the gas detection system suggested that it could be a good choice for nuisance immunity as measuring two types of gases would allow for a confident confirmation of fire. Gas detectors also were found to be unaffected by the variable environmental factors such as dust concentration.

A scaling analysis of optical densities with volume provided an indication that smoke detector certification tests could be tested in smaller volumes. Chin's analysis did not show a clear trend between the response times of detectors or signatures for smoldering and flaming fires, even though the expectation was that detector response times should be affected by smoke density and particle sizes from different fire sources. The research demonstrated there is a substantial need for detection systems with the ability to discriminate between nuisance and fire sources; plus more nuisance source testing needs to be conducted in general. Considering limited testing was performed with the ULD inside of the cargo compartment, there was a large emphasis on the demand for a more systematic way of testing ULDs solely inside of cargo compartments. Chin identified that future research must reevaluate wireless detection systems inside of cargo compartments to adequately test the ability of the technology. There is also an obligation to standardize detection in cargo compartments and a push for more hazard-based requirements on detection systems rather than a time constraint as this testing proved the difficulty of meeting that rule (Chin, 2018).

2.7 Computational Fluid Dynamic (CFD) Modeling

Comparing experimental results with CFD simulations can be extremely useful as part of a research program. A commonly used CFD program, Fire Dynamic Simulator (FDS), allows for the analysis of large eddy simulations for low speed flows which can be exceptionally helpful in understanding smoke and heat transport in a fire. To visualize the display of outputs of the FDS simulation, Smokeview (SMV) is utilized. Validation of FDS results is important in testing as it allows for further analysis without conducting real experiments. Forgoing these experiments saves money, time, labor, and materials needed for testing. Thus, creating a verified and valid model can be used as a more efficient means of analysis in the future.

FDS uses heat transfer and fluid flow calculations to perform predictions on how a fire will interact with its environment. There are multiple user defined fields that can be altered depending on the fire source, environment, and desired mesh field. The mesh field is a critical grid spacing parameter which defines the area that will be used in the simulation. Specified grid points are located in an x, y, and z coordinate system to allow for the creation of a 3-D modeling space. The size of the grid is key when performing simulation runs. Excessively large grid spacing yields inaccurate results. If an extremely small grid size is selected to yield accurate results, the simulation run time can be excessive. Mesh fields are created inside of the model grid allowing the user to simulate large areas and establish finer meshes to better support predictions of spaces that have high importance. The calculations are performed using data incorporated from all grid points within different meshes. (Kevin, 2020).

In 2007, FDS models were created for the inside of an aircraft cargo compartment and validated for potential use in the certification of cargo compartment fire detection (Suo-Anttila). The testing procedure included variations of the fire location, compartment size, and ventilation. Thermocouples, light transmission, and gas species concentration were all validated and verified to prove the 300 second simulation was predicting accurate results. The models were constructed to resemble a Boeing-707 and DC-10. Within each FDS model, fuels were either placed in the middle of the cargo compartment or at the corner or sidewall of the cargo compartment. The fuel sources ignited in the center of the cargo compartment were considered to be the baseline fire scenario while the corner and sidewall fires were labeled as scenario two. All testing conditions modeled an empty cargo compartment, as this is a requirement for certification testing. The accuracy of the prediction was judged based on the results of the ceiling jet arrival time and how well the gas species concentration was simulated as a function of time.

Time based comparisons were made at 0-60 second, 0-120 second, and 0-180 second intervals. The first 60 seconds demonstrated the simulated temperatures followed the experimental test temperatures well; considered excellent when recalling FAA regulations as this is the time at which detectors inside the cargo compartment must alarm if there is a fire. At 120 seconds, the trends in temperatures remain similar but the magnitudes near the fire sources are greater in the simulated model. The light obscuration readings were compared at identical times with the exception of two additional comparison intervals at 30 and 45 seconds. The predicted light obscuration correlated well with experimental readings between 30 to 45 seconds and then diverged from the experimental data around the 120 to 180 second time range, however overall trends were

still well predicted. The gas concentration measurements indicated good agreement for both CO and CO_2 for a majority of the test duration, being compared at the 60 seconds, 120 seconds, and 180 second time intervals. Ultimately, the FDS program achieved its goal of predicting a realistic fire inside of the airplane cargo compartments and the model appears to have the ability to optimize detection system testing for more efficient analysis.

Chapter 3: Methodology

3.1 Experimental Setup

Cargo aircrafts have multiple methods of transferring shipments and luggage. The scope of this project focused on freighters carrying ULDs which minimize the labor required for loading and unloading and maximize the aircraft's cargo space. This specific experimental setup was conducted inside of a DC-10 aircraft with a half-width lower deck container with one angled side, known as an LD3 ULD, placed inside the lower cargo compartment.

3.1.1 Cargo Compartment

All testing occurred inside of the lower cargo compartment of a DC-10 airplane located at the FAATC. A curtain was used to partition off a middle section of the lower cargo compartment, with a volume of approximately 1600 ft^3. A second curtain was provided at the doorway to the cargo compartment in lieu of closing the large door to the

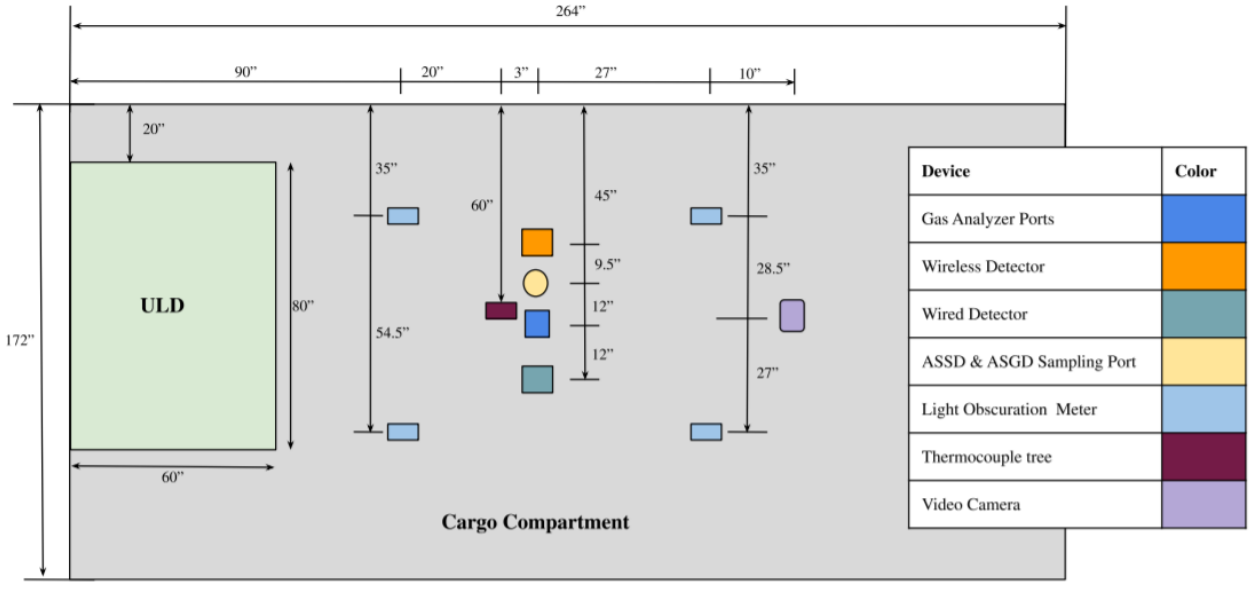

Figure 3.1. Ceiling plan of cargo compartment, ceiling thermocouples not shown.

compartment at the beginning of each test. The instrument configuration in the cargo compartment can be located in Figure 3.1.

3.1.2 Unit Loading Device

The tests were conducted using an LD3 ULD prototype assembled at the FAATC with a volume of approximately 159 ft^3. The ULD was positioned at one side of the cargo compartment with a 20-inch gap between the ULD and cargo compartment container wall as this position would be a likely location in realistic flight scenarios. Most LD3 ULDs have either solid or canvas doors. However, for this project, a solid plexiglass door was fitted to the container using a piano hinge for viewing purposes and ease of access

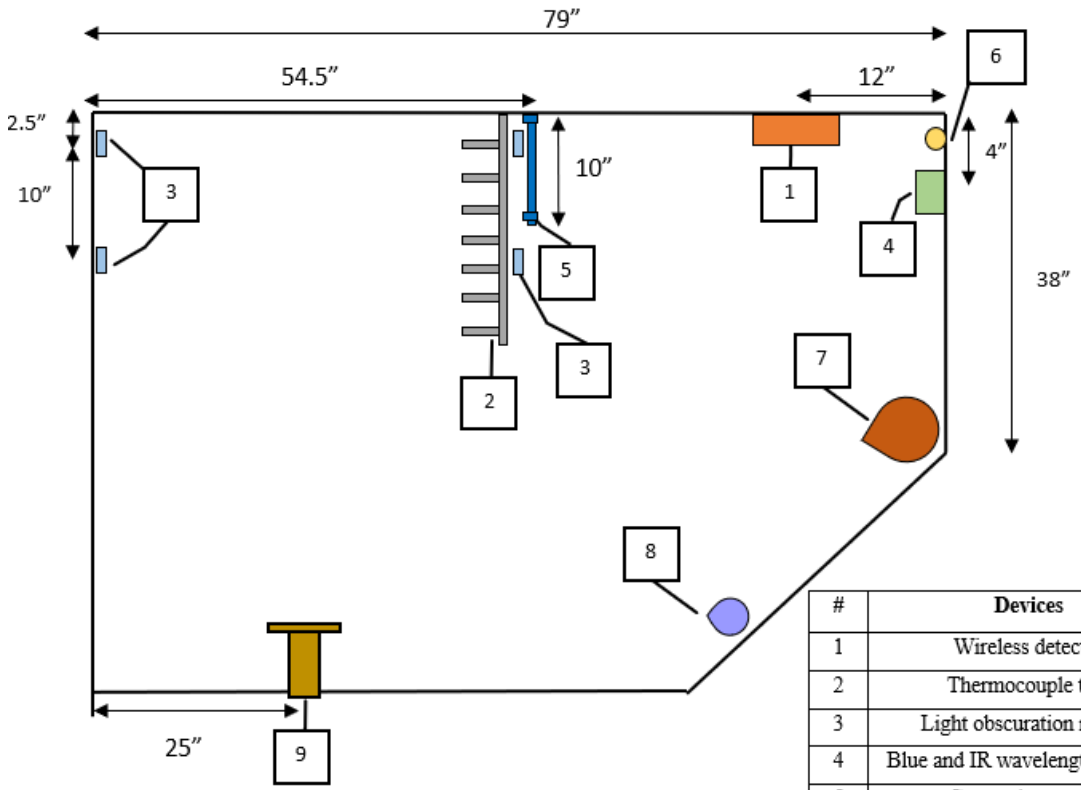

#	Devices
1	Wireless detector
2	Thermocouple tree
3	Light obscuration meters
4	Blue and IR wavelength detector
5	Gas analyzer ports
6	ASSD & ASGD Sampling Port
7	Infrared Camera
8	Video Camera
9	Fuel Placement

Figure 3.2. Elevation view of ULD, ceiling thermocouples not shown.

between testing. Placement of instrumentation inside the ULD can be found in Figure 3.2 and 3.3.

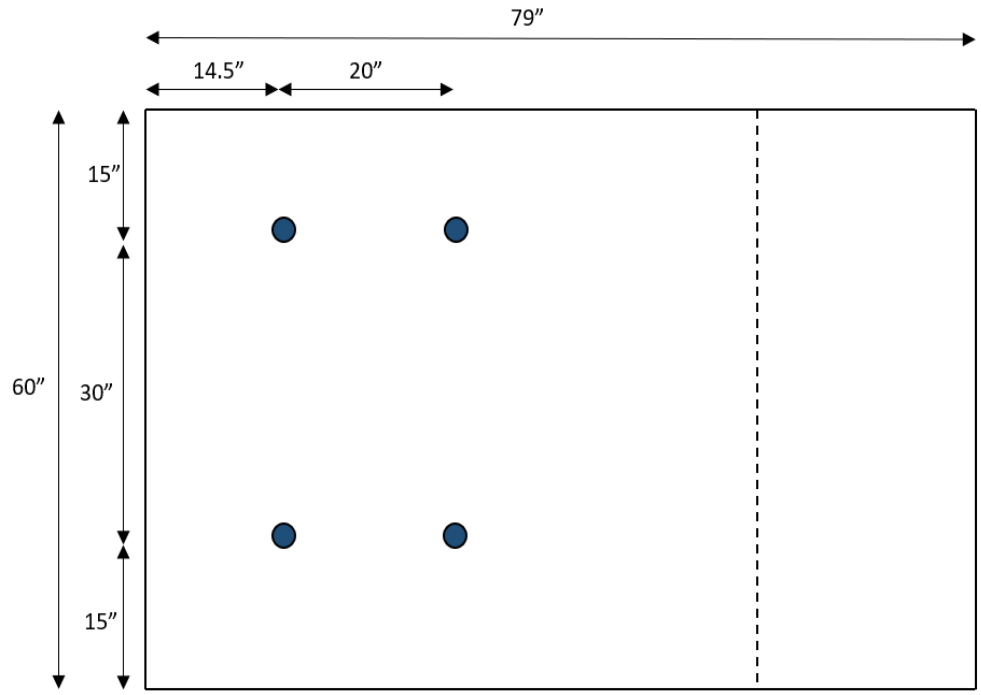

Figure 3.3 Ceiling view of ULD, thermocouples only.

3.2 Varying Leakage Rates

To account for a variety of ULD shapes and sizes, a leakage rate test method was created to provide three different leakage rates. The initial ULD was standardized as the small leakage rate model (SLRM), as no modifications or alterations were applied to the container. The second ULD model was constructed with a column of 1-inch diameter holes down the middle of the ULD on the right side of the door spaced 5 inches apart, yielding a medium leakage rate model (MLRM). The third ULD model was built with a second column of holes migrating down the left side of the ULD door, providing the large leakage rate model (LLRM). The container shape and alignment of holes in the ULD for the leakage rate is shown in Figure 3.4. To reproduce the MLRM and SLRMs, duct tape was applied to each column of 1-inch holes to inhibit potential gas and smoke seeps. CO_2 leakage rate tests were performed on each ULD model to quantifiably measure the respective leakage rates in cubic feet per minute. The testing process required pumping a large quantity of CO_2 into the ULD and then measuring the slow

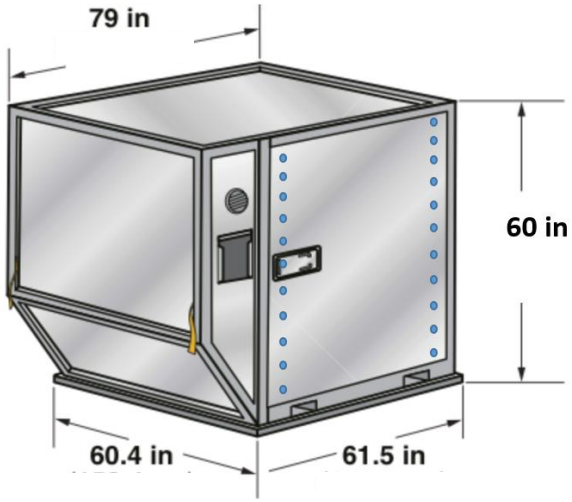

Figure 3.4. LD3 ULD with columns of holes for varying leakage rate models.

decrease in gas concentration in the compartment over time. The process was performed on each leakage rate model. The results of each test are presented in the next chapter.

3.3 Instrumentation

Comprehensive data collection was conducted throughout each test to provide unique detail on the smoke characteristics inside the ULD and cargo compartment. Many instruments were positioned in both testing areas to account for volume and environmental effects, while a select few were placed only inside the ULD. The configuration of instruments inside the ULD and cargo compartment can be viewed in Figures 3.1, 3.2, and 3.3.

3.3.1 Light Obscuration Meters

Light obscuration was a key metric used to characterize smoke. Light obscuration meters measure the amount of white light received by a photocell transmitted through the smoke. Four light obscuration meters were placed inside of the ULD and two were positioned in the cargo compartment varying in distance from the ULD. The interior top meters were placed 2.5 inches from the ceiling while the bottom meters were placed 10 inches from the ceiling. The closest cargo compartment meter was 30 inches from the ULD and the second meter was placed 50 inches beyond the first one. Both cargo compartment light obscuration meters were spaced 2.5 inches down from the ceiling. The data acquisition (DAQ) system collected voltages received from the light obscuration meter transmitter which gradually dropped as the smoke levels increased.

The DAQ system continuously collected voltages from the light obscuration meters throughout the testing period. The instrument was turned on before the ignition of

$$O_u = \left[1 - \left(\frac{V_s}{V_c}\right)^{1/d}\right] * 100 \qquad (3.1)$$

any fuel to determine the ambient clear air voltage and remained on until the test was complete. The raw voltages were converted to percent obscuration per foot (O_u) by using equation 3.1 from UL217. The smoke density meter readings with smoke, V_s, and smoke density meter readings with clear air, V_c, were both required as part of the calculation. The distance apart for light obscuration meters in UL217 is recommended to be 5 feet, the ULD set up used in testing only allowed for a distance, d, between all the light obscuration meters to be 4.54 feet (ANSI/UL217).

3.3.2 Gas Analyzers

Four gas analyzer stations were used in the testing area: station 1 and 2 in the cargo compartment and station 3 and 4 in the ULD. Each set of analyzers had one intake tube flush with the ceiling with the second intake tube positioned 10 inches down from the ceiling. The analyzers had the ability to measure the percent of oxygen, carbon dioxide, and carbon monoxide. Transport times were recorded by measuring the response time for each station after smoke had entered the gas analyzer inlet. The documented value was subtracted from the DAQ response times after testing was complete.

The FAA gas analyzers collected the gas by volume in terms of percent concentration. The values of the CO and CO_2 in percent were found to be extremely low, thus, the data was converted into parts per million (ppm). To better understand the development of the gas concentrations, the change in concentration was observed. The conversion formula used to adjust the raw percent concentration data to the change in gas concentration in ppm, ΔGC_{ppm}, can be found in equation 3.2. The initial gas concentration in percent concentration, $GC_{\%,initial}$, was identified at the beginning of

$$\Delta GC_{ppm} = \left(GC_{\%,t} - GC_{\%,initial}\right) * 10{,}000 \quad (3.2)$$

each test by averaging the gas concentration levels several seconds before the fuel was ignited to pinpoint the ambient air condition. The gas concentration in percent concentration at a given time, $GC_{\%,t}$, was selected to determine the change in gas concentration at that current moment. The DAQ was setup with the limited ability to only detect gas concentrations above 70 ppm for CO and 190 for CO_2. Discrete points were graphed at the time of the first change in gas concentration to avoid the appearance of a step-like function.

3.3.3 Thermocouples

K-type thermocouples measured the rise in temperature during each test in the cargo compartment and ULD. Thermocouples were placed along the ceilings of the ULD and the cargo compartment. The cargo compartment ceiling had 25 thermocouples spaced evenly 29 inches apart while the ULD ceiling had 4 thermocouples distributed above the fuel shown in Figure 3. Separate thermocouple trees were also arranged inside the ULD and in the cargo compartment with each thermocouple positioned 3.5 inches and 3 inches apart, respectively, totaling 7 thermocouples for each tree.

3.3.4 Blue and IR Wavelength Detector

Blue and IR signals were evaluated inside the ULD to complete a comprehensive analysis of the airborne smoke particles released from the fuel. The device utilized a blue 470 nm LED light and IR 850 nm LED light. A blue light can register particles around 450-490 nm while an IR light detects particles around 700-1000 nm (Karp, 2018).

The blue and IR wavelength outputs were recorded by the DAQ system in the form of a voltage reading. Typical blue and IR readings are expressed in terms of signals; thus, the raw readings for both the blue and the IR wavelength voltages, V_{new}, were

converted to signals through equation 3.3. The initial voltage collected by the DAQ system reflected the ambient air voltage represented as $V_{ambient}$.

$$Signal = \frac{V_{new} - V_{ambient}}{V_{ambient}} \qquad (3.3)$$

3.3.5 Air Sampling Smoke Detectors (ASSD)

Multiple types of smoke detectors were located in the testing area for comparative results. One category of detector needed in the experiments is labeled as a Very Early Smoke Detection Apparatus (VESDA), an aspirating smoke detector by Xtralis. The VESDA-E VEA model VEA-040-A10, inlet tube located inside of the ULD, provides pinpoint addressability through utilizing microbore tube networks. This model is used most in restricted access areas and regions of high spot detector density. Sampling point sensitivities for this system are framed into 3 settings categorized by light obscuration; standard at 2.5 %/ft, enhanced at 1.3 %/ft, and high at 0.5 %/ft (Xtralis 922, 2019). For testing purposes, the detector was set to the highest sensitivity to provide the fastest time to detection.

A second ASSD model attached to the cargo compartment was the VESDA-E VEU detector model VEU-A10 which is known to be the highest sensitivity aspirating smoke detector (Xtralis VESDA-E VEU, 2019). The response notifications given by the system were based on predetermined light obscuration settings. “Alert” occurred at 0.025 %/ft, “Action” at 0.0438 %/ft, and “Fire 1” at 0.0625 %/ft (Xtralis 864, 2019). When analyzing detector response times, the time at which “Fire 1” occurred was the time documented as the response time.

Both models utilize tubing networks that run from the area being protected to the detection chamber. The air from the protected area is actively drawn through the tubing

by an aspirating fan in the detector house. Once the sampled air is brought to the detector, the air is analyzed for characteristics that would suggest a fire was occurring in the protected area.

3.3.6 Air Sampling Gas Detectors (ASGD)

Air sampling gas detectors (ASGD) were also utilized during testing. ASGDs can sense multiple types of gases. For this project, the ASGDs were used to sense CO, CO_2, and hydrogen (H_2). Two types of ASGD systems were used to cover the ULD and cargo compartment. The same ASSD tubing was used for the ASGD system to minimize waste in the testing area, meaning the detector and inlet placement were identical. The ULD ASGD system used two Sensepoint XCL gas detectors model XCL-VEA-CO and XCL-VEA-H_2. The cargo compartment was protected by three VESDA ECO gas detectors; models ECO-D-B-41, ECO-D-B-49, and ECO-D-B-14.

3.3.7 Wireless Smoke Detectors

Further technology comparisons led to the implementation of two WES^+ wireless smoke detectors by Space Age Electronics (SAE). One wireless detector was placed inside of the ULD next to the ASSD tubing inlet while the second wireless detector was placed alongside the ASSD inlet in the cargo compartment. The units, powered by batteries, were connected to a home base station though radio signals. Although not used during testing, these units have the capability of sending radio signals to strobe and horn call points. The base station, at normal smoke levels, provided a constant green LED. When one of the wireless detectors registered smoke, the base units would indicate such with a flashing red LED. The wireless detectors were chosen based on their transmission

abilities and proved to work in an aircraft environment involving metal walls and long distances from the base station.

3.3.8 Wired Smoke Detector

The DC-10 aircraft used during testing was supplied with a Whittaker Model 601 optical beam smoke detector on the cargo compartment ceiling and used during testing. The smoke detector functions by using light scattering concepts and wiring. The detector's response to smoke was monitored though a voltage output when enough was produced in quantities that created at least 3-5 %/ft light obscuration. For testing purposes, the smoke detector was set to alarm at 4 %/ft light obscuration.

3.3.9 Video Camera

To record individual tests, two GoPro video cameras were utilized to provide a visual record of individual tests, one was placed inside the ULD and the second in the cargo compartment. The GoPro inside the ULD was directed at the fuel source in the lower right corner and the GoPro in the cargo compartment was positioned behind the line of ceiling detectors and directed at the plexiglass door, shown in Figures 3.1 and 3.2. An infrared (IR) camera was also placed inside of the ULD as a backup device for the GoPro cameras. The data found from this footage was tracked but the thermal data was not used for comparisons for the scope of this project.

3.4 Fire Sources

The fuels burned for this experimental program consisted of materials that were intended to replicate a real fire scenario as well as nuisance sources. The materials tested consisted of heptane, polyethylene (PU) foam, suitcases, shredded paper, wood chips, baled cotton, lithium ion batteries, smoke generators, a humidifier, and talcum powder. Incorporating a

variety of fuel sources allowed each test to have unique smoke signatures, allowing for in-depth understanding of smoke in realistic settings. The goal was to analyze an assortment of fuels that would generate contrasting mean particle diameters, heat release rates (HRR), particle counts, and CO and CO_2 yields (Fabian, 2007). The fuels were chosen and ignited based on their ability to flame or smolder, as the type of fire determines the smoke particle size and quantity of smoke generated. The flaming fires, produced by fuels such as heptane and flaming polyethylene (PU) foam, have smaller mean particle sizes in comparison to the smoldering fires which tend to lean towards greater sized mean particle dimensions. Smoldering fires commonly produced by smoldering PU foam, wood, and cotton, generate low amounts of heat but a greater density of smoke. Wood, paper, PU foam, and heptane were also chosen as test fuels as these sources are tested by Underwriter Laboratories (UL) in UL268 to certify smoke alarms (Smoke Detectors, 2016). Suitcases, cotton, and lithium ion batteries are some of the most common items found onboard aircrafts with lithium ion batteries being the most popular material to cause a fire (FAA Office of Security, 2020).

3.5 Standard Procedure

Before testing was conducted at the FAATC, a Health and Safety Plan was drafted to identify safety measures that must take place prior, during, and after each test. Details on this report can be found in Appendix A.

Using a DAQ system, the instruments in the testing area were turned on several seconds before the fuel was ignited for each test to document the ambient air signature before the introduction of new smoke particles. Active data collection consisted of documenting the ignition time and all detector response times on the DAQ system. See

Appendix B for a more complete version of the steps taken during each test and the test data template filled out before and during each test. The same protocol was used in every test in order to ensure reproducible results. The data collection ended once the door of the cargo compartment was opened. After each test run, the data collected would be exported from the DAQ system to a unique folder labeled by fuel and leakage rate. To minimize the time between tests, once the test was completed, fans were placed inside of the ULD and cargo compartment to quickly remove the smoke from the testing area and the cargo compartment door was opened fully. The next test began once all light obscuration meters displayed voltage levels identical to values prior to testing and detectors were reset.

During each test, instrument and detector response times were reported to create a comparison between tested fuels and their individual smoke signatures. The ASGDs and ASSDs inside the ULD and the cargo compartment each had separate transport times, calculated by measuring the time taken for the instruments to register the smoke. The transport times were subtracted from the raw detector response times to demonstrate an accurate timed result.

Chapter 4: Data

4.1 Basic Calculations:

4.1.1 Mass Loss Rate of Heptane

The mass loss rate per unit area, $\dot{m}''$, of heptane in varying volumes and pool sizes were calculated using equation 4.1. The density of heptane, $\rho_{heptane}$, was assumed to be 684 kg/m^3. The pan diameter, d_{pan}, initial volume of heptane before burn, $V_{heptane}$, and burn time, t_{burn}, were all recorded before each test to accurately calculate each mass loss rate.

$$\dot{m}'' = \left(\frac{\rho_{heptane} * V_{heptane}}{t_{burn}}\right) / 0.25\pi {d_{pan}}^2 \qquad (4.1)$$

Table 4.1 Heptane MLRPUA for varying diameter pool fires.

Case	Pool Diameter (m)	Heptane Volume (mL)	Burn Time (s)	$\dot{m}''$ (kg/m^2-s)
1	0.102	15	174	0.00727
2	0.102	20	220	0.00767
3	0.203	20	95	0.00444
4	0.203	40	133	0.00634

Computing the MLRPUA was imperative for further analysis and comparison when constructing the FDS model in the next chapter. Recording the burn times of each individual test was further beneficial as it provided detail on the amount of time it would take to conduct each heptane test. Ultimately, efficient testing was of top priority, thus, the shortest burn time was chosen, case 3.

4.2 Full Scale Test Results:

Displays of detection response times, blue and IR signals, and gas concentrations versus light obscuration are presented in this section. Demonstration of the smoke concentration differences between the ULD versus the cargo compartment was provided through analysis of the LLRM ULD tests. This ULD model creates the greatest smoke signature

magnitude in the cargo compartment, thereby yielding the smallest difference in smoke signature magnitudes between ULDs and the cargo compartment. The smoldering and flaming PU foam tests were chosen for data review in this section. This fuel was ignited two separate ways to account for varying types of smoke particles released during different combustion processes. Graphs of data from all other fuels that were tested in this project can be found in Appendix C.

4.2.1 Light Obscuration and Detector Response Times

Light obscuration for the smoldering PU foam test over the duration of the test is presented in Figure 4.1 along with the detector activation times. To account for potential instrument error, the light obscuration inside the ULD was generated from the average of the two light obscuration meters at the highest position in the ULD. The light obscuration in the cargo compartment was identified from the light obscuration meter closest to the ULD (for most test scenarios the furthest light obscuration meter detected minimal levels of light obscuration). The significant time gap between the light obscuration profile

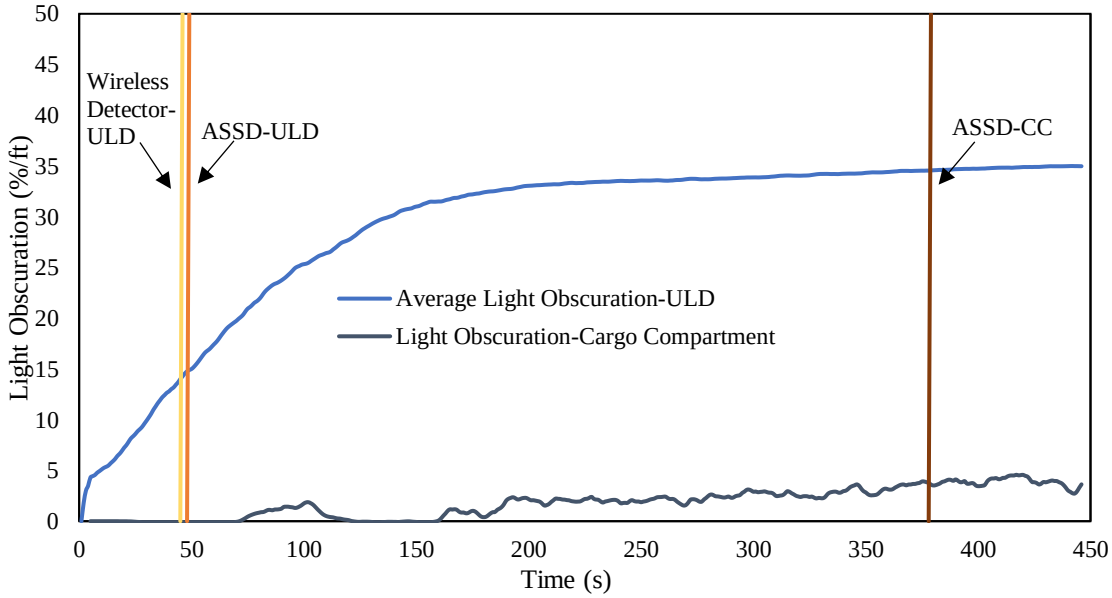

Figure 4.1. Smoldering PU foam – LLRM - Light obscuration inside ULD and the cargo compartment versus detector activation.

inside the ULD versus the light obscuration in the cargo compartment provides insight on the effectiveness of instrument placement. The vertical lines in Figure 1 display the times at which each detector was activated. The wireless detector inside of the ULD was first to alarm at 44 seconds, while the ASSD inside the ULD alarmed at 47 seconds. These activations were relatively similar in comparison to the ASSD in the cargo compartment which alarmed at 378 seconds. The wireless and wired detectors inside the cargo compartment did not activate over the duration of this test due to lack of light obscuration in the cargo compartment.

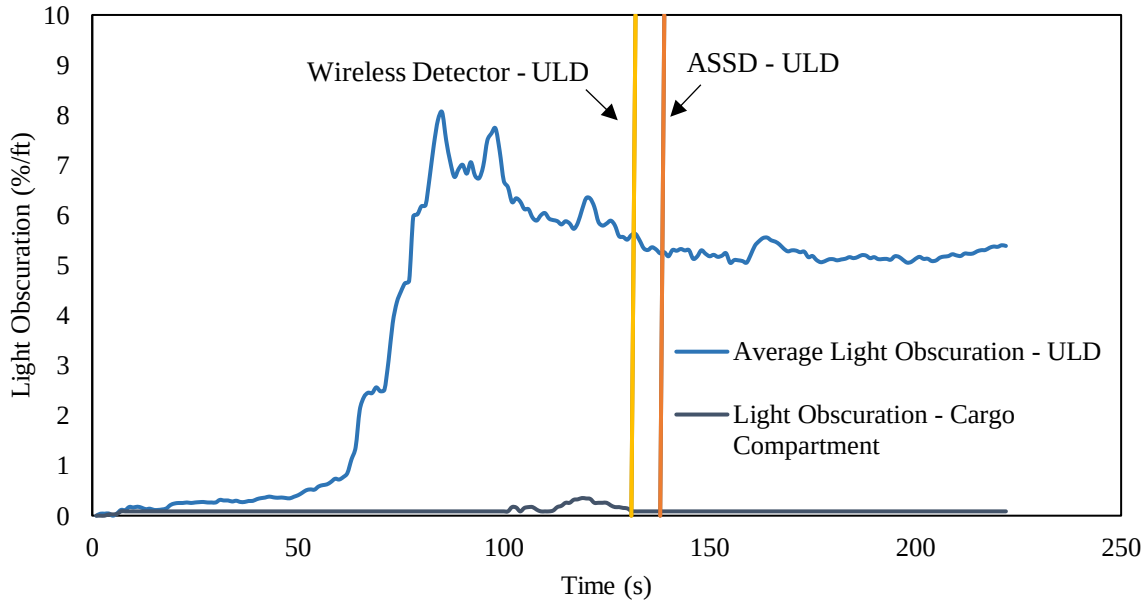

Figure 4.2. Flaming PU foam – LLRM - Light obscuration inside ULD and the cargo compartment versus detector activation.

The flaming PU foam test results for light obscuration and detector activation times is shown in Figure 4.2. The light obscuration in the ULD is shown to be peaking around 8.06 %/ft which is much greater than the amount received by the light obscuration meter in the cargo compartment which only reached a maximum level of 0.34 %/ft. The wireless detector and ASSD inside of the ULD responded to the fire within 10 seconds of

each other, however, as expected from to the extremely low light obscuration in the cargo compartment, none of the cargo compartment detectors activated during the test.

4.2.2 Light Obscuration and Blue, IR, and Blue + IR Signal

The smoldering PU foam test results from the Blue + IR wavelength detector compared with the average light obscuration levels inside the ULD are shown in Figure 4.3. Separate profiles were graphed to indicate the differences between the Blue signal and the IR signal. The sums of the Blue and IR signal were also plotted and observed to

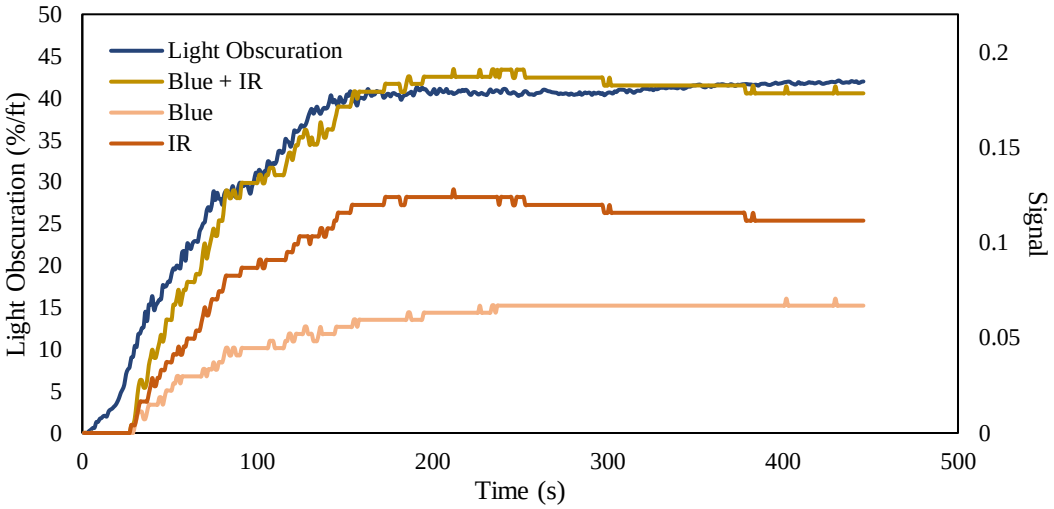

Figure 4.3. Smoldering PU Foam – LLRM – Light obscuration and Blue + IR, Blue, IR Signals.

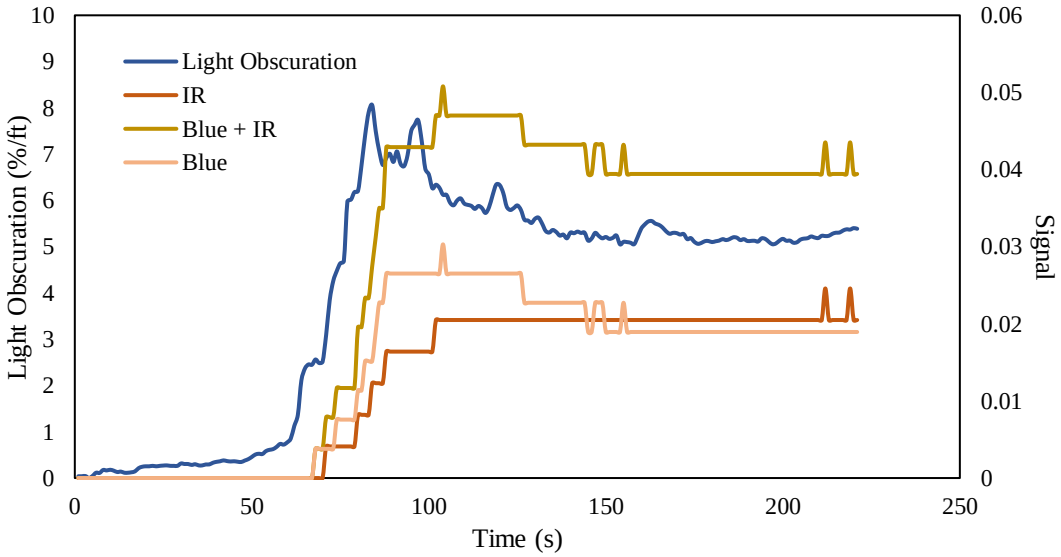

Figure 4.4. Flaming PU Foam – LLRM – Light obscuration and Blue + IR, Blue, IR Signals.

follow the light obscuration measurements relatively well, peaking around the same time before leveling out.

The flaming PU foam test results showing the same measurements as for smoldering PU foam is found in Figure 4.4. Although the concentration of smoke is much less than the concentration made from the smoldering PU foam test, the correlation between the sum of the Blue and IR wavelengths and the light obscuration inside the ULD is fairly good.

4.2.3 Light Obscuration and Gas Concentrations

The results of the CO_2 gas concentration collected by the gas analyzers inside the ULD and the light obscuration in the ULD for the smoldering PU foam test are graphed in Figure 4.5. The distinct triangle markers on the graph show the time at which the concentration of CO_2 was first achieved. The intake tube for station 4 was located just under the ULD ceiling and intake tube for station 3 was placed 12 inches down from the same position.

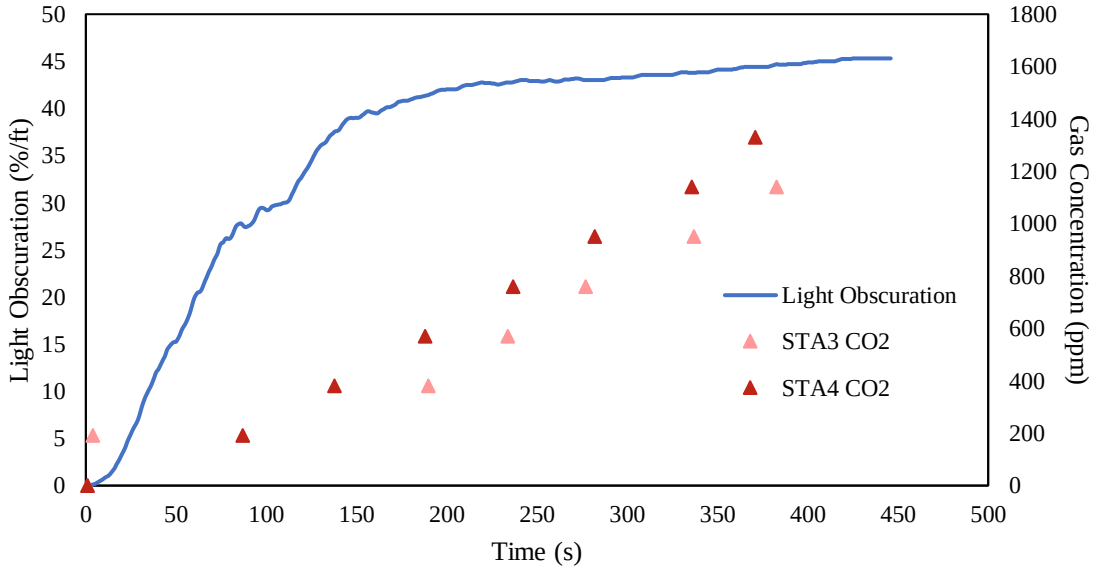

Figure 4.5. Smoldering PU Foam – LLRM– Light obscuration and gas concentrations inside ULD

The flaming PU foam test results demonstrating the CO_2 gas concentration and light obscuration levels can be found in Figure 4.6. The triangle indicators in this type of combustion reveal the gas concentration levels increased faster in comparison to the light obscuration levels suggesting the instrument which responds to the fire source fastest is dependent on how the fuel source is ignited and the mode of combustion. The CO_2 gas concentration levels shown in Figure 4.5 responds to the smoke signature in the air several seconds slower than the light obscuration increase. However, for Figure 4.6 the CO_2 concentration appears to detect faster than the light obscuration levels. This finding suggests that the instrument which detects the smoke signature the fastest is also fuel dependent.

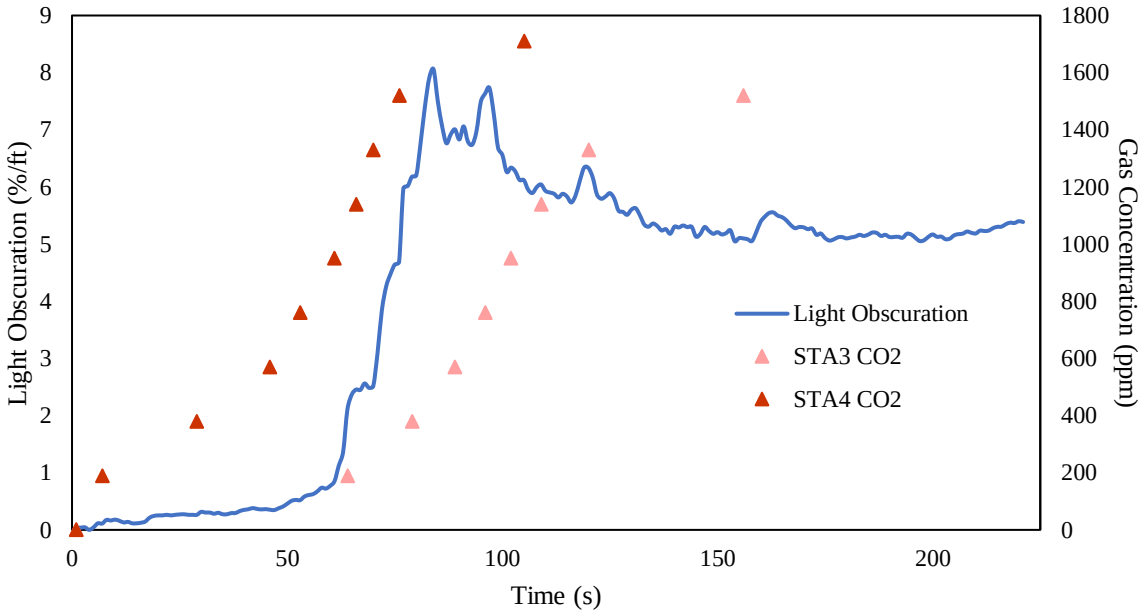

Figure 4.6. Flaming PU Foam – LLRM– Light obscuration and gas concentrations inside ULD.

As the gas analyzers also measured the CO levels, further gas technology analysis pertaining to the ASGD system measuring CO was performed. The smoldering PU foam test results, shown in figure 4.7, demonstrate the ASGD system measured gas concentration levels approximately in the middle of the gas analyzer range. The results

suggest the ASGD interpretations are within good range of the FAA instrument readings, meaning if the gas analyzers reacted well to the fire scenarios, the ASGD systems would hypothetically follow suit.

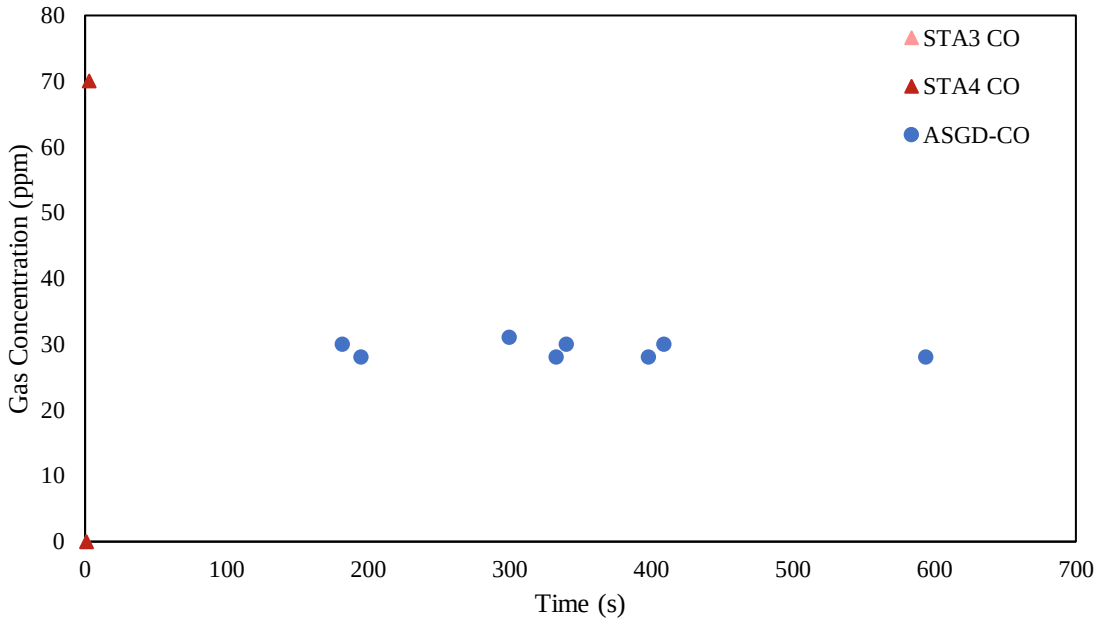

Figure 4.7. Smoldering PU Foam Test – LLRM- Gas analyzers and ASGD measuring CO.

4.2 Leakage Rate Data

4.2.1 Leakage Rate Tests

The leakage rates test results, determined by using equations 4.2 and 4.3, can be found in Table 4.2. The first step in calculating the leakage rate was to find the value of tau, τ. To begin, the CO_2 concentration levels were graphed versus time in minutes. A line of best fit was placed over the data to find an exponential equation which would match the form shown in equation 4.2. Once tau was extracted from the formula, the value was placed in equation 4.3 where it was then multiplied by the volume of the ULD, V_{ULD}, which was found to be 151.23 ft^3.

$$C = C_0 * e^{(-t/\tau)} \quad (4.2) \qquad Leakage\ Rate = \tau * V_{ULD} \quad (4.3)$$

As expected by their test type and number of holes, the calculated leakage rates showed the SLRM had the lowest leakage rate and the LLRM had the highest leakage rate.

Table 4.2 ULD Leakage Rates

Test Type	**ULD Category**	**τ (min$^{-1)}$**	**Leakage Rate (cfm)**
ULD 1 - No holes	Small Leakage Rate Model (SLRM)	0.025	3.78
ULD 2 - 1 Column of holes	Medium Leakage Rate Model (MLRM)	0.037	5.60
ULD 3 - 2 Columns of holes	Large Leakage Rate Model (LLRM)	0.058	8.71

4.2.2 Leakage Rate Effects

To demonstrate the effects of ULD leakage rates, light obscuration levels from the LLRM, MLRM, and SLRM ULD tests from each type of PU foam test were analyzed. This section analyzes only the PU foam tests as it can be assumed to be representative of

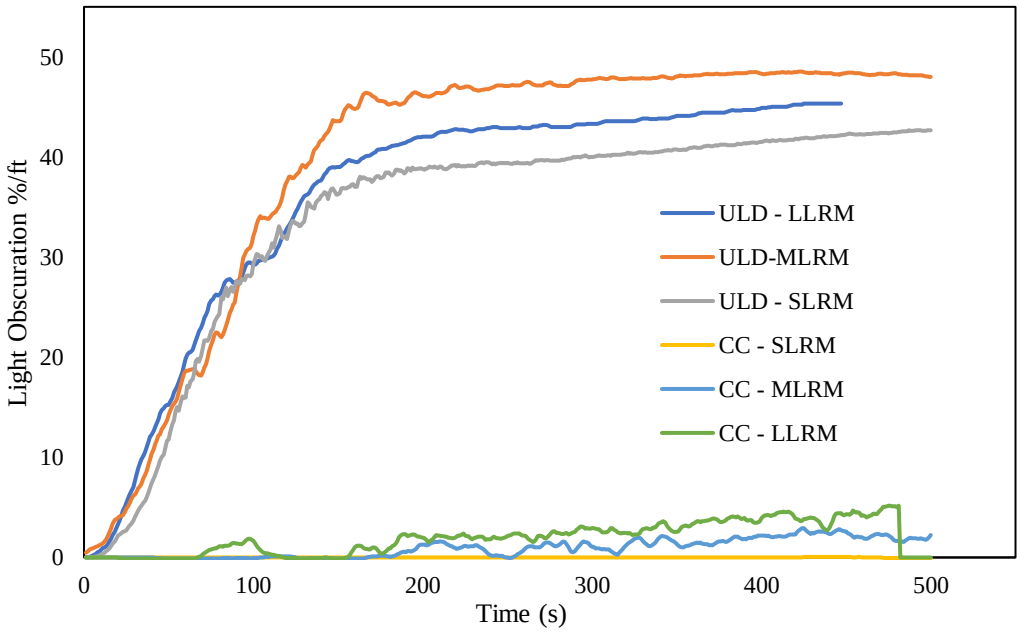

Figure 4.8. Smoldering PU foam tests - Leakage rate effects on light obscuration.

all other fire sources. The three different leakage rate tests conducted for each fuel provided insight on the effects of tightly sealed containers. The light obscuration results from all three smoldering PU foam tests are shown in Figure 4.8. The graph demonstrates the light obscuration levels are altered in both the ULD and the cargo compartment depending on the applied leakage rate. The light obscuration in the cargo compartment was greatest in the LLRM test reaching a maximum level of 5.17 %/ft. The MLRM test created the second greatest light obscuration level in the cargo compartment of 3.75 %/ft while the cargo compartment light obscuration was nonexistent in the SLRM test. Interestingly, the interior ULD light obscuration did not follow the same trend. The MLRM test produced the greatest obscuration of 48.5 %/ft with the LLRM test following in second with a maximum of 45.3 %/ft. The SLRM test generated the least amount of smoke reaching a maximum peak of 42.7 %ft. These tests were only conducted once, thus the repeatability of the results is unknown.

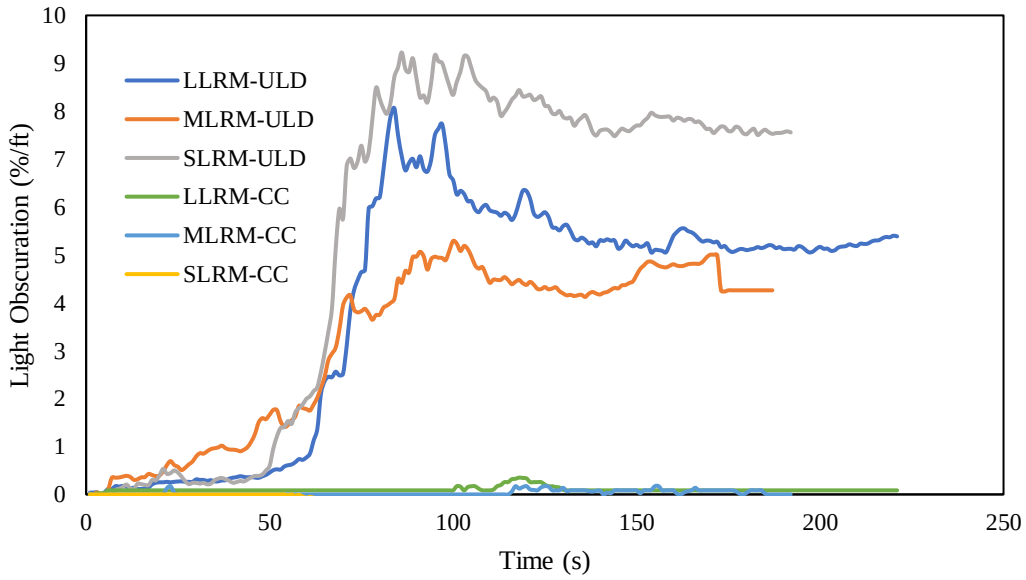

Figure 4.9. Flaming PU foam tests - Leakage rate effects on light obscuration.

The light obscuration results for flaming PU foam for all three types of leakage rate tests are displayed in Figure 4.9. The graph shows an extreme difference between the light obscuration levels inside the ULD versus in the cargo compartment. As anticipated, the light obscuration in the cargo compartment was nonexistent in the SLRM test while the MLRM test achieved a small increase in light obscuration in the cargo compartment peaking at 0.173 %/ft and the LLRM test created the highest light obscuration in the cargo compartment of 0.352 %/ft. The SLRM test created the greatest light obscuration level inside the ULD reaching a maximum of 9.23 %/ft. At a peak of 8.06 %/ft, the LLRM test produced the second greatest light obscuration level in the ULD. The MLRM test yielded the least amount of light obscuration with a maximum of 5.29 %/ft.

Chapter 5: Results

5.1 Location Effects on Detection Times

The activation times from the ASSD systems and wireless detectors located in the ULD and cargo compartment are shown in Table 5.1. The table shows the activation times for the LLRM ULD tests only. All eight fuel sources presented in Table 5.1 provided adequate smoke allowing for at least one detector to alarm in each test. The table is split between the smoldering fire tests and flaming fire tests. Although each smoldering fuel source produced varying amounts of smoke, the average activation time of the ASSD in the ULD is average 364 seconds faster than the ASSD in the cargo compartment. For the tests where both wireless detectors activated, the average activation time of the ULD wireless detector is 322 seconds faster than the cargo compartment wireless detector. However, there were six tests where the cargo compartment wireless detector never activated in the entire duration of the test (these instances are identified in Table 5.1).

The ULD detectors also responded more quickly than detectors in the cargo compartment for flaming fuel sources. For the flaming fuel sources neither the cargo compartment ASSD nor the cargo compartment wireless detector activated in either test, thus, an average activation time difference was not calculated. The inactivity of both detectors suggests the flaming smoke particles were unable to escape the ULD in sufficient quantity even when the leakage rate was largest. Interestingly, the ULD ASSD had a faster average activation time in the smoldering fuel tests in comparison to the flaming fuel tests while the ULD wireless detector had a faster average activation time in the flaming fuel tests in comparison to the smoldering fuel tests.

Table 5.1. Activation Times and Differences

Fire Type	Fire Source	ASSD			Wireless Detector		
		ULD Activation Time (s)	CC Activation Time (s)	Time Difference (s)	ULD Activation Time (s)	CC Activation Time (s)	Time Difference (s)
Smold.	Smold. PU Foam	46	378	332	44	NA	CC detector never alarmed
	Wood	62	184	122	58	430	372
	Cotton	91	467	376	119	NA	CC detector never alarmed
	Wires	47	467	420	257	NA	CC detector never alarmed
	Paper	116	190	74	112	383	271
	Batteries	370	1228	858	735	NA	CC detector never alarmed
Smoldering Average		122	436	364	221	407	322
Flame	Flame PU Foam	133	NA	CC detector never alarmed	90	NA	CC detector never alarmed
	Heptane	241	NA	CC detector never alarmed	168	NA	CC detector never alarmed
Flaming Average		187	NA	NA	179	NA	NA

A graphical representation of Table 5.1 is presented in Figures 5.1 and 5.2 to illustrate the magnitude of the activation time difference. The graph in Figure 5.1 demonstrates that the ASSD in every smoldering fuel test provided a faster activation time in the ULD while the cargo compartment activation time had a delayed response time between 74 seconds and 858 seconds. The flaming tests indicate that the ULD ASSD activates at a similar time compared to the smoldering ULD ASSD, however, the

cargo compartment ASSD in the flaming tests do not follow the same pattern and instead never activate.

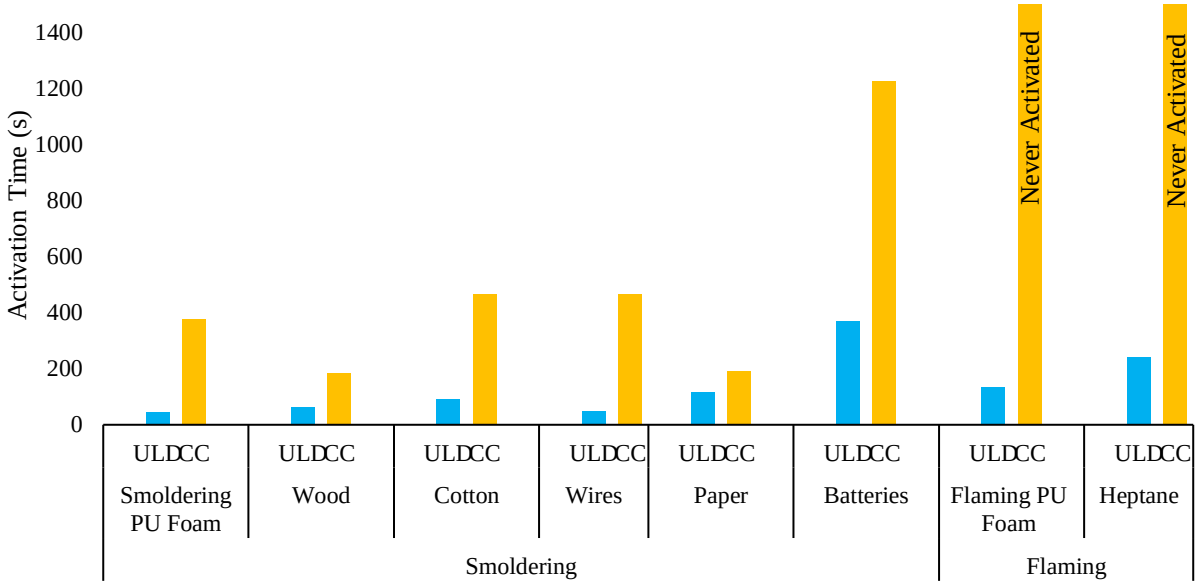

Figure 5.1 ASSD activation times compared - LLRM ULD Tests

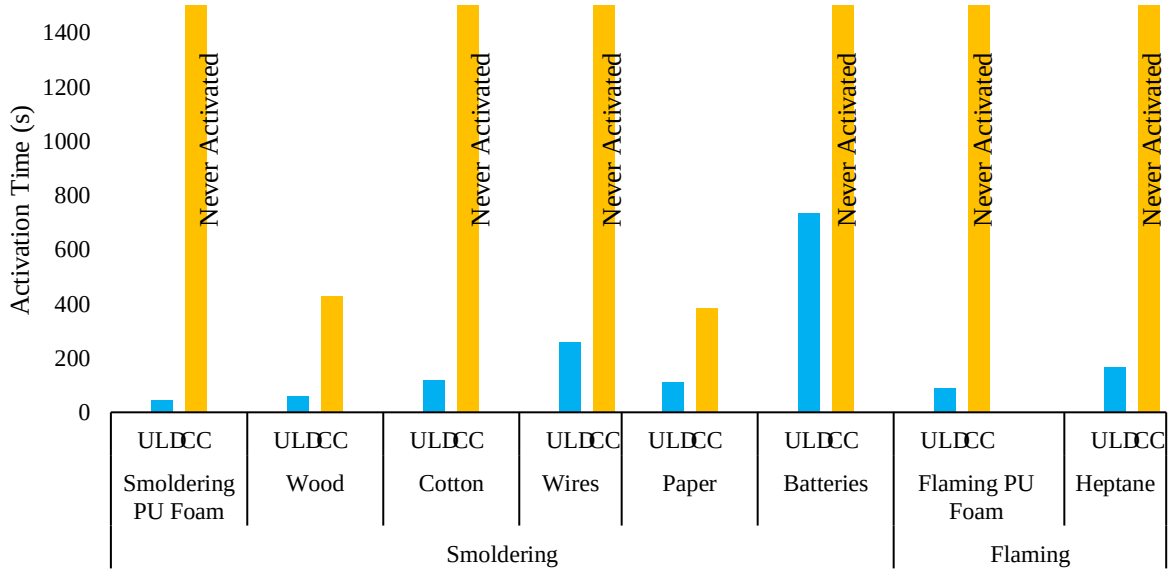

Figure 5.2 Wireless detector activation times compared - LLRM ULD Tests

The graphical representation of the wireless detector activation times is shown in Figure 5.2. The graph further shows that the ULD wireless detector activation times exceed the cargo compartment wireless detector activation times in every test,

inconsequential of whether the fuel was flaming or smoldering. In six of the eight tests, the cargo compartment wireless detector never activated. Considering the faster activation times of the ULD detectors than the cargo compartment detectors, the next section will solely focus on the abilities of the detectors inside of the ULD.

5.2 Detection Technology Effects on Detection Times

Focusing solely on the detectors inside of the ULD, a deeper comparison of the activation times for various detection technologies included inside of the ULD was performed. The LLRM ULD tests remained the focus of this evaluation. The ASSD, ASGD measuring CO[1], and wireless detector were compared together grouped by fuel in Figure 5.3. Evaluating the activation times revealed the wireless detector was first to activate for five of the eight tests, while the ASSD detector activated first for two of the

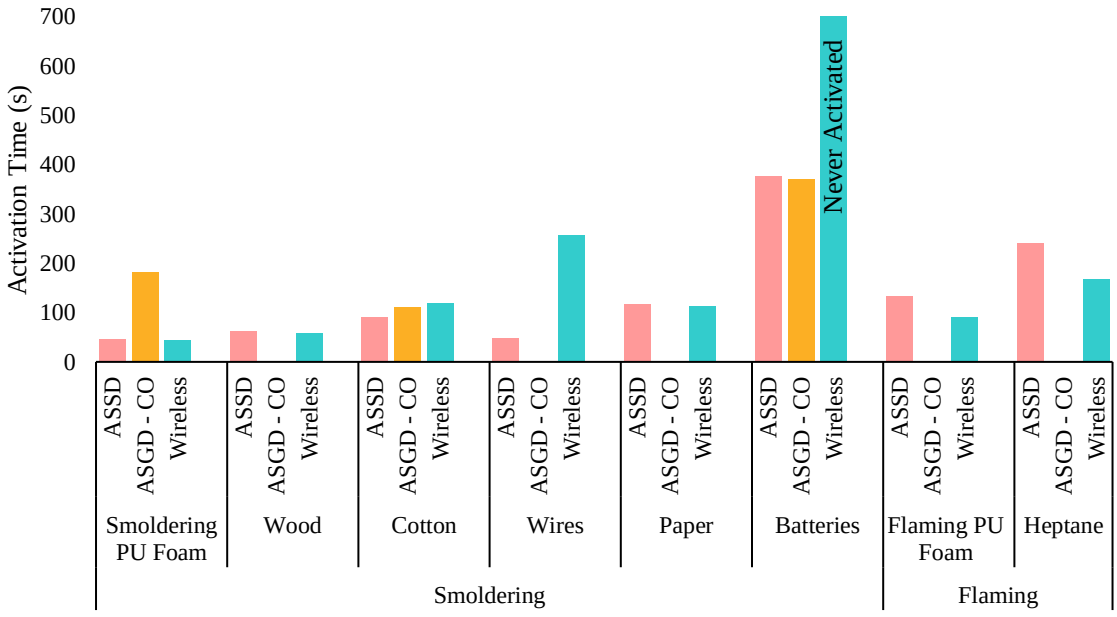

Figure 5.3 Activation times of detectors inside ULD – LLRM ULD tests

[1] Data for the ASGD measuring CO was only recorded for three tested fuels.

tests and the ASGD measuring CO activated first for one test. Each detector was set to unique thresholds set by the manufacturer; thus, the results could vary if more restrictive threshold were set on any of the detection systems. More in-depth analysis shows the wireless detector activated first for both flaming tests and activated first for three of the five smoldering tests. However, the wireless detector failed to activate in the battery test[2].

Table 5.2 Light obscuration at detection activation time for largest leakage rate.

Fire Type	Fuel	Detector Activated	Light obscuration %/ft at location of detector
Smoldering	Smoldering PU Foam	Wireless Detector-ULD	13.81
		ASSD-ULD	14.68
	Cotton	Wireless Detector-ULD	4.92
		ASSD-ULD	2.48
	Wood	Wireless Detector-ULD	3.60
		ASSD-ULD	4.45
	Wires	Wireless Detector-ULD	7.33
		ASSD-ULD	12.84
	Paper	Wireless Detector-ULD	64.83
		ASSD-ULD	66.10
	Batteries	Wireless Detector-ULD	28.25
		ASSD-ULD	25.21
Flaming	Flaming PU foam	Wireless Detector-ULD	6.57
		ASSD-ULD	4.88
	Heptane	Wireless Detector-ULD	7.75
		ASSD-ULD	11.74

[2] The wireless detectors were not changed after each set of tests; therefore, the detector was subjected to soot from past tests that may have affected its ability to activate properly.

The light obscuration at the time of activation of each detection technology was recorded and is displayed in Table 5.2 and visually represented in Figure 5.4. The results show a wide variety of light obscurations have the ability to activate wireless detectors and ASSDs depending on the fuel source. When comparing the light obscuration levels between the wireless detector and ASSD for the same fuel, it was revealed that the light obscuration levels which activated the alarms of both detectors are extremely similar to one another. The average difference in the light obscuration readings was found to be 2.46 %/ft, meaning the two technologies activate at extremely similar smoke density levels. The thresholds set by the manufacturer was the largest influence in this set of results.

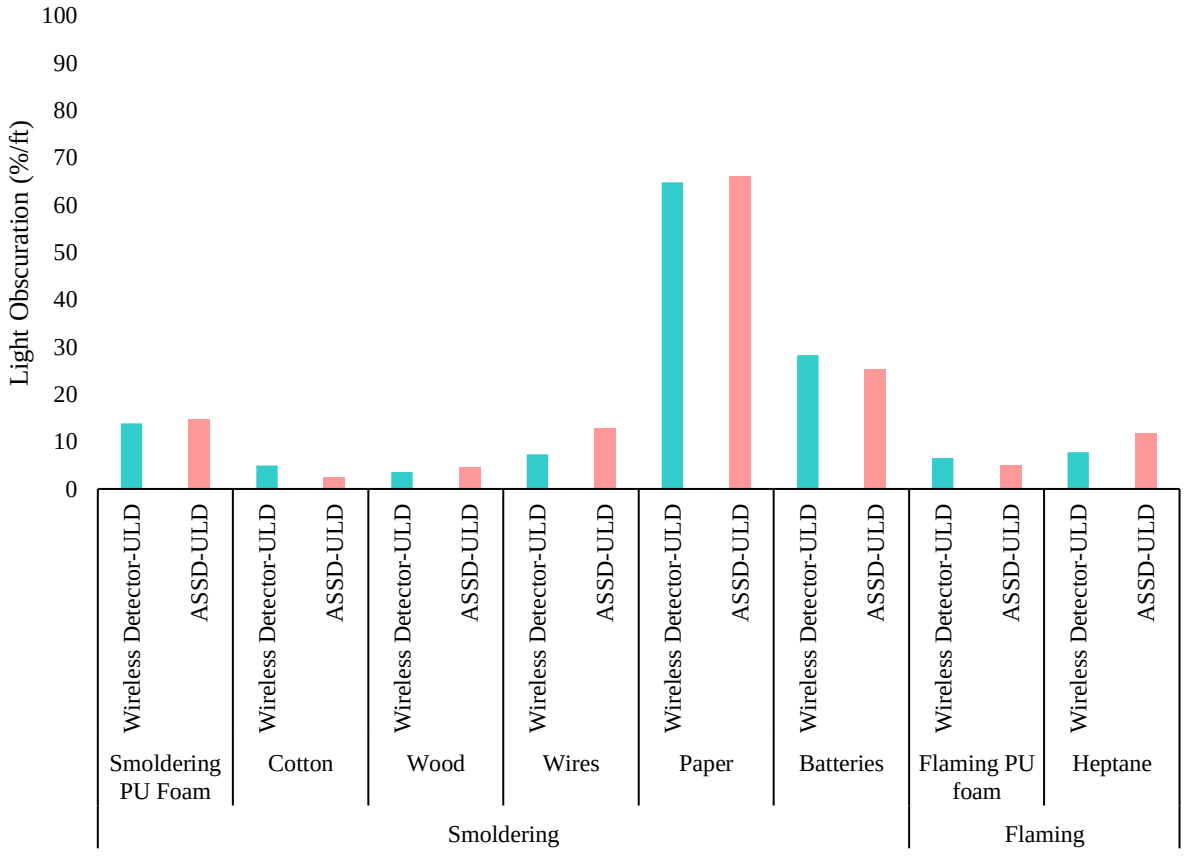

Figure 5.4 Light obscuration at time of activation per detector technology.

In Figure 5.4, the fuel which generated the highest light obscuration before the time of activation for both technologies was found to be paper[3]. The fuel which produced the smallest amount of concentration before the time of activation for both technologies was found to be cotton.

The Blue+IR wavelength detector was found to provide results with good correlation to the light obscuration levels. Although there is a several second delay in increase for the Blue+IR signal, the slopes of both instruments have similar trends indicating the Blue+IR technology has the capability of performing well in a real detector which could activate during a fire. The Blue+IR signals were not set to alarm to the fuel source at a specific level, thus, comparison with the activation times for ASSD, ASGD, and wireless detectors is not possible.

The gas concentration inside the ULD was also analyzed to determine how the smoke signature was changing in time. The values for the time of first rise in gas concentration and the rate of rise for CO and CO_2 for each fuel are displayed in Table 5.3. A visual representation of the results is shown in Figures 5.5 and 5.6. The smoldering PU foam test did not create enough CO for detection by the gas analyzers and the wires test did not create enough CO or CO_2, thus, those spots were labeled NA in Table 5.3. The bar graphs in Figures 5.5 and 5.6 show no bar for those tests to represent the lack of an adequate gas concentration.

[3] Many of the fuel sources created large amounts of soot. Instruments were not cleaned before each new fuel source which may reason why the paper test had the highest light obscuration as it was the last tested fuel source.

Table 5.3 Gas concentration first increase and rate of rise.

Test Type	Fuel	Time of first concentration rise (s)		Rate of rise (ppm/s)	
		CO	CO_2	CO	CO_2
Smoldering	Smoldering PU Foam	NA	6	NA	3.13
	Cotton	96	45	0.79	5.99
	Wood	33	4	2.61	15.14
	Wires	NA	NA	NA	NA
	Paper	16	4	3.44	18.94
	Batteries	152	5	29.70	0.77
Flaming	Flaming PU Foam	65	7	1.08	20.62
	Heptane	136	18	0.52	19.44

The findings show for every test, CO_2 was the first gas detected by the gas analyzers and for the smoldering PU foam test it was the only gas detected. On average, the first indication of CO was around 69 seconds after the first indication of CO_2. The

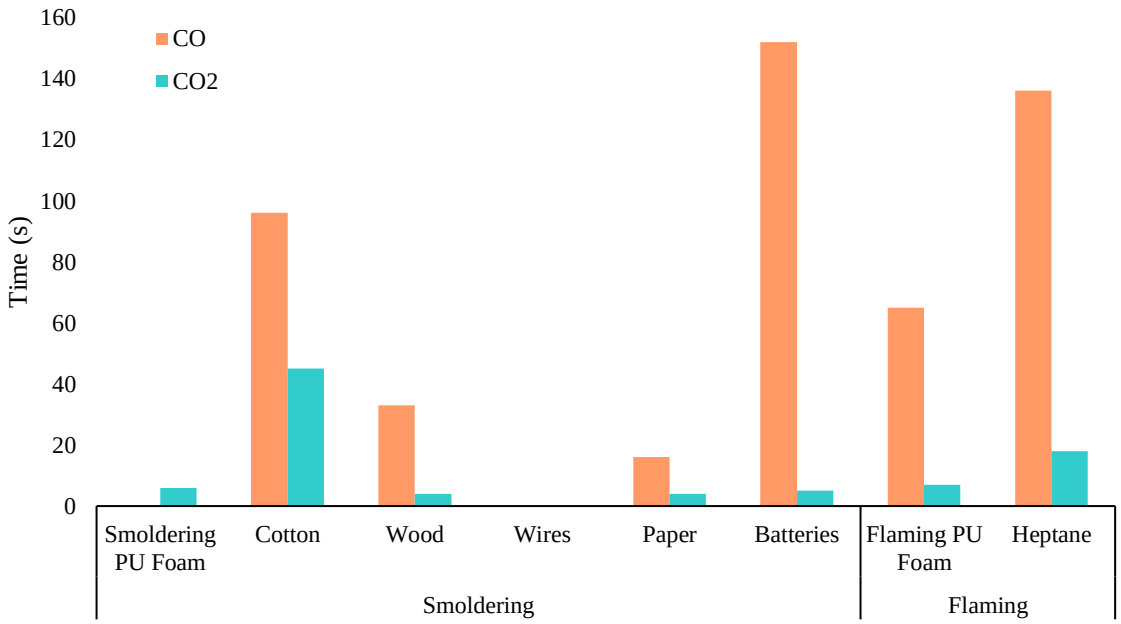

Figure 5.5 Time of first gas concentration increase.

fuel source which created the fastest CO_2 detection time was observed to be paper and wood, with batteries and both foam tests following closely behind. Cotton was found to take the longest for CO_2 concentration detection.

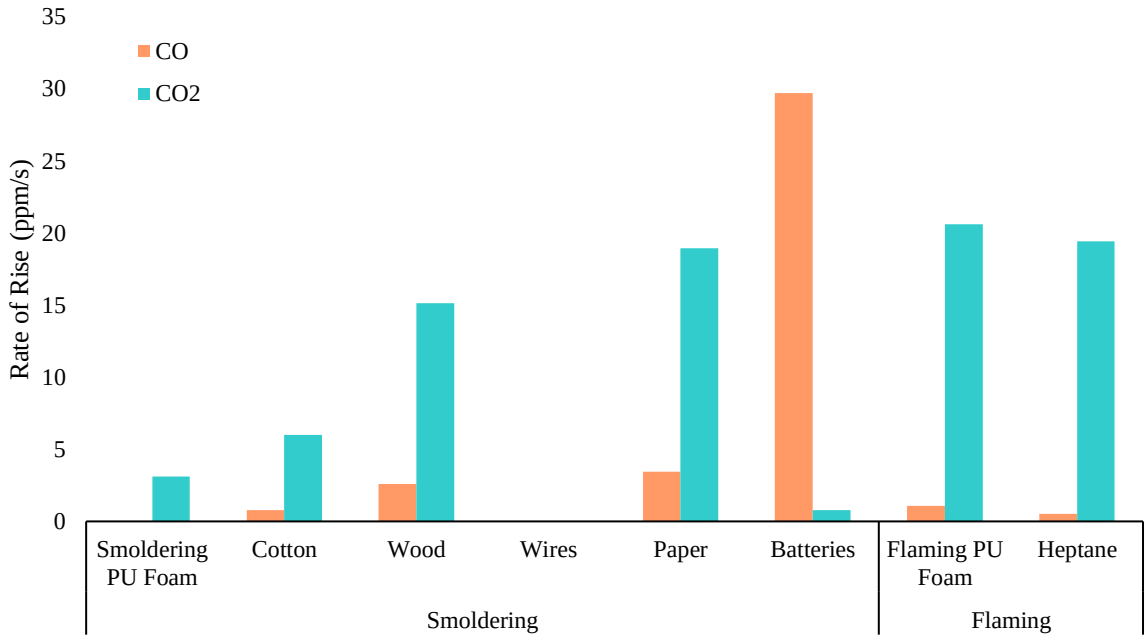

Figure 5.6 Average gas concentration rate of rise.

The gas rate of rise of the concentration of CO_2 increased much faster that for CO, with the exception of the batteries test which showed the CO concentration to increase dramatically within a short period of time. On average, the CO_2 concentration had a rate of rise nearly 14 ppm/s greater than the CO rate of rise, suggesting the small volume in the ULD allowed for the CO_2 levels to increase much faster than the CO levels. The flaming PU foam created the greatest CO_2 rate of rise while the batteries created the fastest CO rate of rise, with the paper fuel generating the second fastest CO rate of rise. Cotton was found to have the lowest CO rate of rise while the batteries had the lowest CO_2 rate of rise. This indicates the first concentration increase and rate of rise were shown to be fuel dependent.

5.3 Leakage Rate Comparisons

The leakage rate results demonstrated that for the Boeing smoke generator only, there is a direct correlation between the light obscuration in the cargo compartment and the ULD leakage rate. The expected results were hypothesized that the greater the leakage rate, the greater are the light obscuration levels in the cargo compartment. Conversely, the

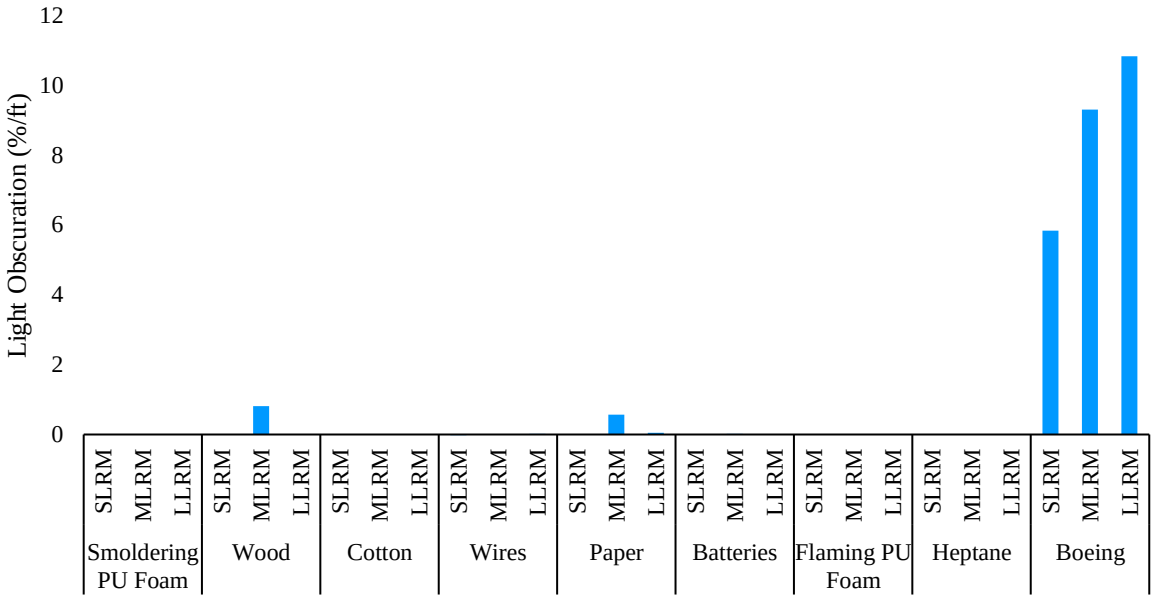

Figure 5.7 Light obscuration at 60 seconds in the cargo compartment.

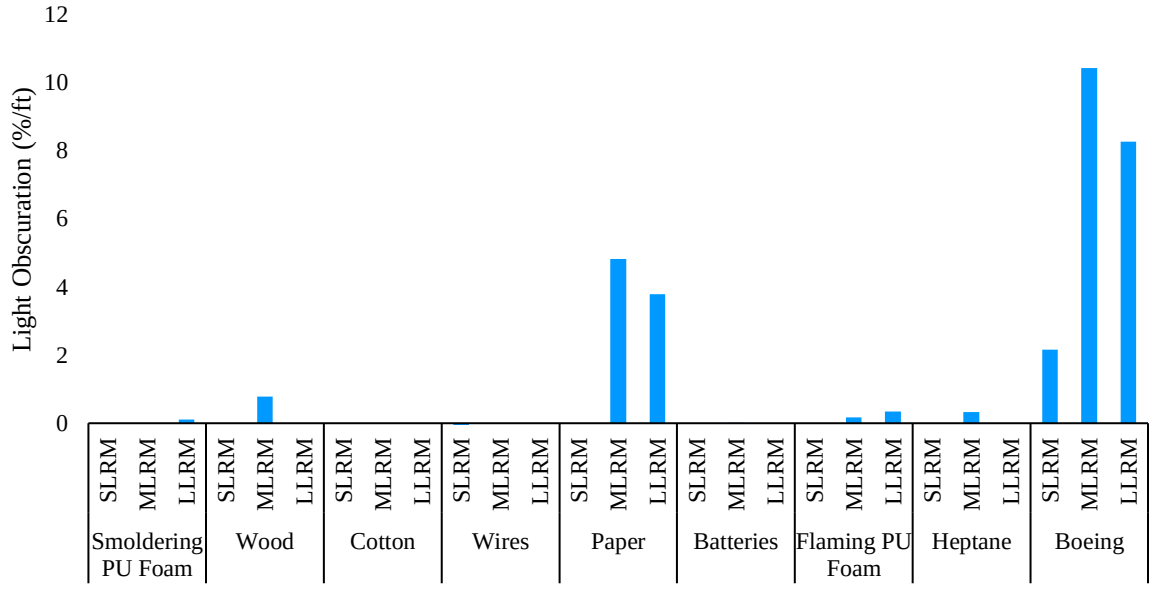

Figure 5.8 Light obscuration at 120 seconds in the cargo compartment.

smaller the leakage rate, the less are the cargo compartment light obscuration levels. The Boeing smoke generator is the only fuel source to follow the expected trend and only at the 60 second mark. Shown in Figures 5.7 and 5.8, the light obscuration at 60 seconds and 120 seconds in each test demonstrate this trend does not always occur. The other eight fuel sources show the leakage rate does not have a direct trend on the light obscuration. This suggests there is low reproducibility of each test.

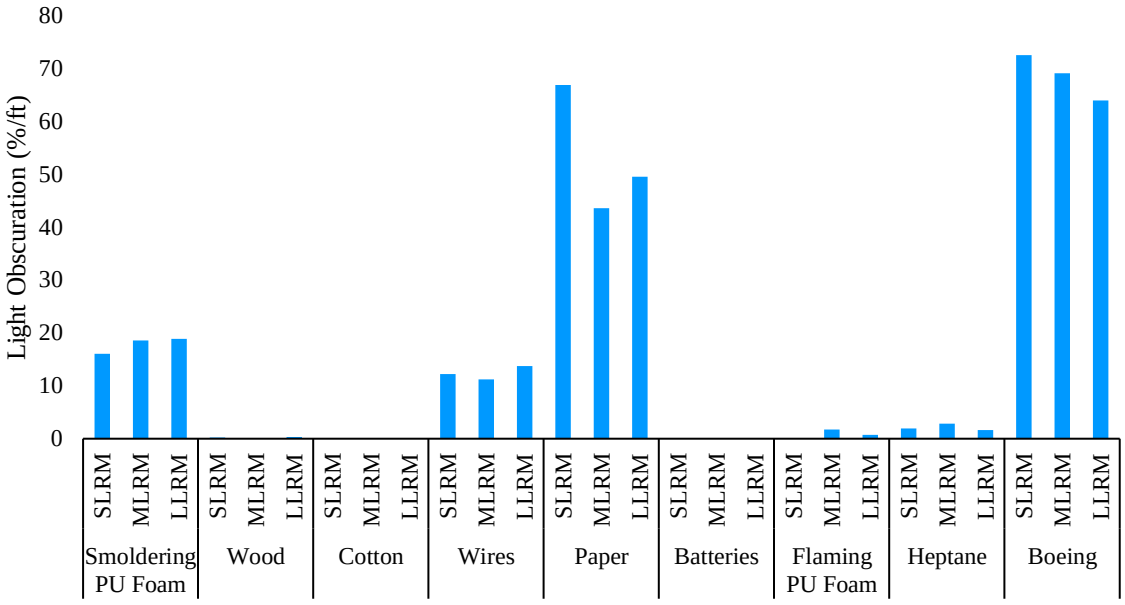

Figure 5.9 Light obscuration at 60 seconds in the ULD.

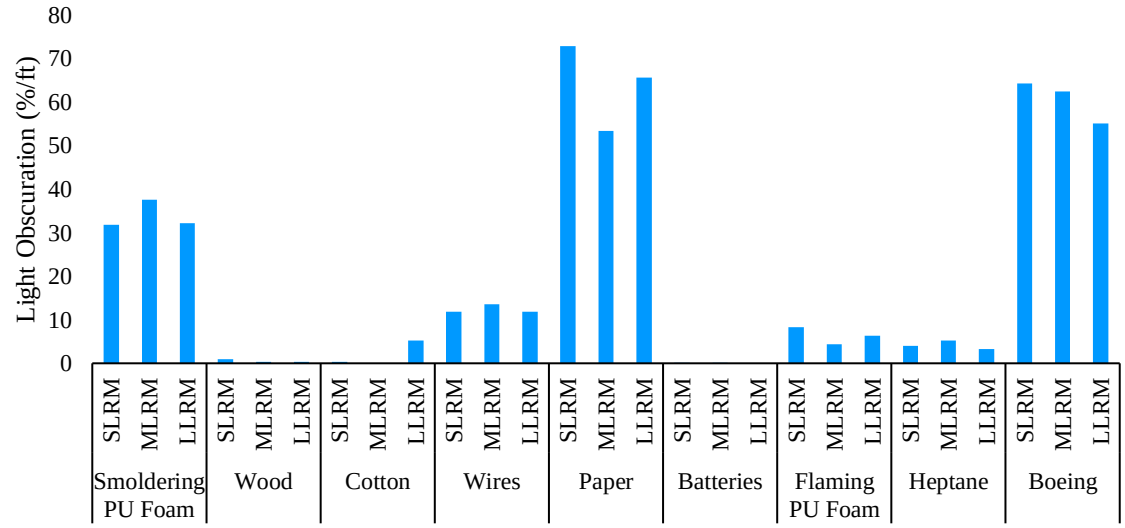

Figure 5.10 Light obscuration at 120 seconds in the ULD.

The light obscuration inside of the ULD also did not always follow an expected trend when comparing the leakage rates. It was hypothesized the SLRM ULD would generate the greatest light obscuration level inside the ULD and the LLRM ULD would have the lowest light obscuration level because it allows the most smoke to escape. However, in Figures 5.9 and 5.10, the results showed the Boeing smoke generator to be the only fuel source to follow the expected trend. For several of the fuels, it was found the MLRM ULD created either the lowest or greatest light obscuration level, which does not match any known hypothesis. Other fuels indicated the leakage rate did not affect the light obscuration levels inside the ULD at all, showing the light obscurations at 60 seconds and 120 seconds were all within 5 %/ft for different leakage rates. Comparing the leakage rates reiterates there is a lack of reproducibility of each test.

Chapter 6: Computational Model

6.1 Model Set-Up

A CFD model of the DC-10 cargo compartment and interior ULD was created to demonstrate the capability of fire modeling software to simulate conditions in an aircraft environment and ability to create results comparable to the experimental results. The demonstration was conducted using FDS (version 6.7.1) and PyroSim (version 6.7.1) and to create a visual representation, Smokeview (6.7.5) was incorporated.

The FDS model, shown in Figures 6.1, 6.2, and 6.3, used three different mesh fields consisting of grid spacing of 10 cm or 20 cm in the x, y, and z coordinate system. The three mesh fields cumulated together to be a 5 m wide, 8.6 m long, and 1.6 m tall space. The first mesh, Mesh1, field involved the ULD and the area closest to it in the cargo compartment. Mesh1 was constructed to be 2.4 m by 5 m with a height of 2 meters with a grid spacing of 1 cm totaling in 20 cells in the x-direction, 50 cells in the y-direction, and 20 cells in the z direction. The second mesh, Mesh2Top, which had a 1 cm grid spacing was made of a 6 m by 5 m by 1 m tall space. Mesh2Top had totaled in 60 cells in the x-direction, 50 cells in the y-direction, and 10 cells in the z-direction. The third mesh field, Mesh3Bottom, was directly beneath Mesh2Top, thus, held the same dimensions as Mesh2Top but had a unique set of cells as this mesh field used a 20 cm grid spacing, as suggested by prior work on CFD modeling (Pongratz). Mesh3bottom had 30 cells in the x-direction, 25 cells in the y-direction, and 5 cells in the z-direction.

Once the mesh fields were created, the cargo compartment framework was modeled to replicate the DC-10 used in the experimental testing. Using the diagram in Figure 3.1 the cargo compartment was constructed with measurements taken at the

FAATC. To place the layout of the cargo compartment, obstructions were placed to simulate walls of the aircraft. Under the assumption the cargo compartment aircraft walls were composed of aluminum, the wall material was given aluminum properties (Aircraft

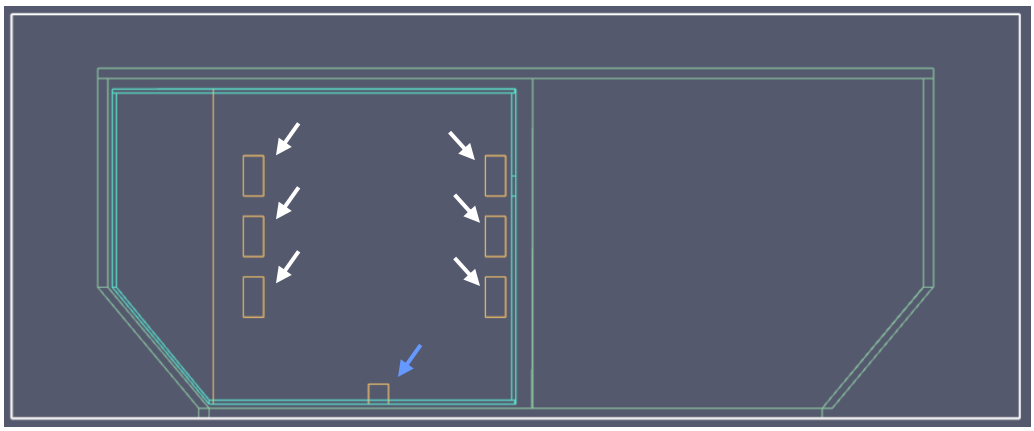

Figure 6.1 Elevation side view of FDS simulation.

and Aerospace). The curtain area covered by flexible plastic drapes in the experimental testing was assumed nonexistent for the modeling to keep the simulation realistic for in flight scenarios. The ULD was placed inside of the cargo compartment in the exact location suggested in Figure 3.1. The ULD wall obstructions were also assumed to hold aluminum properties except for the door. The door obstruction was given plexiglass properties to represent the plexiglass door used in the experimental testing.

The ULD was modeled to resemble the LLRM ULD for comparisons with the experimental LLRM heptane tests. The door of the ULD was given three holes on each side totaling in six holes to resemble the largest leakage rate ULD door from the

Figure 6.2 Elevation Front View of FDS simulation.

experimental testing. The area of each rectangular hole was 0.1 m in length and 0.2 m in height. The holes in the ULD door can be seen in Figure 6.1 each outlined in orange indicated by the white arrows. To account for air flow from other crevices of the ULD, another hole was place on the wall adjacent to the ULD door. The area of the hole was constructed to be 0.1 m by 0.1 m and can be found in Figure 6.2 outlined in blue indicated by the white arrow on the left wall of the ULD. Flow measuring devices were placed over each hole to measure the flow rate through each hole to determine the flow area for the model that was equivalent to that in the experiments. FDS simulations were rerun until the leakage rate of the simulated ULD was verified to be correct meaning it was within a range near 8.71 cfm which was the overall leakage rate of the experimental LLRM ULD.

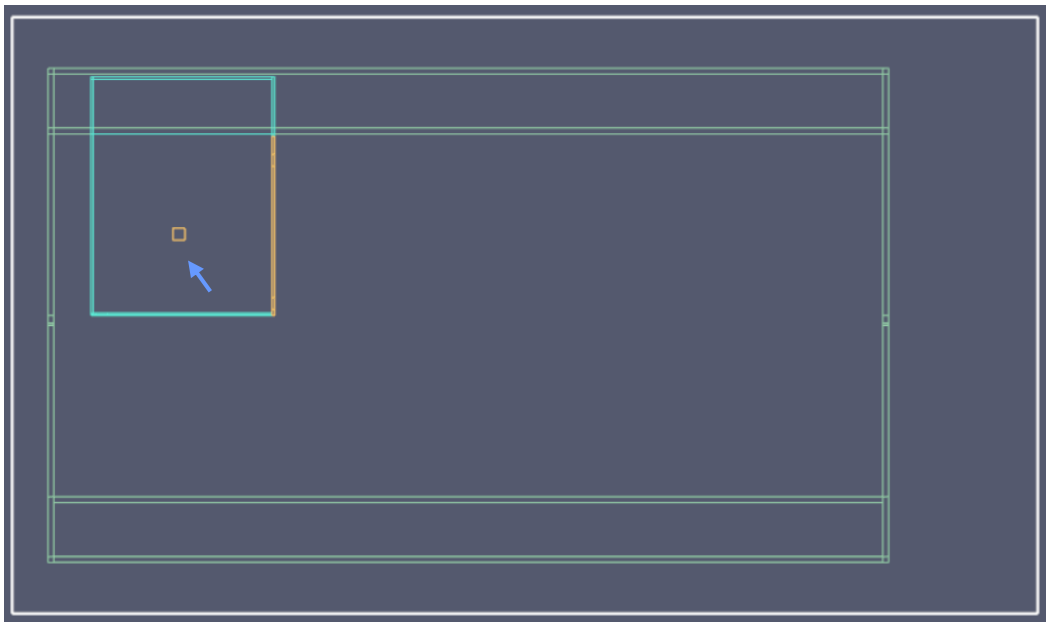

Figure 6.3 Plan View of FDS simulation.

Heptane was used to demonstrate the capability of this model as it is one of the simpler fuel sources to simulate accurately. The source was created under the simple chemistry model using heptane's composition of C_7H_{16}. The surface area of the fuel

source was identified as ‘burner’ and the heat release rate was determined using the calculated values in Table 4.1 which was found to be 0.00444 kg/m^2-s in case 3. The burner location can be found in Figures 6.1, 6.2, and 6.3 outlined in the orange box indicated be the blue arrow in the center of the ULD floor. The burner surface was prescribed to have a unique ramping function which would best mimic the experimental heptane characteristics. The ramp up time was set to reach maximum mass loss rate within the first 10 seconds and set to decrease from the maximum mass loss rate in the last 10 seconds of the test. The entire 3D view of the model structure can be found in figure 6.4. The devices were added later to confirm the accuracy of the model.

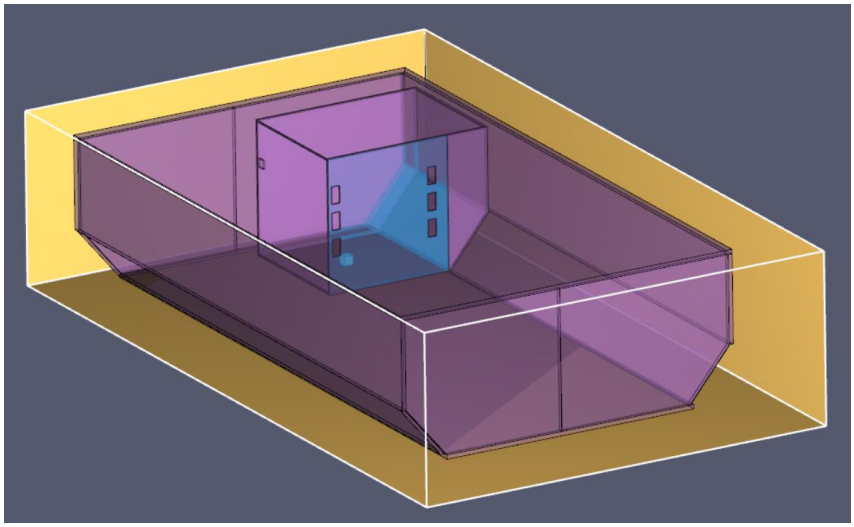

Figure 6.4 3D View of FDS simulation.

Devices were placed inside the cargo compartment and ULD to measure the accuracy of the model against the experimental results. Thermocouples were the main source of comparison. Thus, the entire compilation of thermocouples used in the experimental testing was placed in the model, meaning one thermocouple tree in the ULD, one thermocouple tree placed in the cargo compartment, and identical experimental test layouts for the ceilings of the ULD and cargo compartment . All FDS thermocouples were placed in the exact spot as the experimental thermocouples. Each thermocouple was

assigned to be made of Chromel and Alumel, the material in used in k-type thermocouples (Button, 2015). For comparisons between experimental light obscuration and simulated light obscuration, optical density devices were placed in the ULD and cargo compartment in their respective experimental testing locations.

Smoke detectors and aspirators were also implemented into the model for comparison between manufactured detectors and simulated detectors. The smoke detectors placed inside the ULD and the cargo compartment were set to measure the soot concentration under the Cleary model using photoelectric technology (Justin). The aspirators mimicked the ASSD system used in the experimental testing. Aspirator samplers were first placed at the exact location of the experimental testing ASSD intake point and then followed by an aspirator system in the same spot which would detect the smoke concentration. The aspirator inside of the ULD resembled the VEA ASSD system, set to have a 40 second transfer delay with a flowrate of 0.35 l/min. The aspirator in the cargo compartment modeled the VEU ASSD system with a transfer delay of 27 seconds and a flowrate of 57.9 l/min.

Measuring the simulated gas concentrations was performed through placing CO and CO_2 detectors inside of the ULD and cargo compartment. Each detector was placed in the exact same position as the ASGD systems in the experimental tests and measured the gas concentration by volume fraction. The FDS results were converted using equation 3.2 similar to the experimental gas analyzer results.

The FDS simulation parameters were modified to meet the experimental testing environment. The model was adjusted to run for 300 seconds, as this was the time in which the experimental test finished. The test was modeled under the very large-eddy

(EMS) simulation type. The average ambient temperature in the testing facility was calculated to be 28.5 °C with an average humidity of 62 %.

6.2 Model Results

The FDS model generated results in Smokeview which are shown in figure 6.5. The program causes the model to appear jagged as this is how the program snaps to the chosen grid size. The yellow area indicates the space outside of the cargo compartment but inside of the mesh field while the pink walls indicate the place of the ULD and cargo compartment, similar to the view in figure 6.4. Smokeview was set to show the soot density of the smoke and the heat release rate per unit volume (HRRPUV) being produced from the fuel source. The ULD appears to be darker than the rest of the model as this is a snapshot of the program after 200 seconds has passed. It can be visually seen that the ULD holds the smoke inside for a considerable amount of time before there is visible smoke in the cargo compartment.

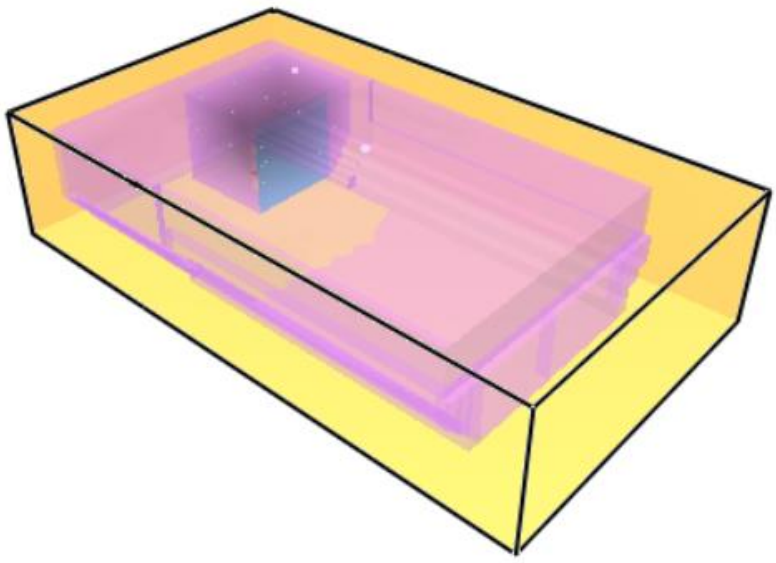

Figure 6.5 FDS results in Smokeview.

6.2.1 Leakage Rate Comparisons

The first check for the FDS model was to examine the total flow rate escaping through the holes in the ULD, labeled as the leakage rate. Each hole in the ULD provided its own

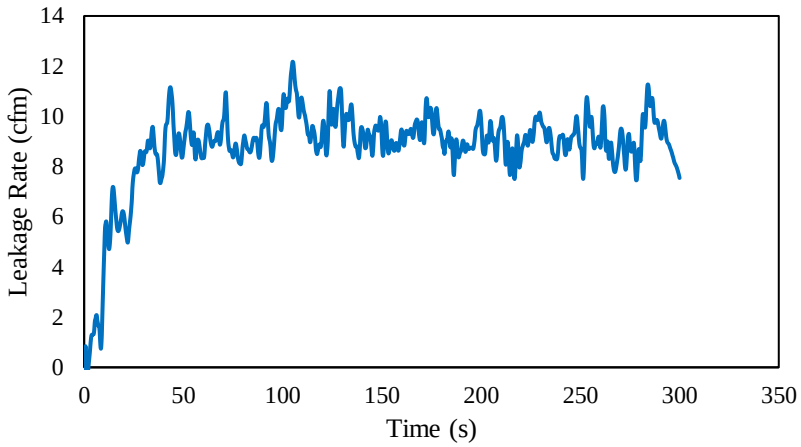

Figure 6.6 Simulated ULD leakage rate.

flow rate, which when summed together, determined the ULD leakage rate. The leakage rate was graphed versus time in Figure 6.6 to demonstrate how it changed throughout the simulation. The simulation was run multiple times until a leakage rate was found that was similar to the one from the experimental LLRM ULD. The final simulated test provided an average leakage rate of 8.78 cfm for the ULD model. The model was selected as this result was extremely close to the leakage rate from the experimental LLRM ULD which had a calculated value of 8.71 cfm.

6.2.2 Thermocouple Comparisons

Temperature was the principle metric for comparison between the FDS results and the experimental results. The FDS thermocouples placed in the ceiling of the ULD were compared to the experimental ULD ceiling thermocouples in Figure 6.7. The FDS thermocouples, shown in green profiles, increase almost at the exact same rate as the experimental thermocouples which are demonstrated in the blue profiles. The simulated thermocouple tree inside of the ULD was compared with the ULD experimental thermocouple tree in Figure 6.8. The results show two modes increase similarly, however, at the end of the test, the FDS simulates the thermocouple temperatures to be around 5 °C higher.

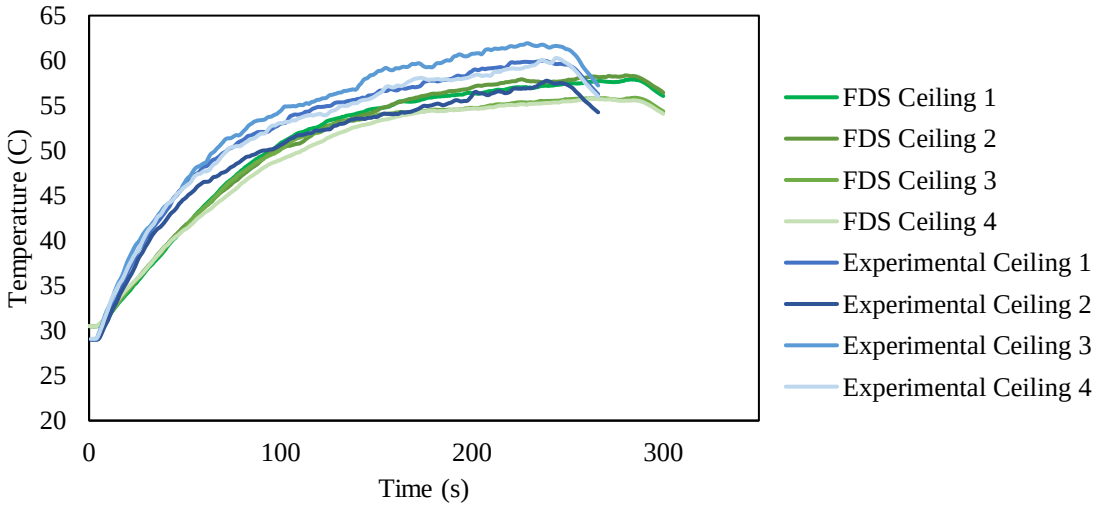

Figure 6.7 FDS versus experimental - Thermocouple comparisons – ULD ceiling

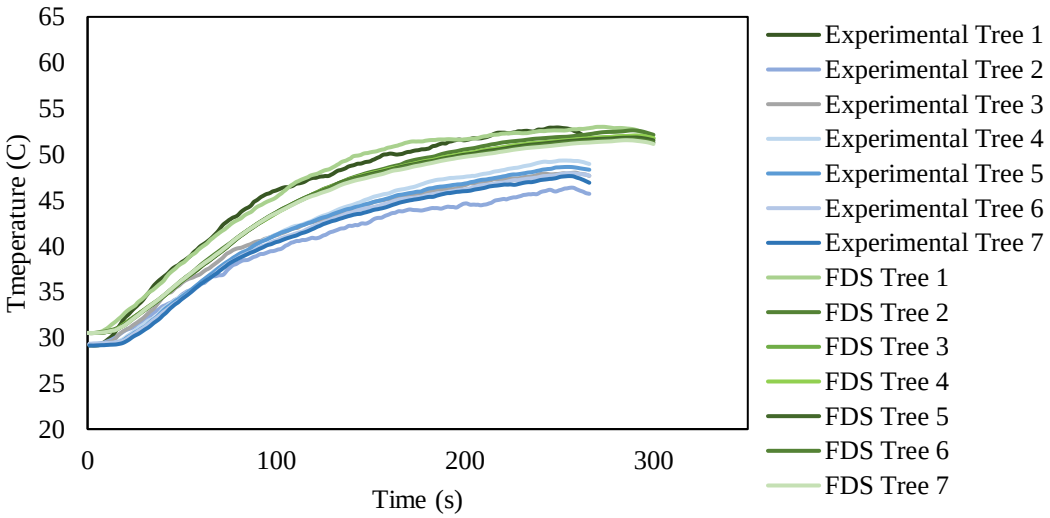

Figure 6.8 FDS versus experimental - Thermocouple comparisons – ULD thermocouple tree

The cargo compartment temperatures were compared next to examine the model's ability to predict temperatures further away from the fire source. The FDS and experimental thermocouples on the ceiling of the cargo compartment were compared in Figure 6.9. Only the row closest to the ULD was compared in this graph to minimize excessive comparisons. The temperatures show the FDS results anticipate an overall

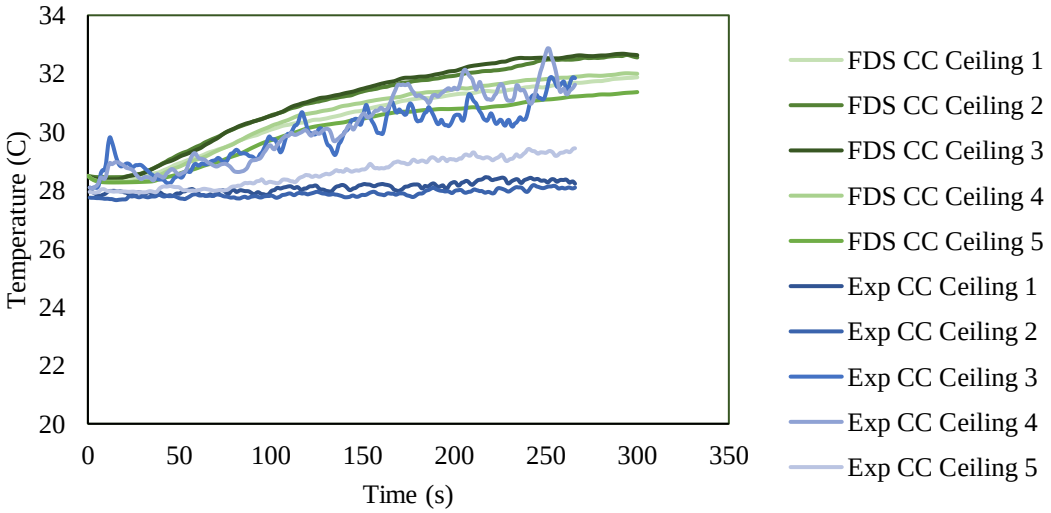

Figure 6.9 FDS versus experimental – Thermocouple comparisons – Cargo compartment ceiling.

higher temperature with the exception of two experimental ceiling thermocouples. Although the simulation produced a disparity in temperature readings, the magnitude of their differences is low.

The cargo compartment thermocouple trees were the last temperatures to compare between the FDS and the experimental results. The correlation between the two modes is shown in Figure 6.10. The predicted and experimental temperatures prove to be almost identical, both ranging between 28 °C and 30 °C for the entire test. Overall, the temperature comparisons at the four separate places in the simulation and experimental tests indicated that the simulated predictions forecasted extremely similar results to the experimental results.

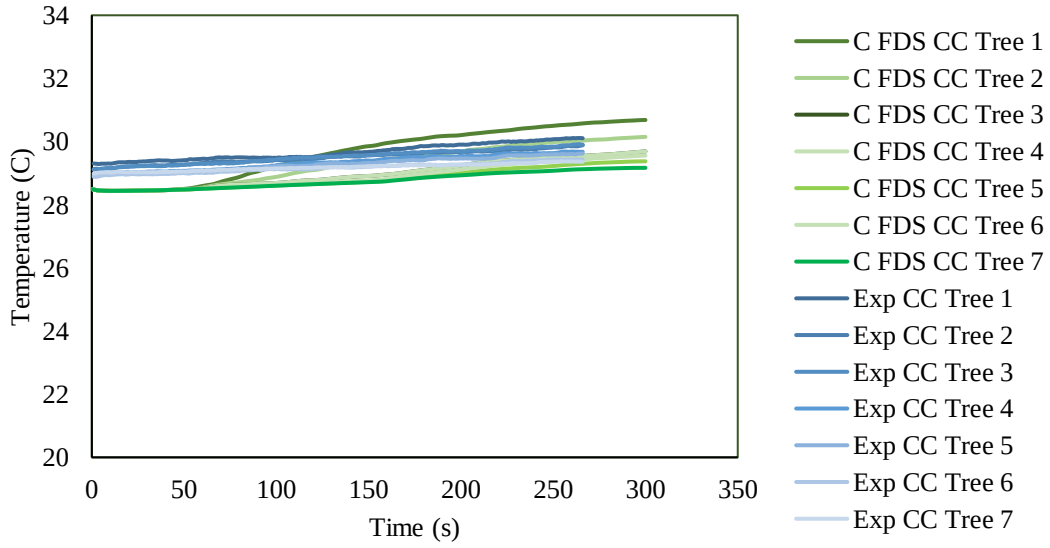

Figure 6.10 FDS versus experimental – Thermocouple comparisons – Cargo compartment thermocouple tree

6.2.3 Light Obscuration Comparisons

The light obscuration in the ULD from the FDS and experimental results are shown in Figure 6.11. The FDS over-predicts the light obscuration early on, but overall, the trend between the FDS and experimental light obscuration is good. The two light obscurations

have extremely similar slopes from 50 seconds to 150 seconds before the experimental profile provides a light obscuration reading slightly higher than the FDS predictions. The overall estimation of the light obscuration was found to be adequate. The cargo compartment light obscuration was nonexistent in the experimental testing, thus, comparison between the FDS light obscuration was deemed irrelevant.

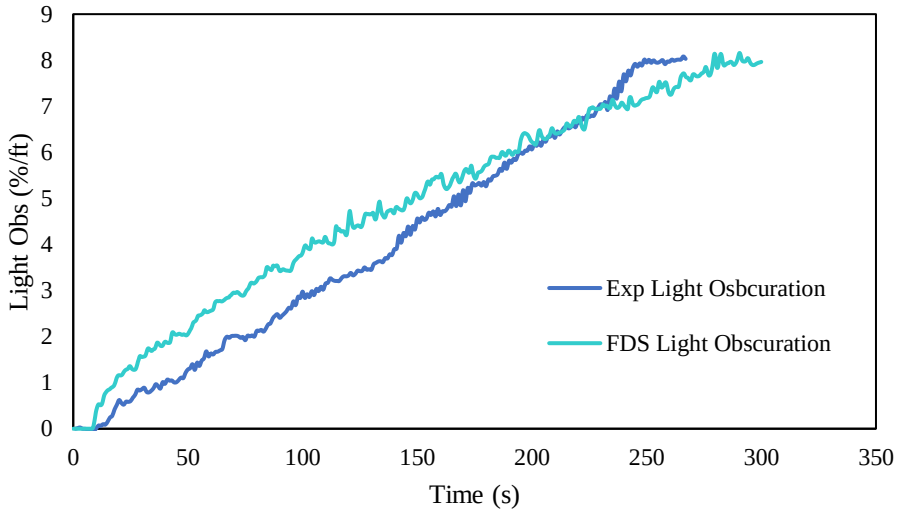

Figure 6.11 FDS versus experimental – Light obscuration comparisons - ULD

6.2.4 Gas Comparisons

The experimental gas analyzers were compared with simulated gas detectors to determine the model's accuracy in estimating gas concentration. The relationship inside the ULD between the experimental CO_2 gas analyzer and the simulated CO_2 gas detector results are displayed in Figure 6.12. The two profiles appear to have similar gas concentration levels for the first half of the test, but towards the second half of the test the FDS estimations begin to have a smaller rate of increase in comparison to the experimental results. There was good correlation between the FDS and experimental results in the beginning of the test. However, towards the end of the tests, the variation between the gas concentration levels and light obscuration levels simulated in the ULD versus in the experimental tests can be reasoned by the placement of the leakage rate holes. Although the FDS leakage rate value was extremely similar to the experimental leakage rate, the exact placement of the FDS holes were not identical to the experimental hole locations. Locating the placement of all the small gaps in the experimental ULD edges and corners

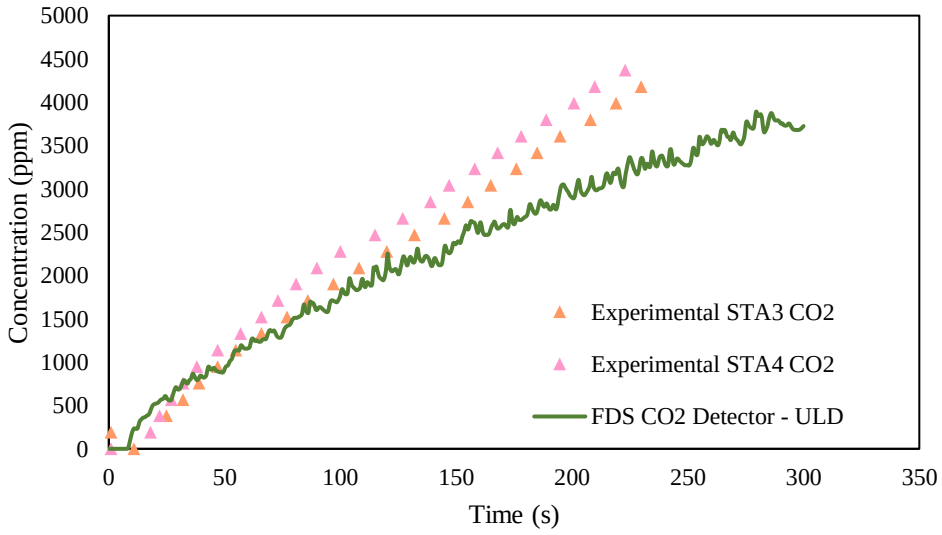

Figure 6.12 FDS versus experimental – CO_2 comparison - ULD

would be nearly impossible, thus, the single FDS hole shown in Figure 6.2 was deemed adequate for this estimation.

The CO concentration levels in the ULD between the FDS predictions and experimental results are demonstrated in Figure 6.13. The FDS results estimated the CO concentration to be much lower than the experimental gas analyzer, however, due to a significantly low amount of data points and concentration levels, advanced analysis cannot be completed. Low levels of CO_2 and CO in the cargo compartment were found in the experimental testing, thus, gas comparison between the FDS and experimental results were not performed.

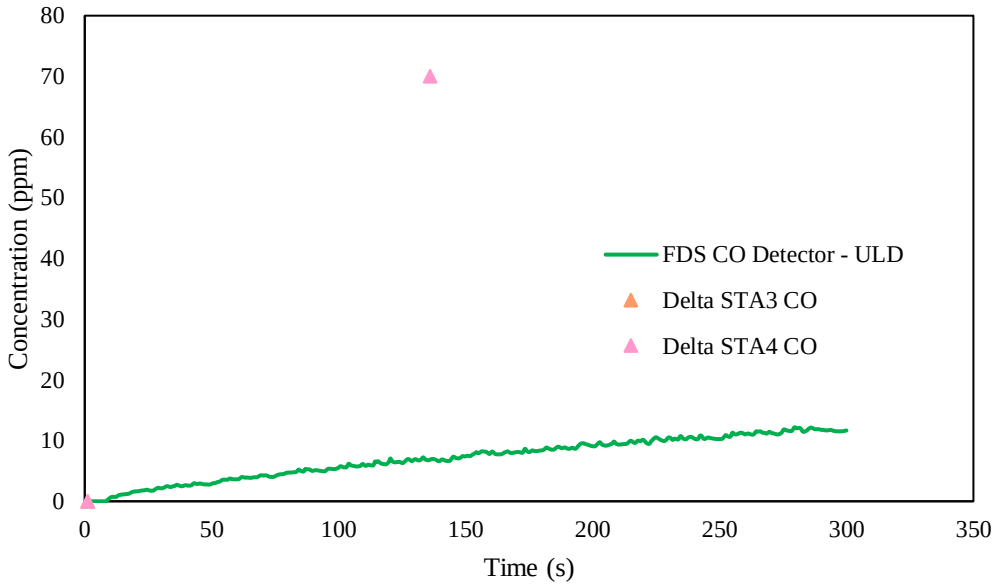

Figure 6.13. FDS versus experimental – CO comparison - ULD

The model proved to be capable of simulating temperature, light obscuration, leakage rate, and gas concentration conditions found in both the ULD and cargo compartment. Primarily, the FDS results compared relatively well to the experimental results, suggesting the model has the ability to predict realistic fire characteristics.

Chapter 7: Conclusions and Future Work

7.1 Conclusions

The safety of humans and cargo on-board aircrafts is a top priority, thus, fast fire detection activation times inside aircraft cargo compartments is particularly essential. Current guidelines describing aircraft smoke detection requirements lack detail and quantitative constraints. The use of ULDs also provide an issue with prompt activation times as the walls act as fire resistant barriers and encapsulate the growing smoke.

This phase of research was a continuation of the analysis of fire detection in cargo compartments in commercial aircraft. The previous phase, conducted by Chin, found ASSD systems yielded good correlation with the light obscuration levels in the cargo compartment. The end of the first phase of experimentation showed there was a need for comparative testing between fire detection in ULDs and cargo compartments. This report, being the second phase of the experimental research, focused on determining a detector technology and location which could cultivate the shortest response time to a wide assortment of fire sources. The effect of ULD leakage rate was also of interest during experimentation. A series of experimental tests were conducted to accurately select the fire detection technology with the best results. To check the results, an FDS model was created and the results between the simulated and experimental outputs were compared.

The first array of analysis concentrated on comparing the smoke characteristics and detector activation times in the ULD and the cargo compartment. The results found smoldering fires have an average activation time difference of 364 seconds for the ASSD detector and 322 seconds for the wireless detector. However, the fuel source did not always generate enough smoke to activate either type of detectors in the cargo

compartment, thus the cargo compartment detectors did not activate for every test. Flaming fire tests showed neither cargo compartment detector activated for either flaming fuel while the ULD detectors activated at about the same time for either fuel. These findings suggest the detector with the shortest response time should be located in the ULD where the fire originates.

The second portion of the analysis was directed to the fire detection technologies inside of the ULD, as this location was found to be more suitable for quick activation times. Overall, the wireless detector outperformed the ASSD and ASGD detectors for five out of the eight tests. The results suggest the wireless detection technology has on average the quickest activation time when tested against a variety of fuels, with the exception of the battery test. However, it should be noted each detector was set to unique thresholds by their manufacturer. These thresholds can be varied by detector type and manufacturer setting, meaning although the wireless detector outperformed the ASSD and ASGD in these experimental tests, the latter could outperform the wireless detector technology if their thresholds were more reduced. Although not compared with the three manufactured fire detectors discussed above, the Blue + IR wavelength detector proved to correlate well with the light obscuration levels.

Gas analysis was performed and showed the CO_2 concentration was detected at much greater levels than the CO in the ULD. The results also demonstrated the CO_2 rate of rise was much greater the CO rate of rise, for all but one test. Both gas evaluation findings suggest, if considering a gas detector in an aircraft, a CO2 detector may yield faster activation times.

The impact of a ULD's leakage rate was observed. The cargo compartment was expected to have a greater light obscuration level with the LLRM ULD and a lower light obscuration level with the SLRM as less smoke would escape, however, the expected pattern was not present in eight out of nine of the tests. The ULD was hypothesized to have the opposite correlation, i.e. a greater light obscuration should occur with the SLRM ULD and a lower light obscuration with the LLRM ULD as this would allow for smoke to escape the container, decreasing the overall smoke density. This expected trend also was not presented in eight out of nine of the tests. While the expected trends were not evident, the likely reason for this behavior is the difficulty in obtaining repeatability of fire signatures from the same fuel sources despite having a detailed test protocol.

The FDS results were compared to the experimental results and showed there was a fair amount correlation between the simulated and experimental temperatures, light obscurations, and gas concentration levels. Differences among the results can be reasoned by the set-up of the ULD leakage rate holes. The results from the FDS model provide a justifiable proof of concept.

With understanding of the main objective and experimental and simulated results, it can be concluded that the detector location with the shortest activation time is inside of the ULD. Within the ULD, out of the manufactured detectors tested, the wireless detector outperformed both air sampling detectors, however, the results could vary if threshold levels were more restrictive.

7.2 Future Research

Future analysis on this research area should first conduct similar tests as the ones performed in this report to verify and confirm the results. During experimental testing, it

was found that several of the wireless output results may have not truly represented the activation time due to the potential of soot build-up from past tests. Thus, future testing should implement rules on replacing the wireless detectors on a systematic basis, at least daily. As recognized earlier, the wireless detector technology showed to outperform the other detector technology, thus, more testing on wireless detectors in aircrafts should be done. Specifically, more research should be done on the robustness, durability, battery life span, and communication network of the wireless detector when inside of a ULD.

ASGD systems were placed in the ULD and ASGD, however, a CO_2 detector was not part of the system due to shipping issues. It would be extremely beneficial to include a CO_2 detector in the next array of testing as this report found CO_2 levels to be much higher than CO levels which were measured by the ASGD.

Nuisance source testing was not a main objective during experimentation. Minimal testing was conducted using talcum powder and humidifiers, but the results were insufficient and inconclusive. Reproducible nuisance source testing would be an imperative aspect of the next phase of research, as this issue is very common in aircrafts. In order to identify a relevant set of sources for nuisance testing, having information on the range in variations in the ambient environment of cargo compartments of commercial aircraft is essential

With future simulated predictions, it may be advantageous for the FDS model to include all three leakage rate models to observe if the computer program could verify the expected trend. With respect to the lack of patterns found with the leakage rate analysis, finding sources overall that could generate reproducible smoke characteristics would be generally most desired. The FDS model created in this project should be redesigned with

various levels of smaller grid spacing to create more accurate results. With smaller grid spacing, more realistic FDS modeling should be done and then compared with the experimental results. In particular, explore the effects of additional ULDs in the cargo compartment and the consequences of extra material in the ULD.

Largely, there is a necessity to quantitatively standardize fire detection systems in aircraft cargo compartments. The well-being of aircraft passengers and cargo relies on future regulations that will expand the current detection testing restrictions.

Appendix A

Test Matrix:

Source/Location	SLRM	MLRM	LLRM
Heptane	• 200 mm diameter pool fires burned 4” off the ground • 20 mL of heptane • Ignited via lighter and test run until flame ceases		
PU Foam (flaming)	• 3.0 by 3.0 by 2.0 in. burned 4” off the ground, near 100 g of foam • Bottom and sides wrapped in aluminum foil • Use of 4 mL of heptane to assist ignition (poured in corner) • Ignite corner • Test run until flame ceases		
PU Foam (smoldering)	• 100 g of foam, cut into pieces varying near 1 x 1 x 1.5 inches • Placed inside of an aluminum foil constructed open box • Smoldering induced via 13” tall hot plate at a constant temperature ranging between 400-600 °F • Test run until the detectors alarm at Fire 1		
Suitcase (soft) (whole suitcase)	• Entire suitcase standing up, filled with 10 cotton XL cotton t-shirts • Smoldering induced via electric charcoal starter at 550 W • Test run until the cargo compartment ASGD and both wired and wireless smoke detectors alarm at Fire 1		
Shredded Paper	• Paper strips approximately 6 – 10 mm in width by 25.4 – 102 mm in length • Shredded paper provided by FAA, which consisted of a mix of 20 lb paper and cardstock • 42.6 g (1.5 oz) tamped down in a 1’ tall metal tube with 1”x1” flue space in the center. Tube was enclosed with wire mesh on bottom. • Tube was placed on a 11.75” high ring stand and ignited via an 8” Bunsen burner with an approximate 6” flame. • Test terminated more than 4 minutes after ignition		
Wood	• 100 g of hickory wood chips • Smoldering induced via 13” tall propane burner at a constant temperature ranging between 400-600 °F		

	• Test run until the detectors alarm at Fire 1 or until more than 20 minutes have passed
Baled Cotton	• 15 g of cotton • Smoldering induced via 13” tall hot plate at a constant temperature ranging between 400-600 °F • Test run until the detectors alarm at Fire 1 or until more than 15 minutes have passed
Lithium Ion Battery	• Place four Lithium Ion Batteries together inside of sealed pipe cage with a single hole at the top • Use a cartridge heater to force thermal runaway
Boeing smoke generator	• Corona Smoke Fluid 135 and CO_2 is supplied • 4 chimney heaters • Position: 68” from the rear doors and 48” from the side wall
Humidifier	• Release water humidifier into air for 30 minutes until ULD reaches a light obscuration below 60%
Baby Powder	• 100 g of baby powder • Fan inserted inside of ULD with direction of airflow facing towards powder • Run test until light obscuration meters observe a reading below 60%/ft

Appendix B

Before Testing Checklist:

#	Equipment Checklist	Location/*Type* (number)	How to check/Turn on	Checked?
1	Wireless Detectors	Inside ULD Inside cargo compartment	1. Check for flashing green light on home base, if flashing the system is ready	
2	Blue/IR Detector	Inside ULD	1. Turn on using outlet power button inside of cargo compartment 2. Check DAQ system for accurate ambient voltage readings.	
3	ULD Lights	Inside ULD	1. Turn on with back switch, turn to brightest mode 2. Charge every 4 hours if not plugged in	
4	Go Pros	Inside cargo compartment (1) Inside ULD (1)	1. Turn on TV screens 2. Flip power switch outside of cargo compartment (connected to orange cord) 3. Turn on Go Pros inside of cargo compartment and ULD, turn on Wi-Fi (use phone to activate Wi-Fi and recording)	
5	Whittaker Detector	Inside cargo compartment	Turn on Whittaker Detector: 1. turn on dual range DC power supply 2. Go to gray box on the ground: a. flip on red switch b. flip on detector switch	

			c. flip on pretest light switch (check the screen to see it on, then turn off before testing begins)	
6	FLIR	Inside cargo compartment	1. Turn on NOT EDMUNDS box next to it. 2. Follow directions on test procedure list to turn on/record	
7	Smoke Meters (1 hour warm up period)	Inside of ULD *New (USB) smoke meters (2)* *Old smoke meters (2)* Inside Cargo Compartment *New (USB) smoke meters (2)*	To turn on: OLD LASERS: a. Turn on power supply (EDMUNDS box) b. turn on lasers (black box) c. Check the voltage of each smoke meter to make sure it is between 8-10 volts d. Check the lasers are working, go inside cargo compartment and ULD and run hand over beam (wear protective glasses) NEW LASERS: a. Turn on computer & open virtual link icon b. Click top device, connect to all c. Open Power Mac PC select 1 sensor and start data collection. Continue this until all 4 smoke meter sensors are open and start each data collection *TO BEGIN RECORDING CHECK TEST PROCEDURE LIST IF ERRORS on Power Max:	

			a. Open virtual link, click disconnect all, and close all windows of Power Max b. Go to USB port inside of cargo compartment and unplug back plugs (one blue and one black), wait several seconds and re-plug them c. Go back to computer and connect to all devices again	
8	Thermocouples	ULD tree (7) ULD ceiling (4) Cargo compartment tree (7) Cargo compartment ceiling (25)	1. Sign into PC and follow directions on test procedure list. 2. Open through MutliDAQ-->PortableDAQTestApp-->ULD file	
9	VESDA Sampling Ports	*CO2 detector* *CO detector* *Hydrogen detector*	VESDA Specialist oversaw set up of these detectors	
10	Gas Analyzers	Inside ULD (2) Inside Cargo Compartment (2)	1. Ask for assistance to turn on (must be trained) 2. Check the switch flow knobs, they should all be facing to the left (towards the ULD). Also make sure the top knobs are pointed in either the left or right direction towards bank A or B (ask to make sure they are not clogged) 3. Scroll on PC window all the way to the right to check that numbers appear	

Sample Test Data Template:

TEST #	
FUEL	
DATE	**__/___/20__**
TIME	

Engineers/Persons Involved:

Weather Record:

Temperature	**Humidity**	**Pressure**

Full Test Run (Yes/No, explain)

Notes:

Appendix C

Light Obscuration and Detector Activation Times

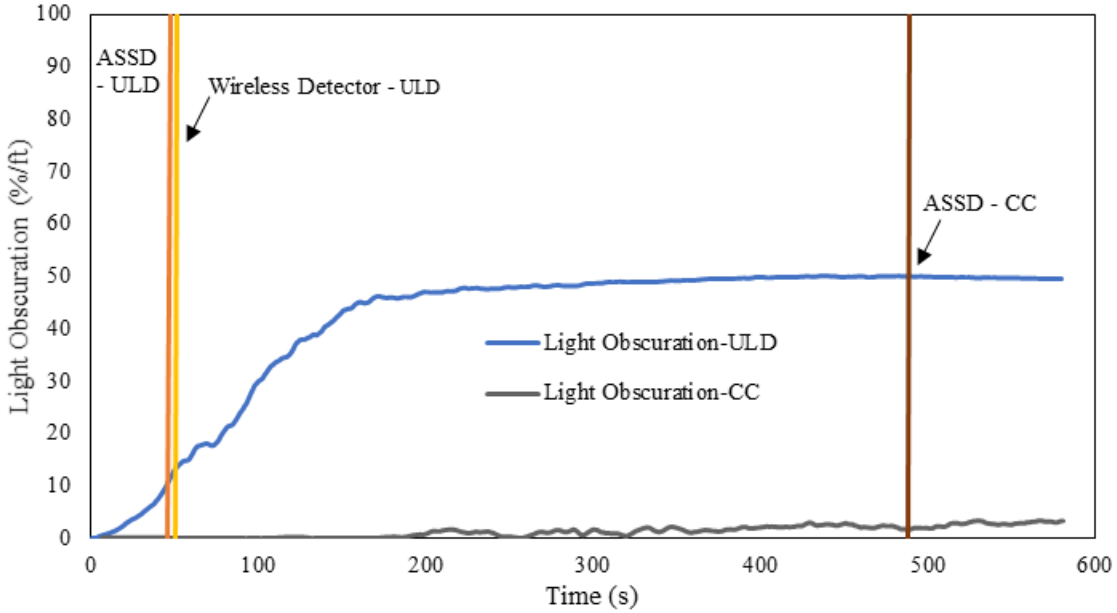

Figure A.1. Smoldering PU foam – MLRM - Light obscuration inside ULD and the cargo compartment versus detector activation.

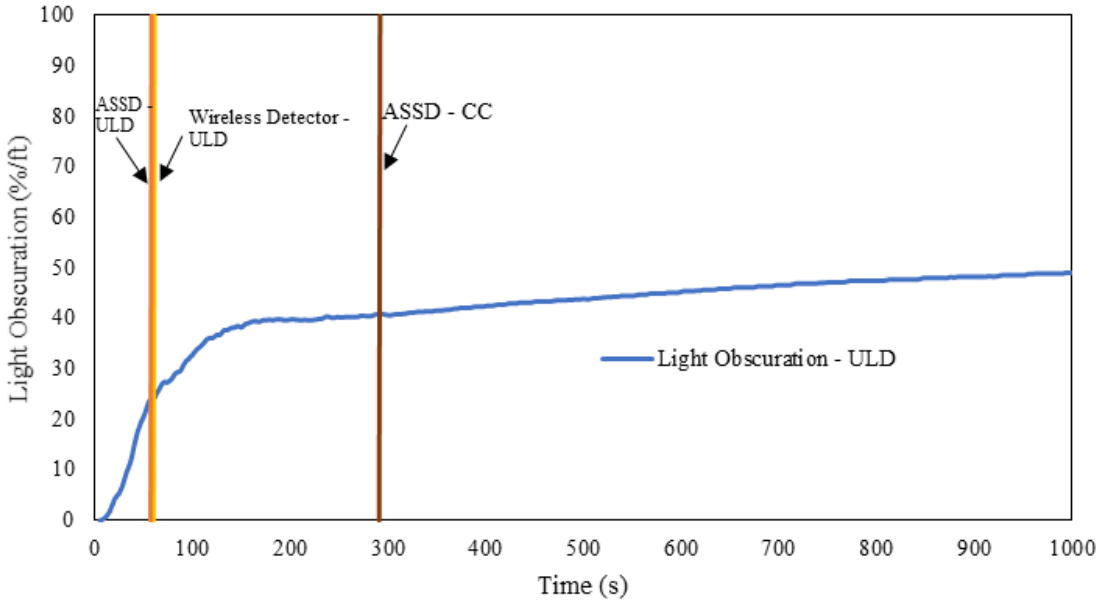

Figure A.2. Smoldering PU foam – SLRM - Light obscuration inside ULD and the cargo compartment versus detector activation.

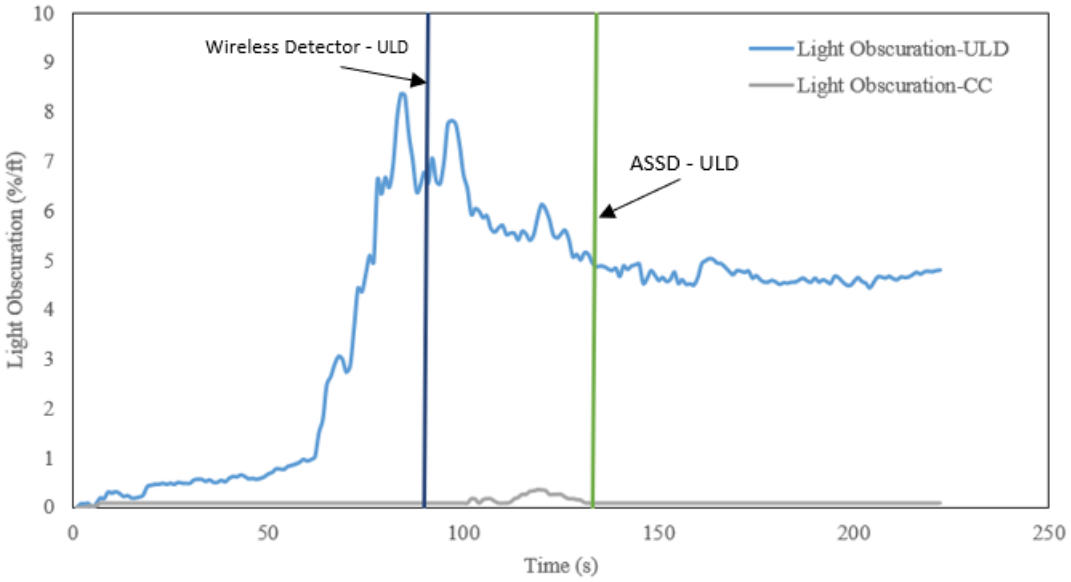

Figure A.3. Flaming PU – LLRM - Light obscuration inside ULD and the cargo compartment versus detector activation.

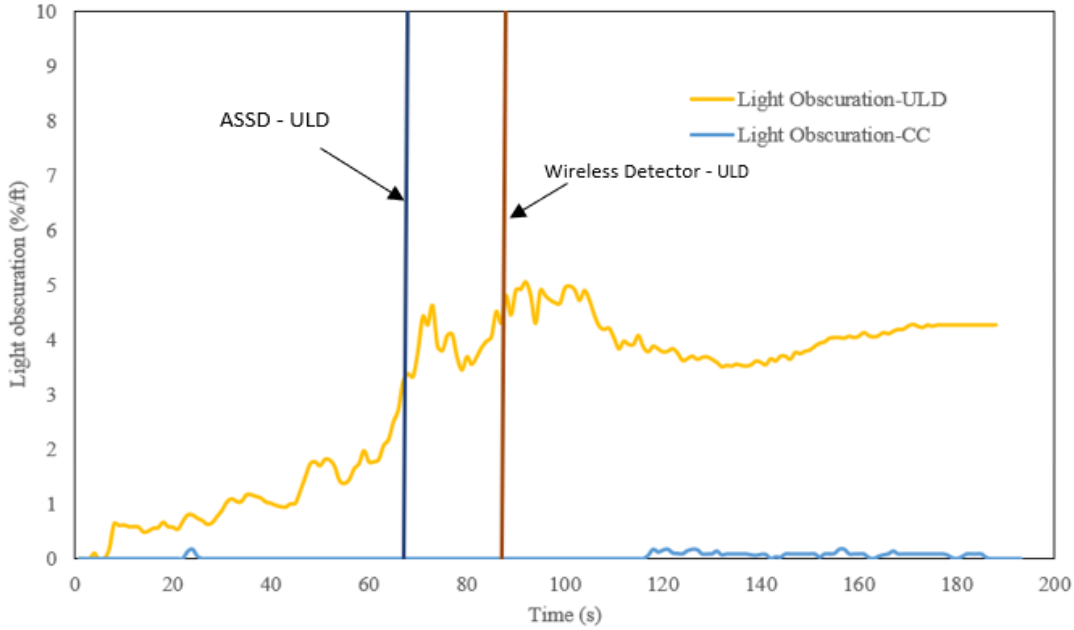

Figure A.4. Flaming PU – MLRM - Light obscuration inside ULD and the cargo compartment versus detector activation.

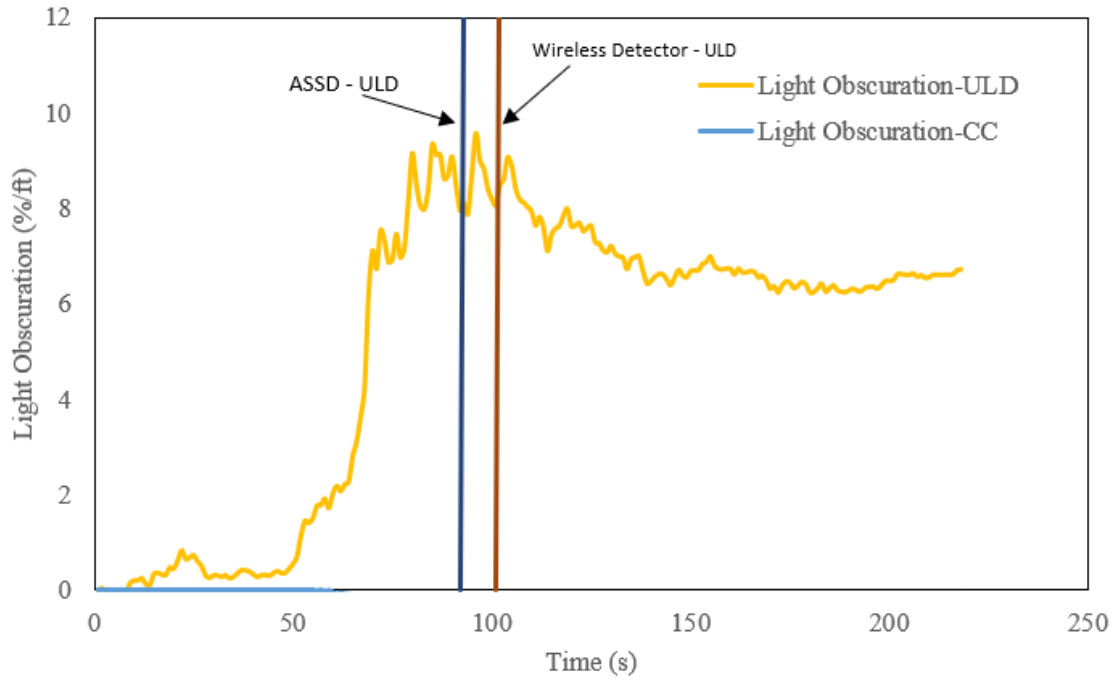

Figure A.5. Flaming PU – SLRM - Light obscuration inside ULD and the cargo compartment versus detector activation.

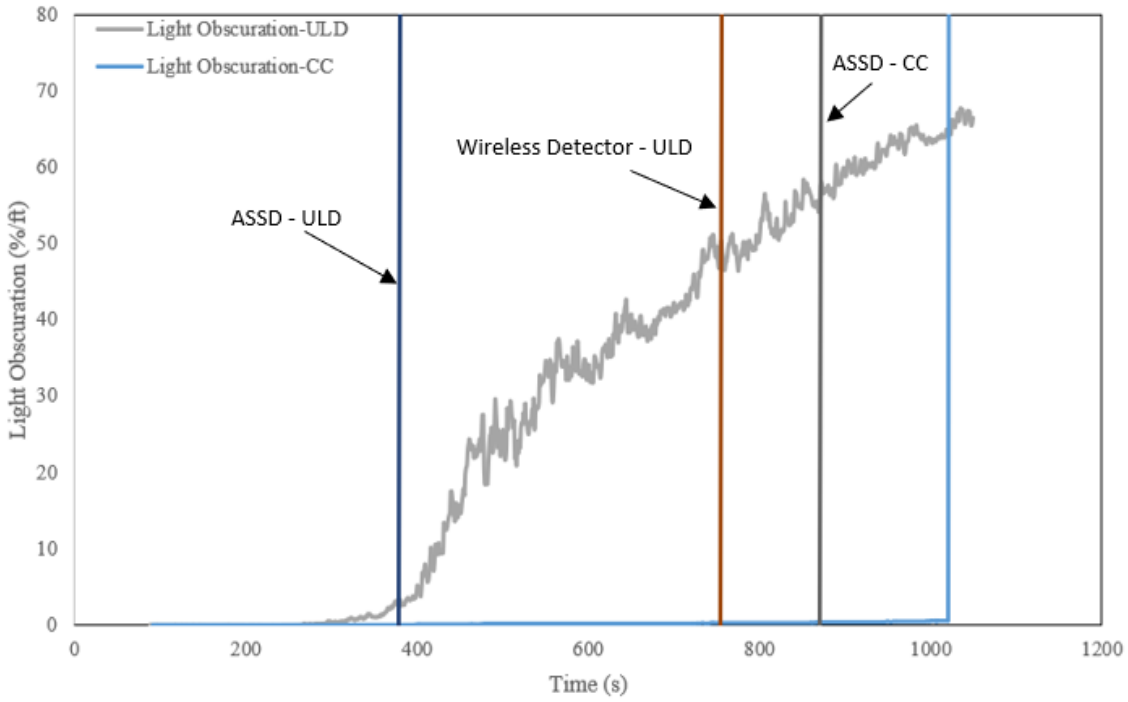

Figure A.6. Suitcase – MLRM - Light obscuration inside ULD and the cargo compartment versus detector activation.

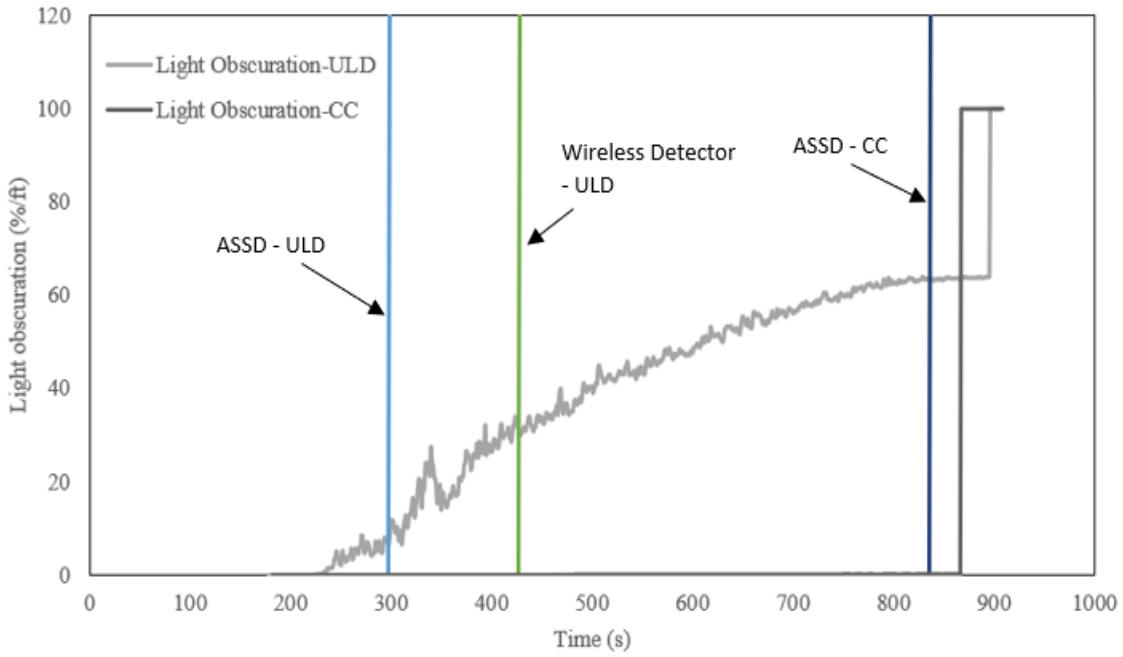

Figure A.7. Suitcase – SLRM - Light obscuration inside ULD and the cargo compartment versus detector activation.

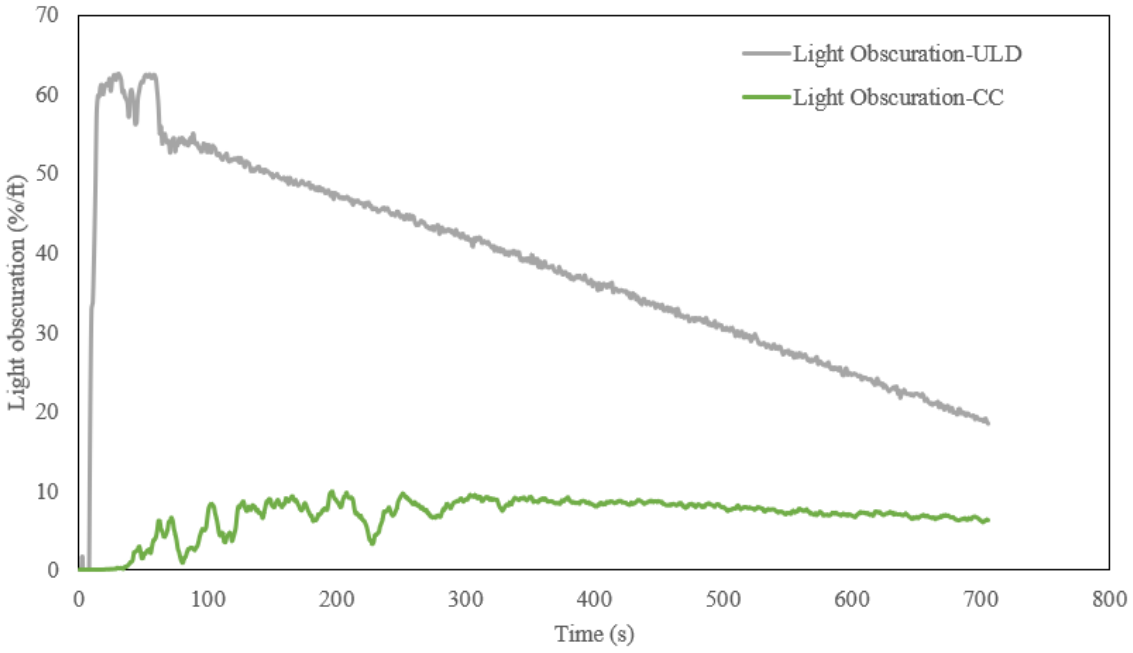

Figure A.8. Boeing Smoke Generator – LLRM - Light obscuration inside ULD and the cargo compartment versus detector activation. (No VEU/VEA Data)

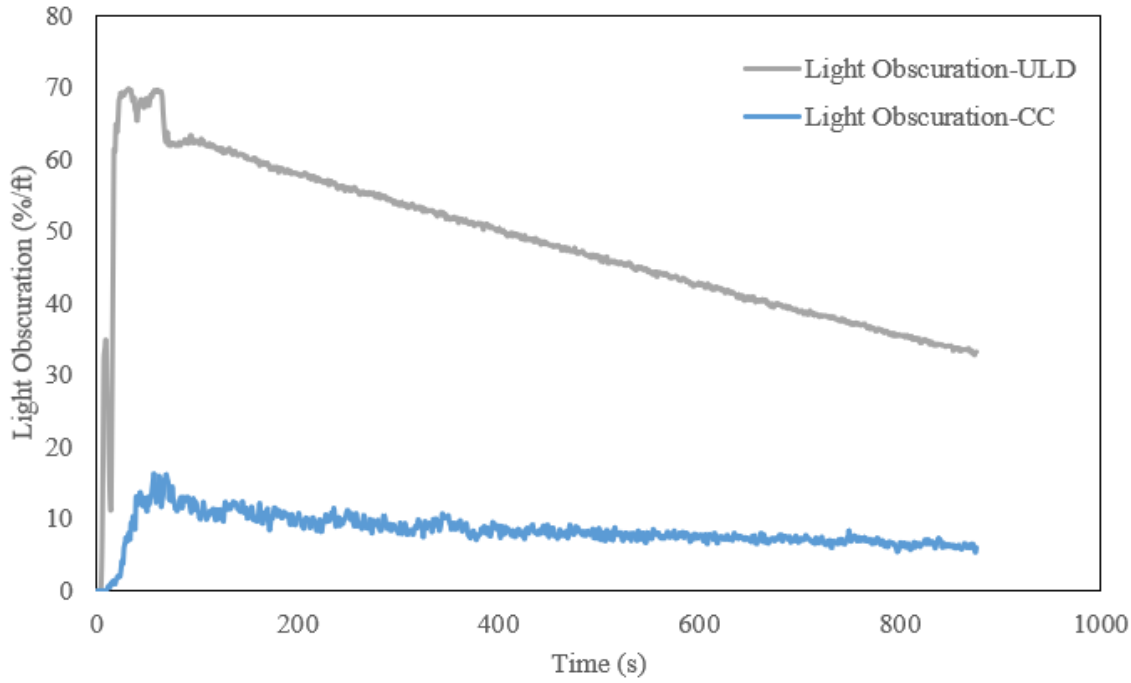

Figure A.9. Boeing Smoke Generator – MLRM - Light obscuration inside ULD and the cargo compartment versus detector activation. (No VEU/VEA Data)

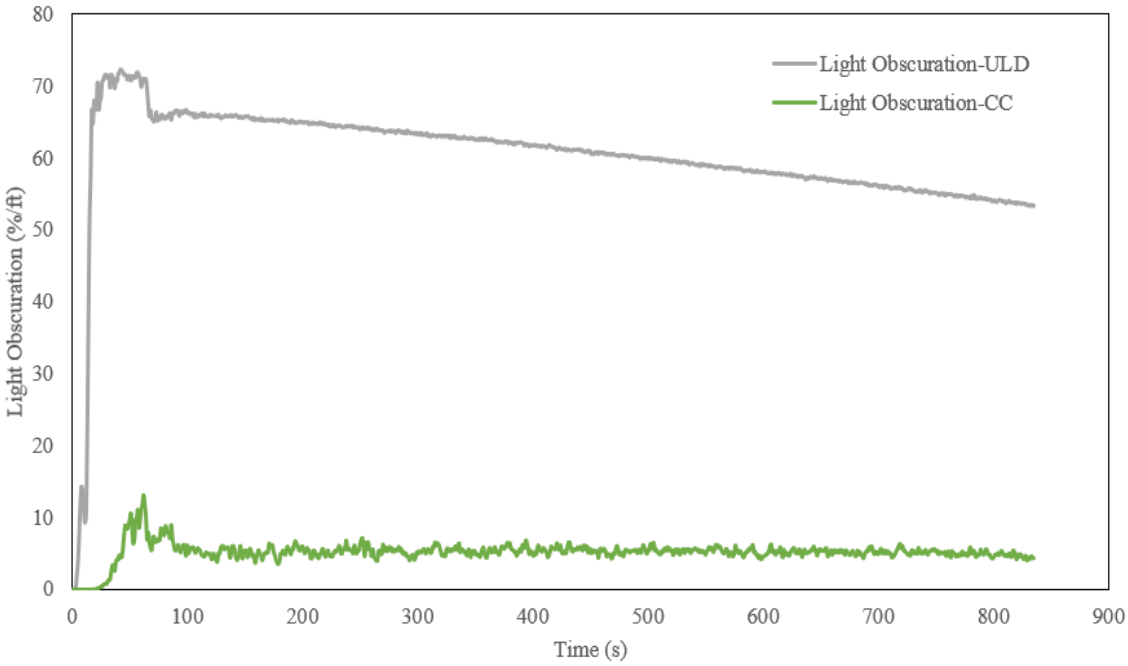

Figure A.10. Boeing Smoke Generator – SLRM - Light obscuration inside ULD and the cargo compartment versus detector activation. (No VEU/VEA Data)

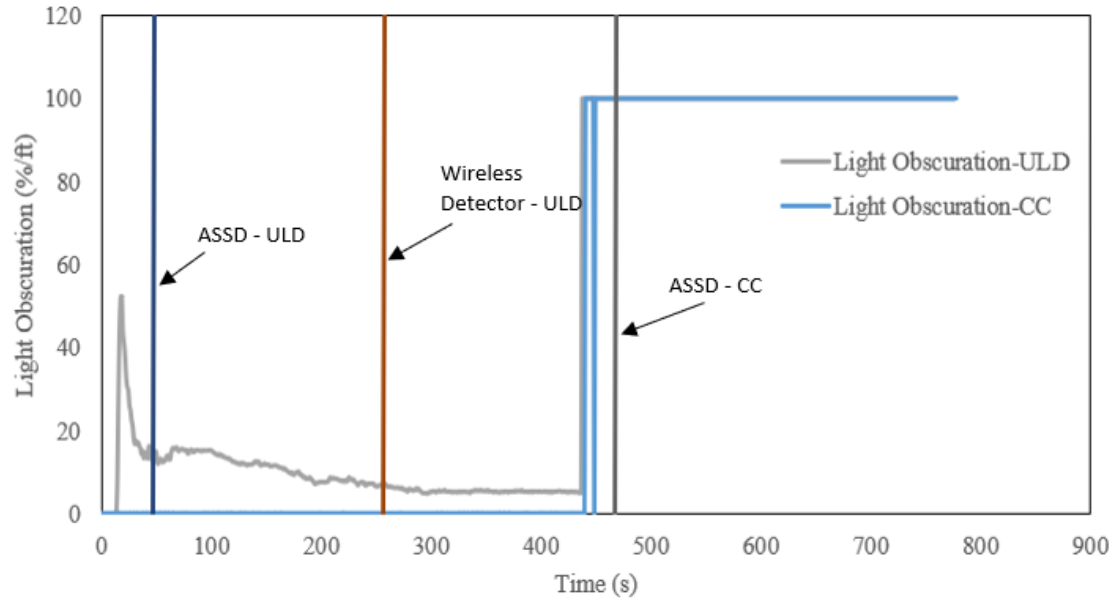

Figure A.11. Wires – LLRM - Light obscuration inside ULD and the cargo compartment versus detector activation.

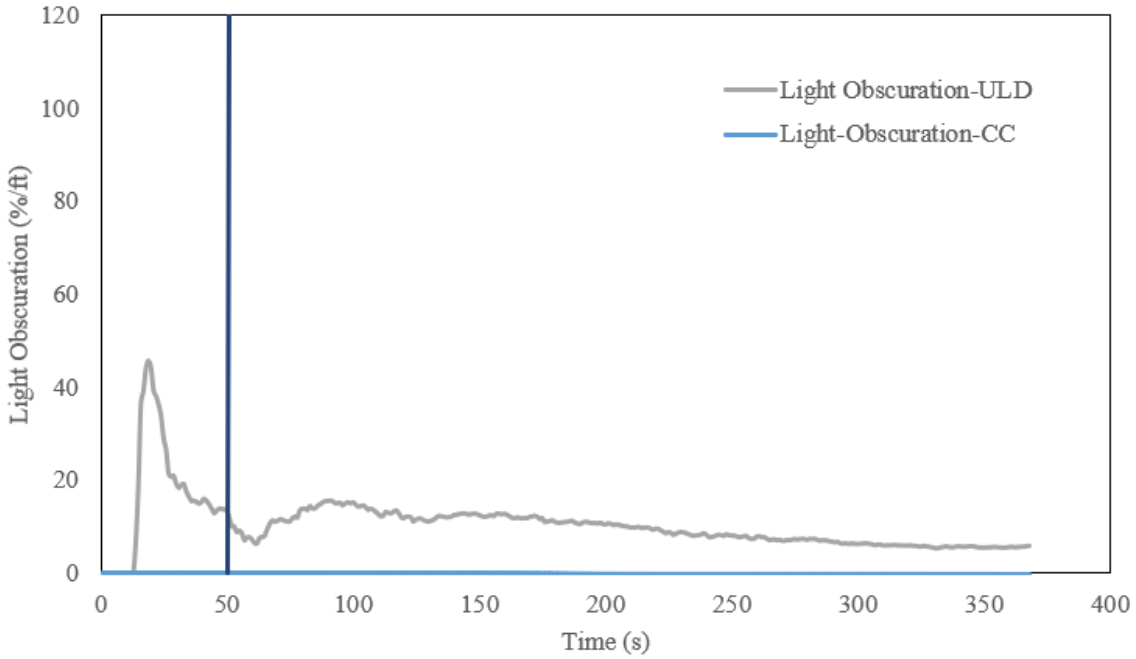

Figure A.12. Wires – MLRM - Light obscuration inside ULD and the cargo compartment versus detector activation.

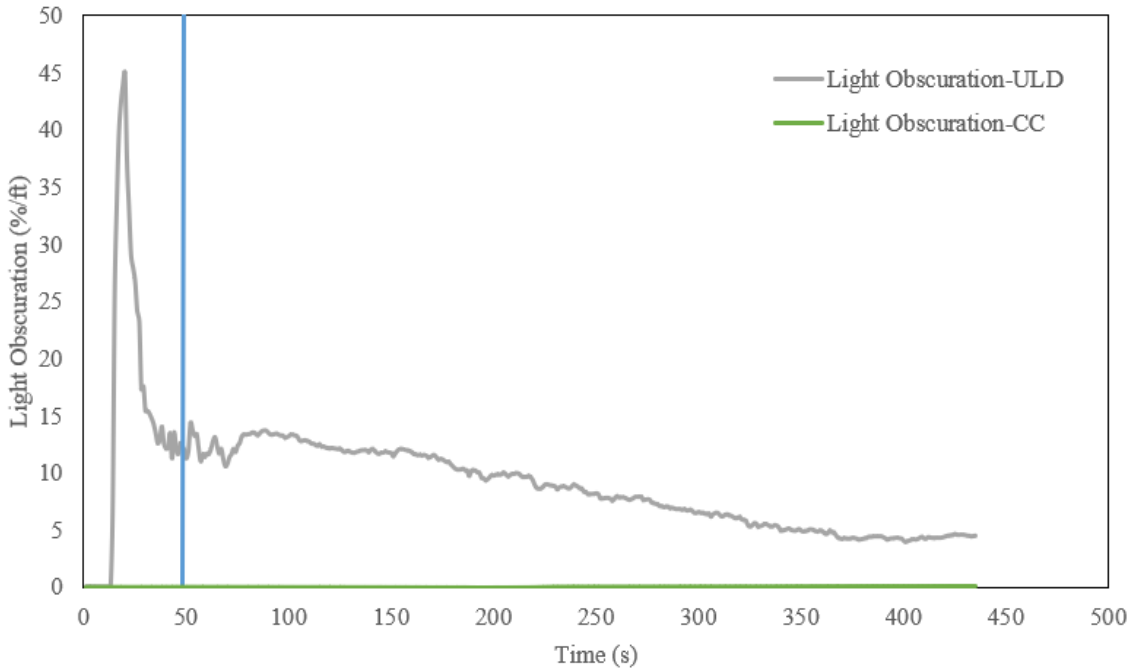

Figure A.13. Wires – SLRM - Light obscuration inside ULD and the cargo compartment versus detector activation.

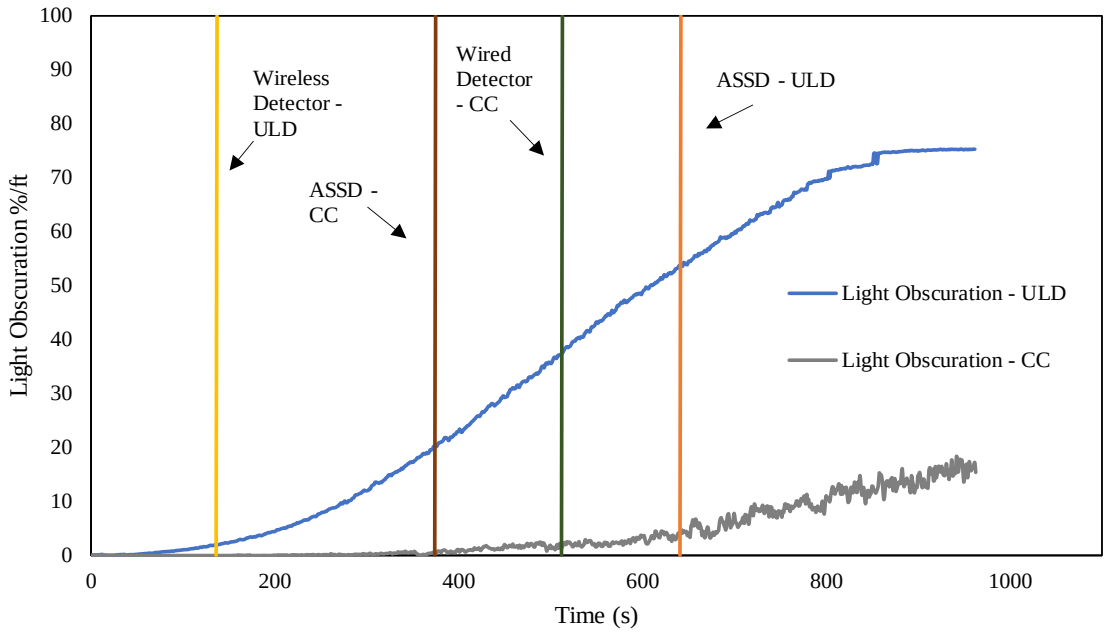

Figure A.14. Wood – LLRM - Light obscuration inside ULD and the cargo compartment versus detector activation.

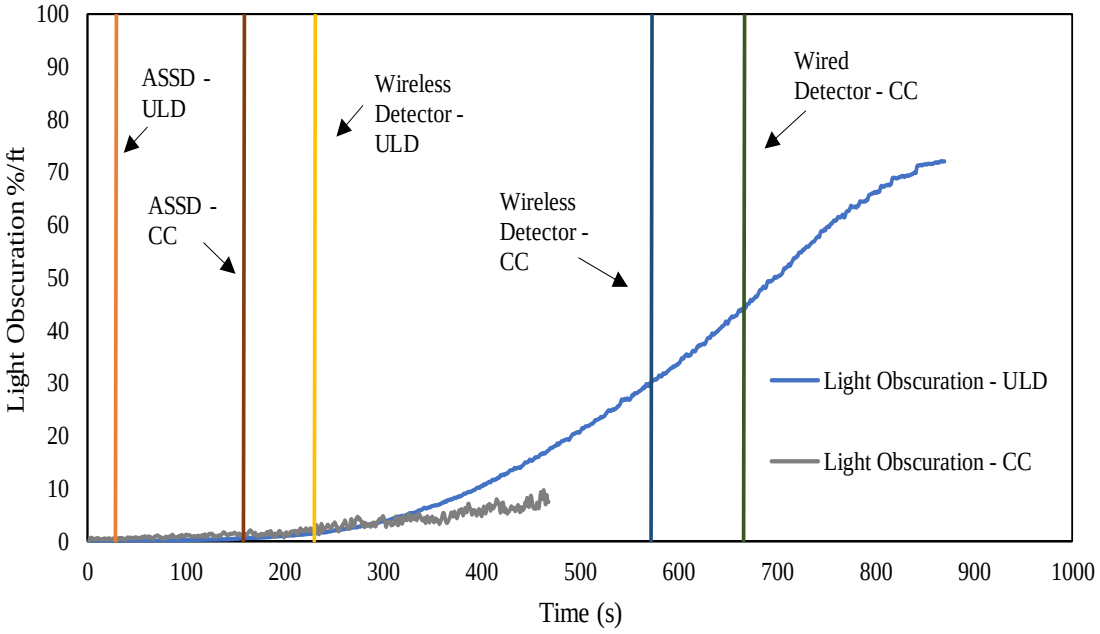

Figure A.15. Wood – MLRM - Light obscuration inside ULD and the cargo compartment versus detector activation.

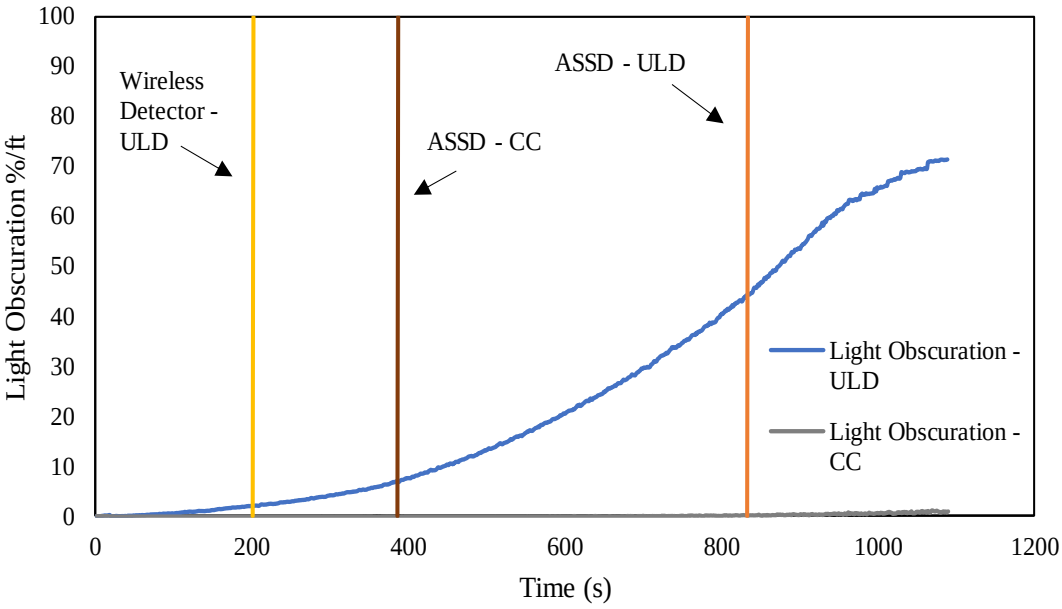

Figure A.16. Wood – SLRM - Light obscuration inside ULD and the cargo compartment versus detector activation.

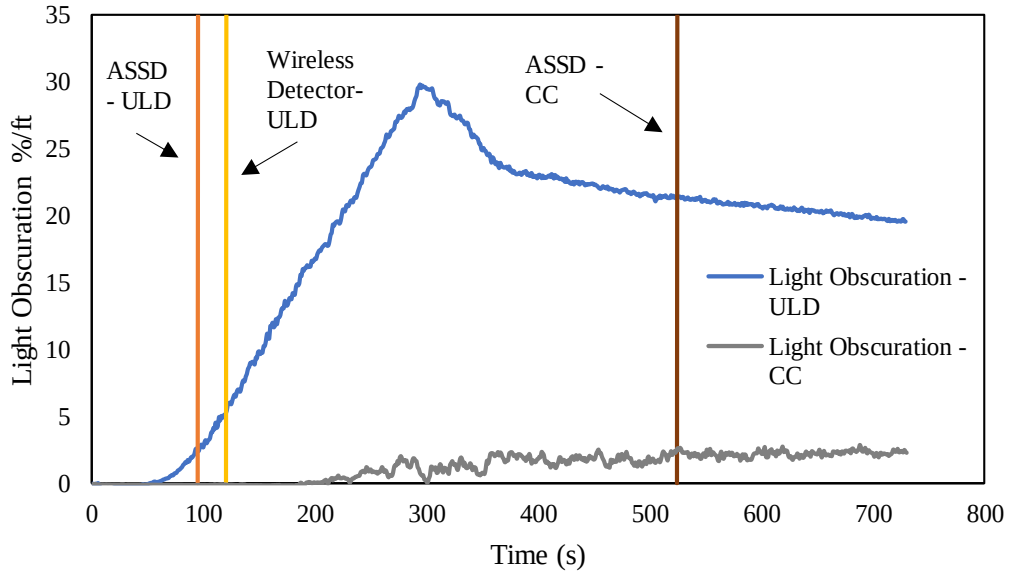

Figure A.17. Cotton – LLRM - Light obscuration inside ULD and the cargo compartment versus detector activation.

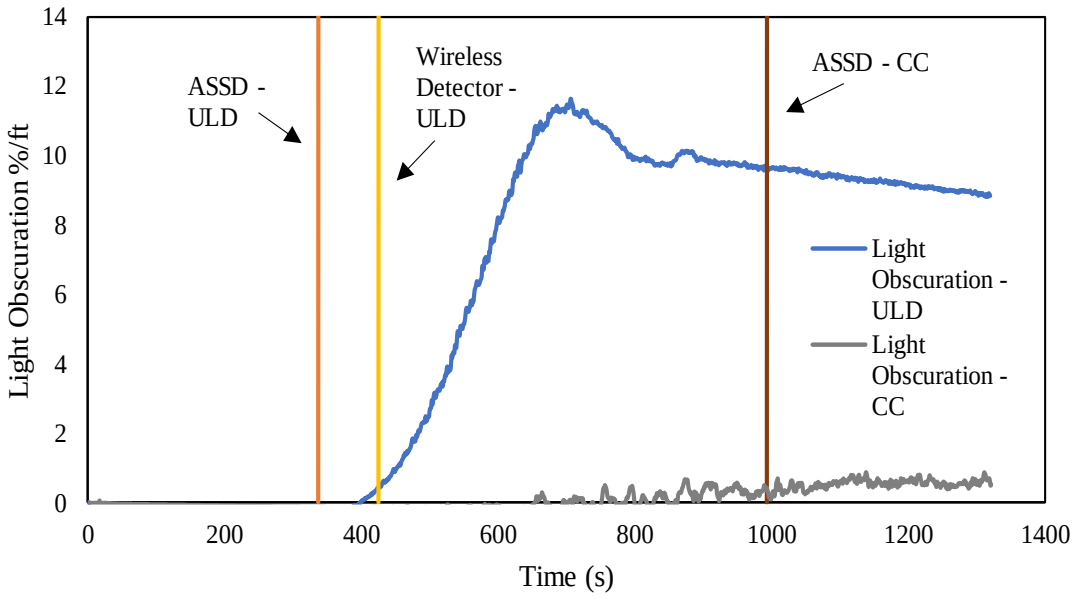

Figure A.18. Cotton – MLRM - Light obscuration inside ULD and the cargo compartment versus detector activation.

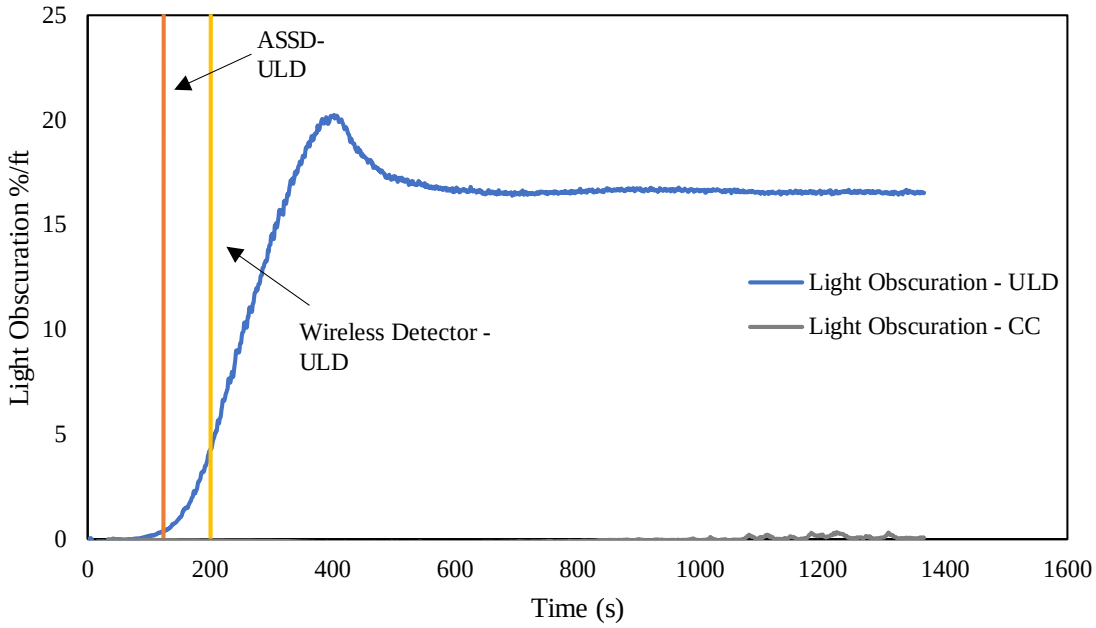

Figure A.19. Cotton – SLRM - Light obscuration inside ULD and the cargo compartment versus detector activation.

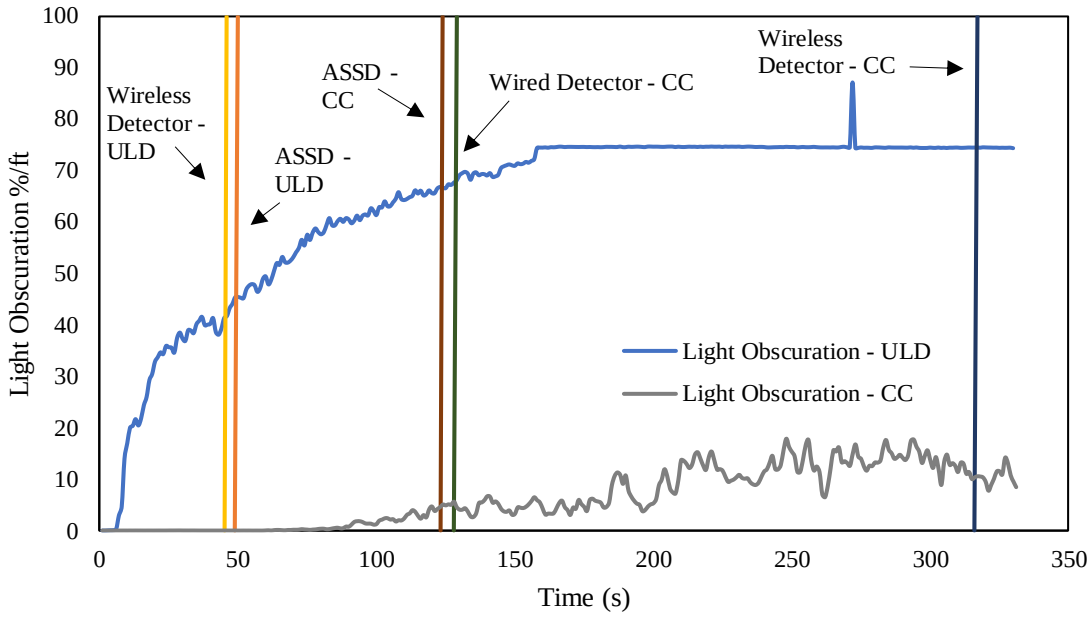

Figure A.20. Paper – LLRM - Light obscuration inside ULD and the cargo compartment versus detector activation.

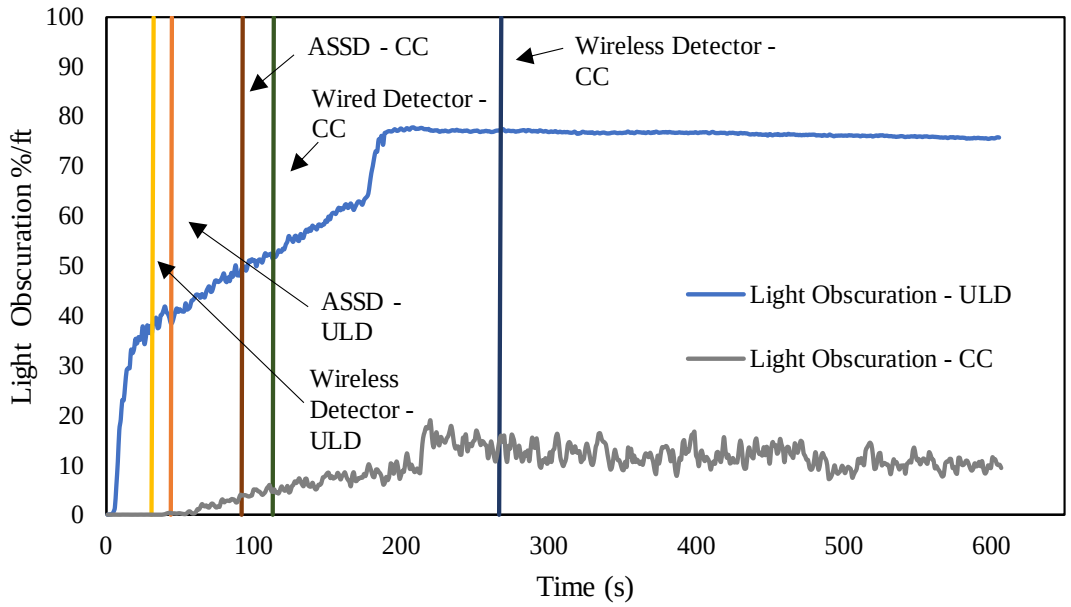

Figure A.21. Paper – MLRM - Light obscuration inside ULD and the cargo compartment versus detector activation.

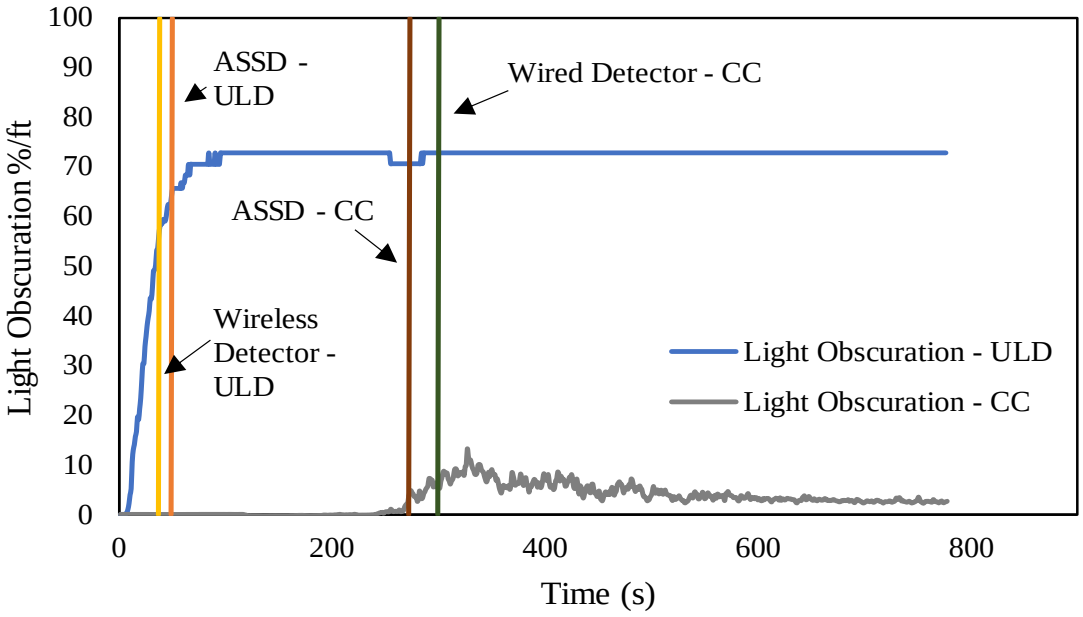

Figure A.22. Paper – SLRM - Light obscuration inside ULD and the cargo compartment versus detector activation.

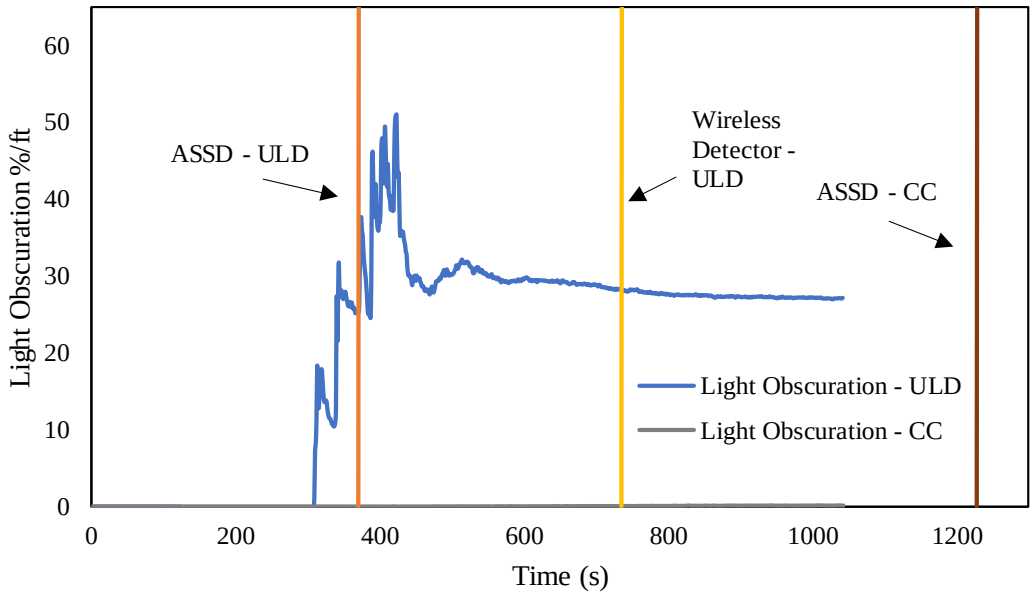

Figure A.23. Batteries – LLRM - Light obscuration inside ULD and the cargo compartment versus detector activation.

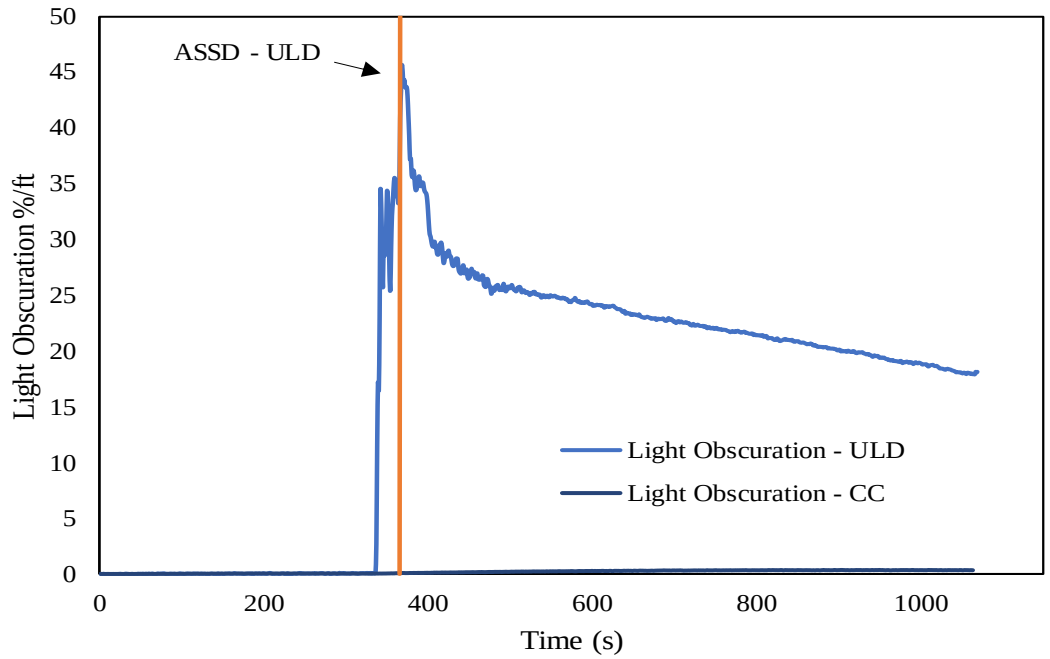

Figure A.24. Batteries – MLRM - Light obscuration inside ULD and the cargo compartment versus detector activation.

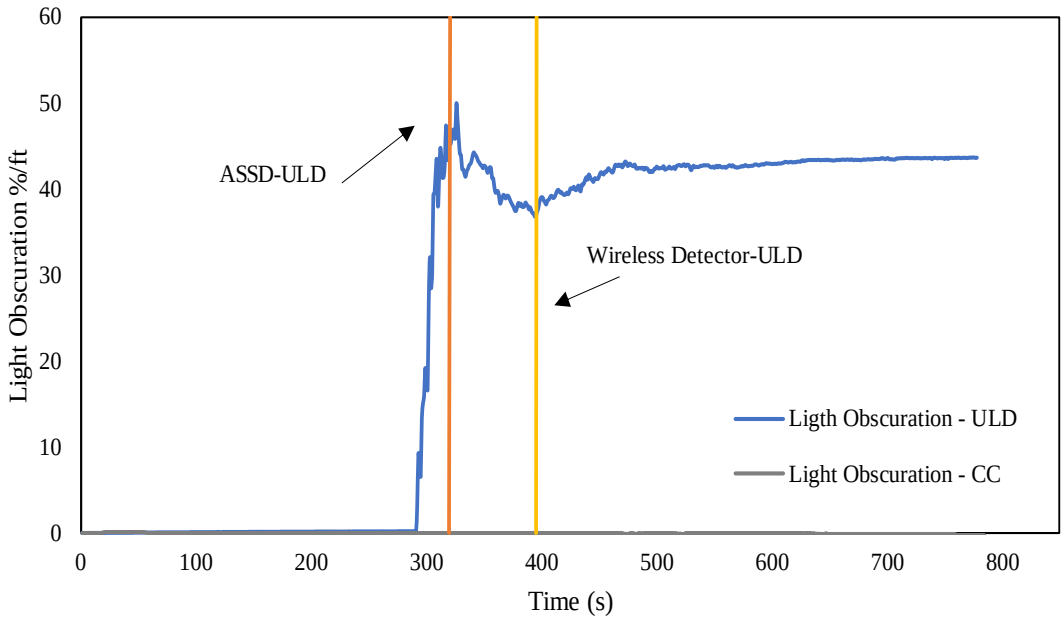

Figure A.25. Batteries – SLRM - Light obscuration inside ULD and the cargo compartment versus detector activation.

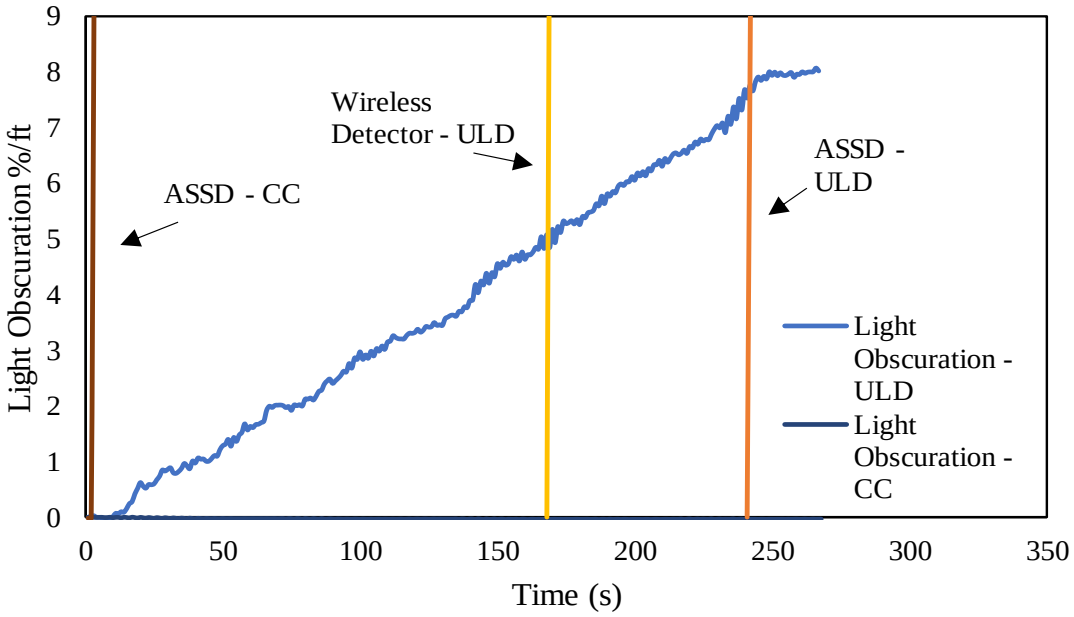

Figure A.26. Heptane – LLRM - Light obscuration inside ULD and the cargo compartment versus detector activation.

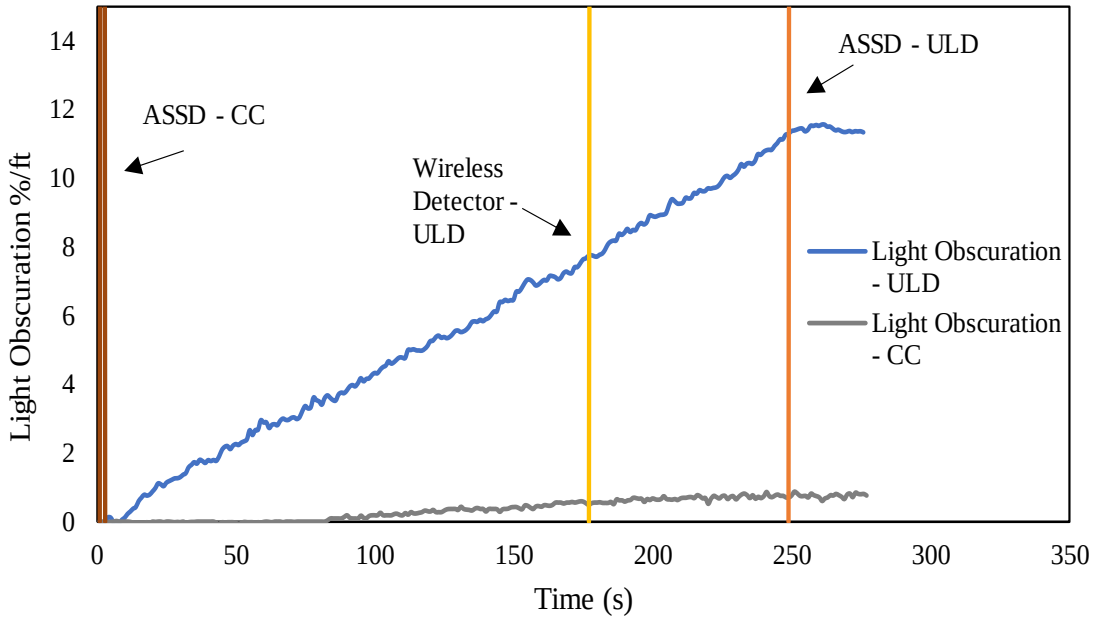

Figure A.27. Heptane – MLRM - Light obscuration inside ULD and the cargo compartment versus detector activation.

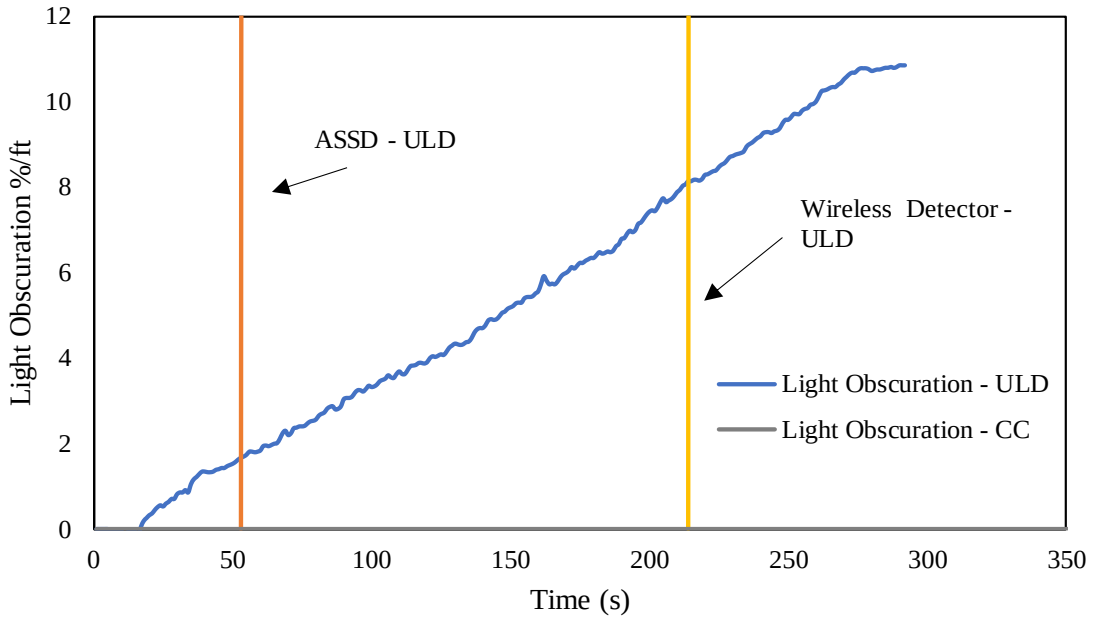

Figure A.28. Heptane – SLRM - Light obscuration inside ULD and the cargo compartment versus detector activation.

Light Obscuration and Blue, IR, and Blue + IR Signal

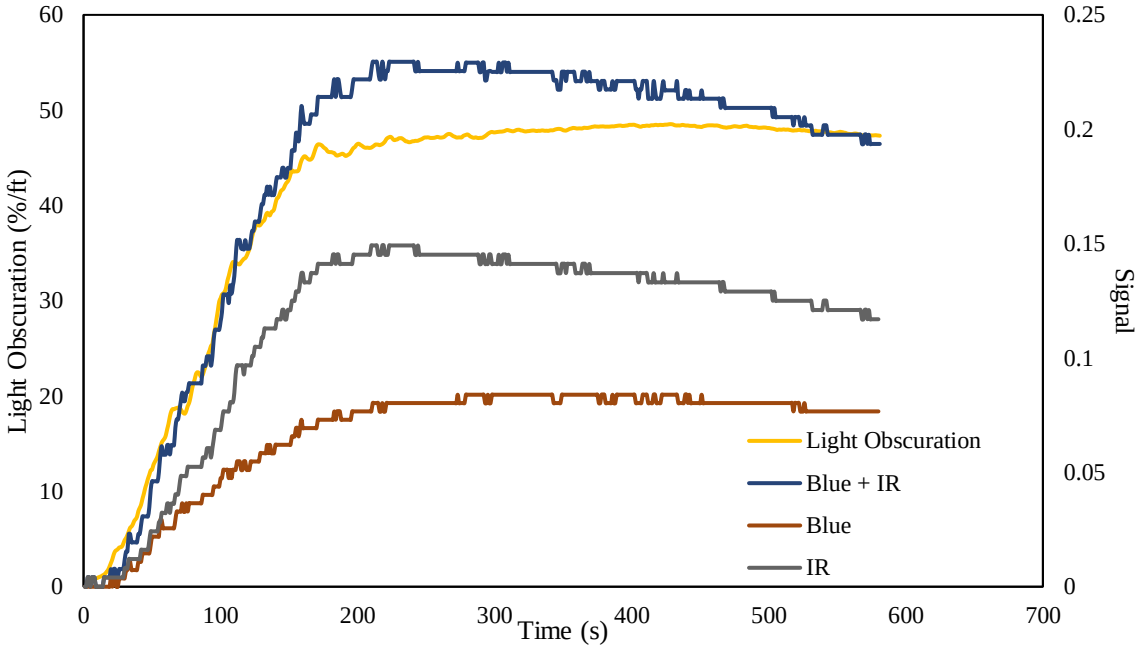

Figure A.29. Smoldering PU foam – MLRM - Light obscuration inside ULD and Blue, IR, and Blue + IR Signal.

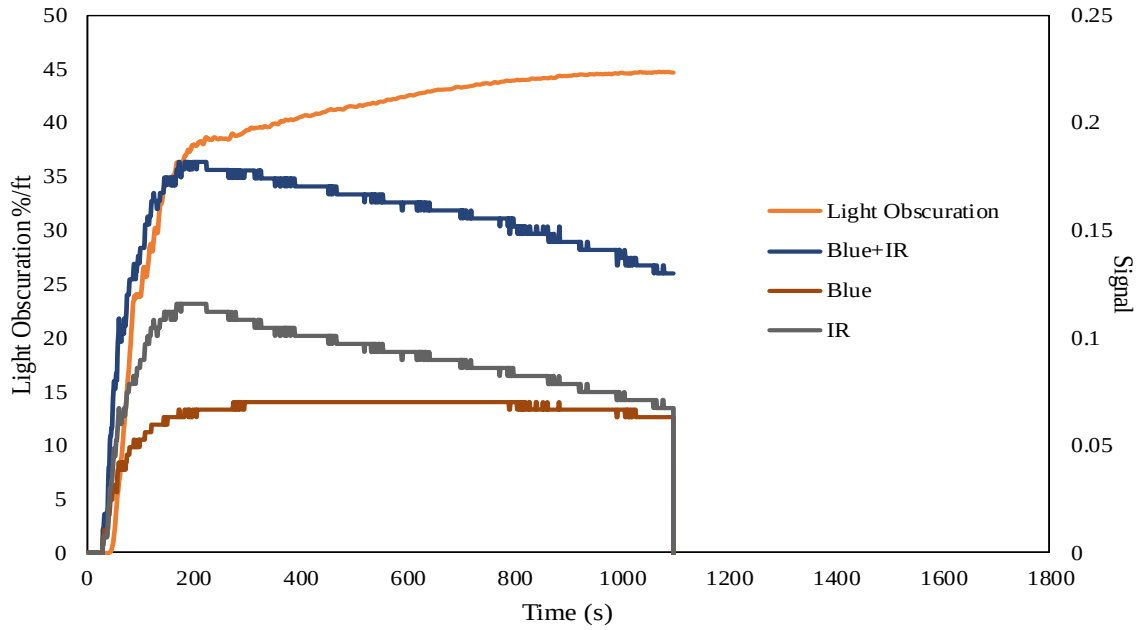

Figure A.30. Smoldering PU foam – SLRM - Light obscuration inside ULD and Blue, IR, and Blue + IR Signal

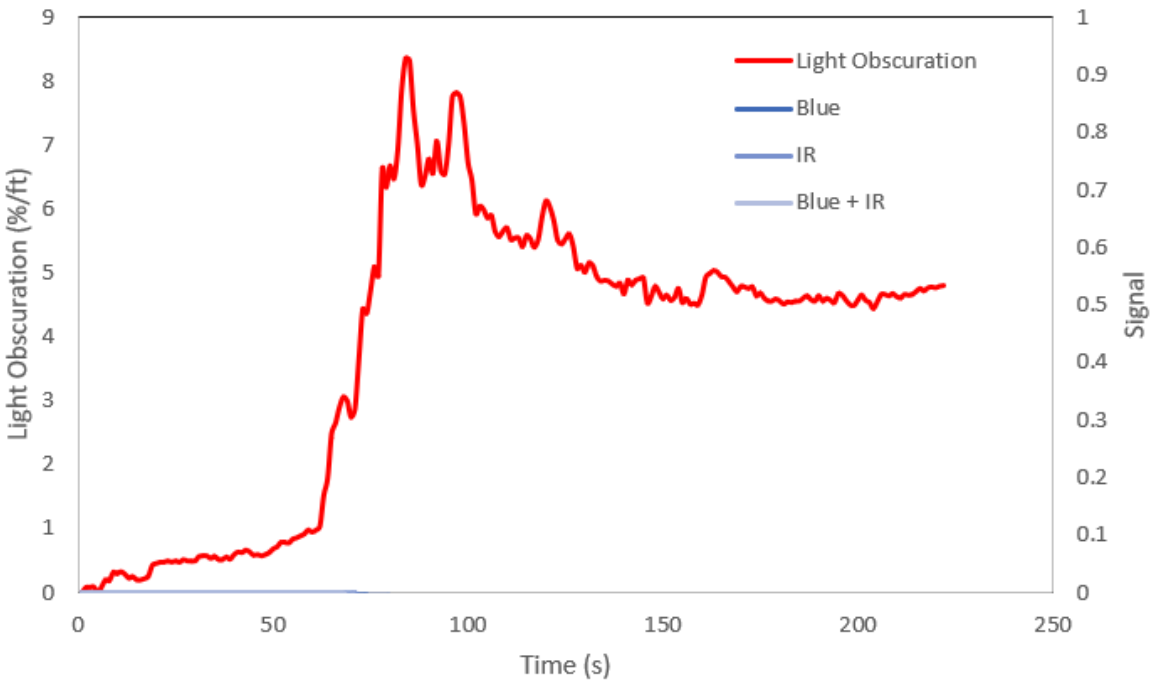

Figure A.31. Flaming PU – LLRM - Light obscuration inside ULD and Blue, IR, and Blue + IR Signal

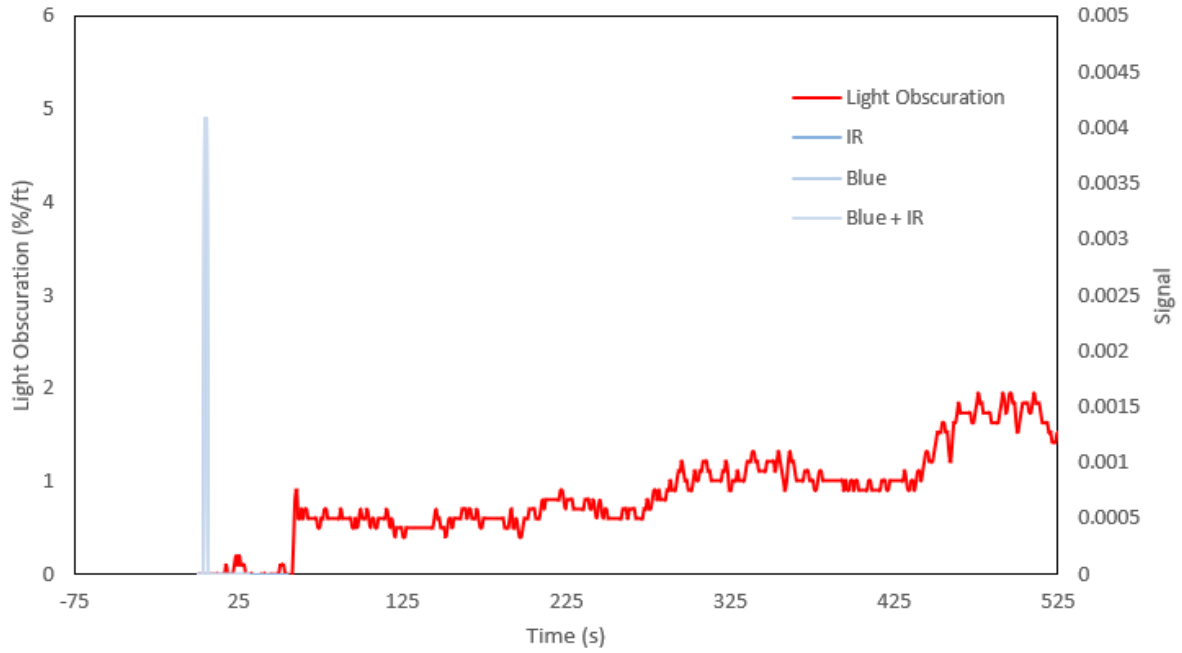

Figure A.32. Flaming PU – MLRM - Light obscuration inside ULD and Blue, IR, and Blue + IR Signal

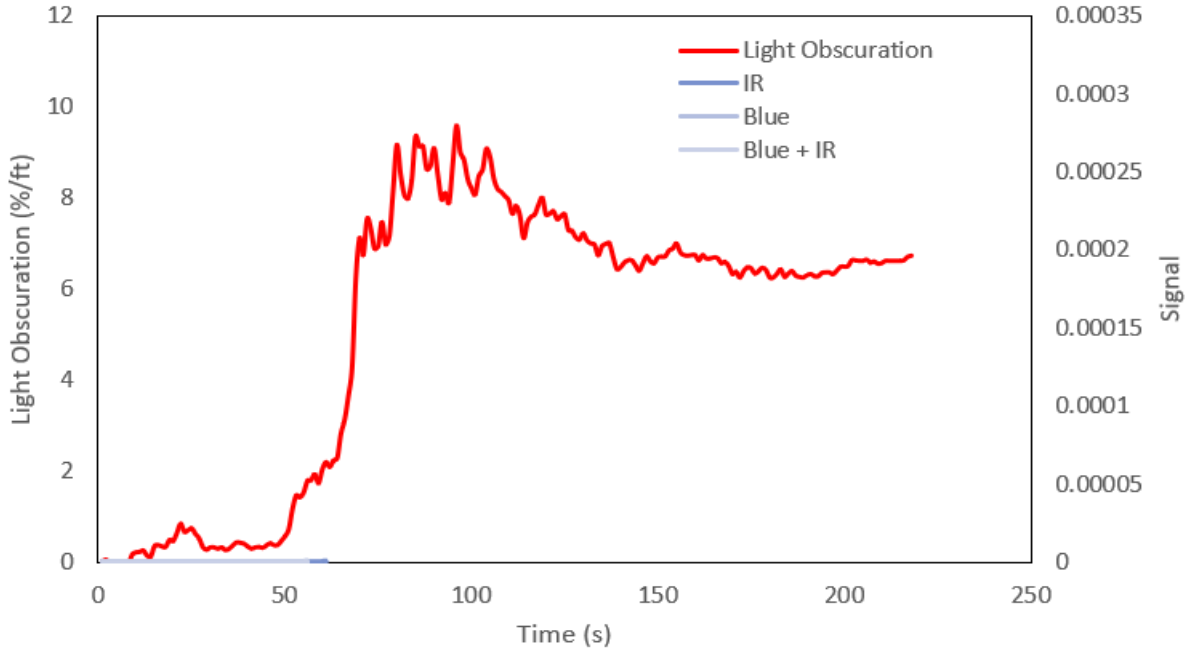

Figure A.33. Flaming PU – SLRM - Light obscuration inside ULD and Blue, IR, and Blue + IR Signal

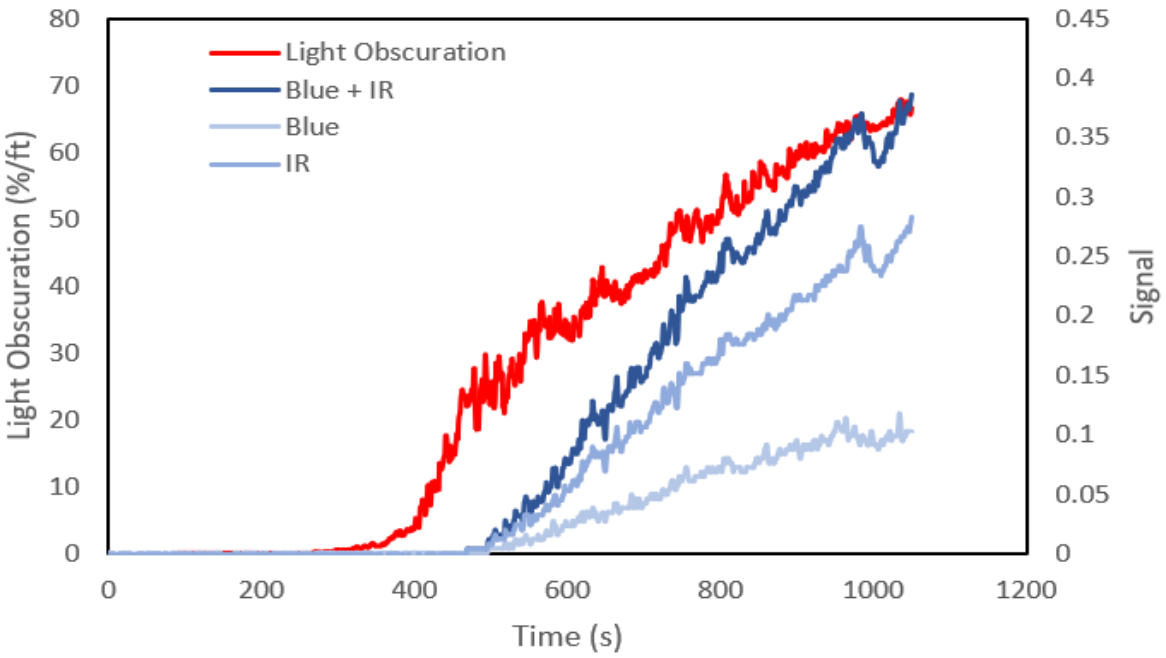

Figure A.34. Suitcase – MLRM - Light obscuration inside ULD and Blue, IR, and Blue + IR Signal

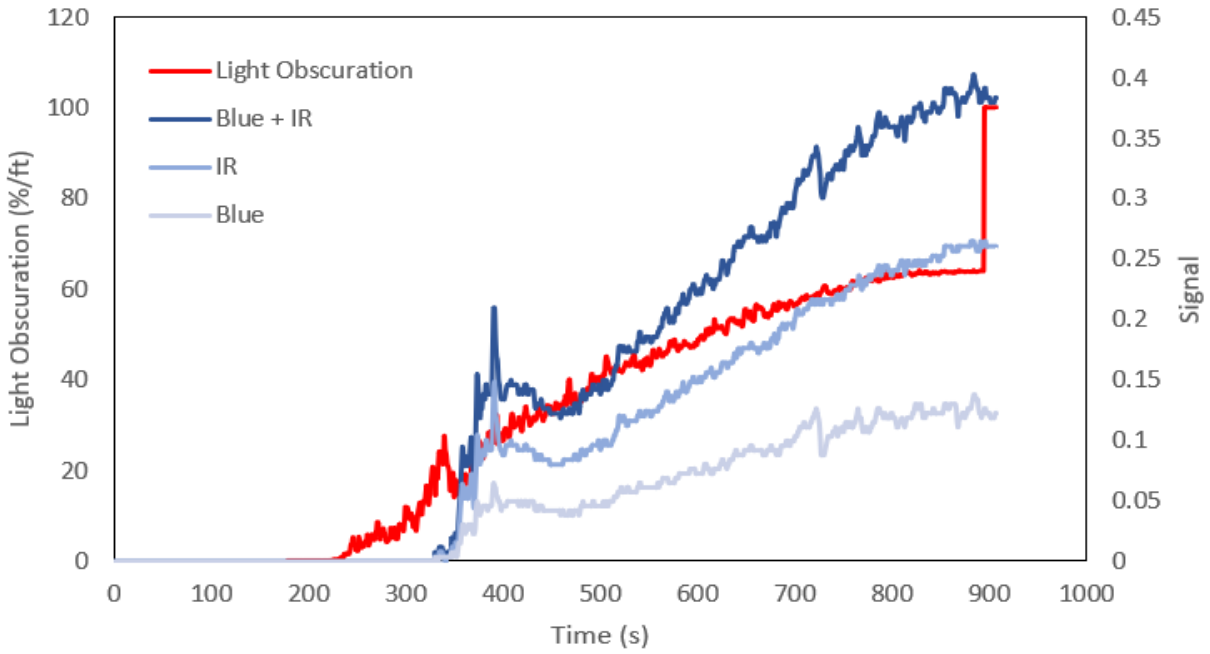

Figure A.35. Suitcase – SLRM - Light obscuration inside ULD and Blue, IR, and Blue + IR Signal

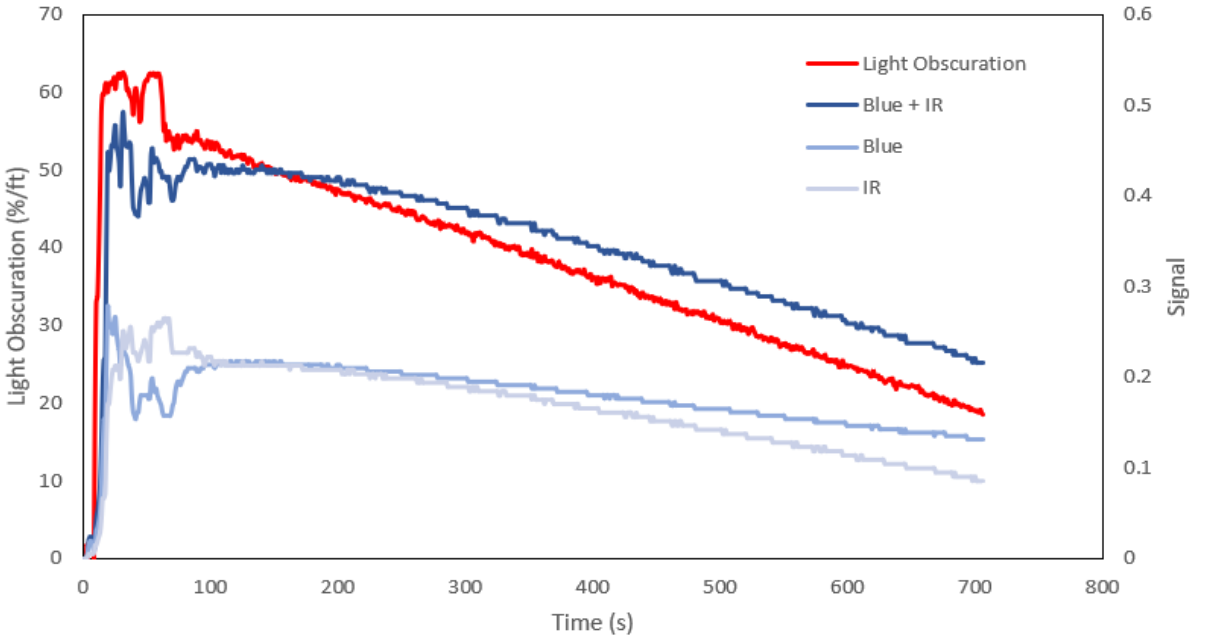

Figure A.36. Boeing Smoke Generator – LLRM - Light obscuration inside ULD and Blue, IR, and Blue + IR Signal

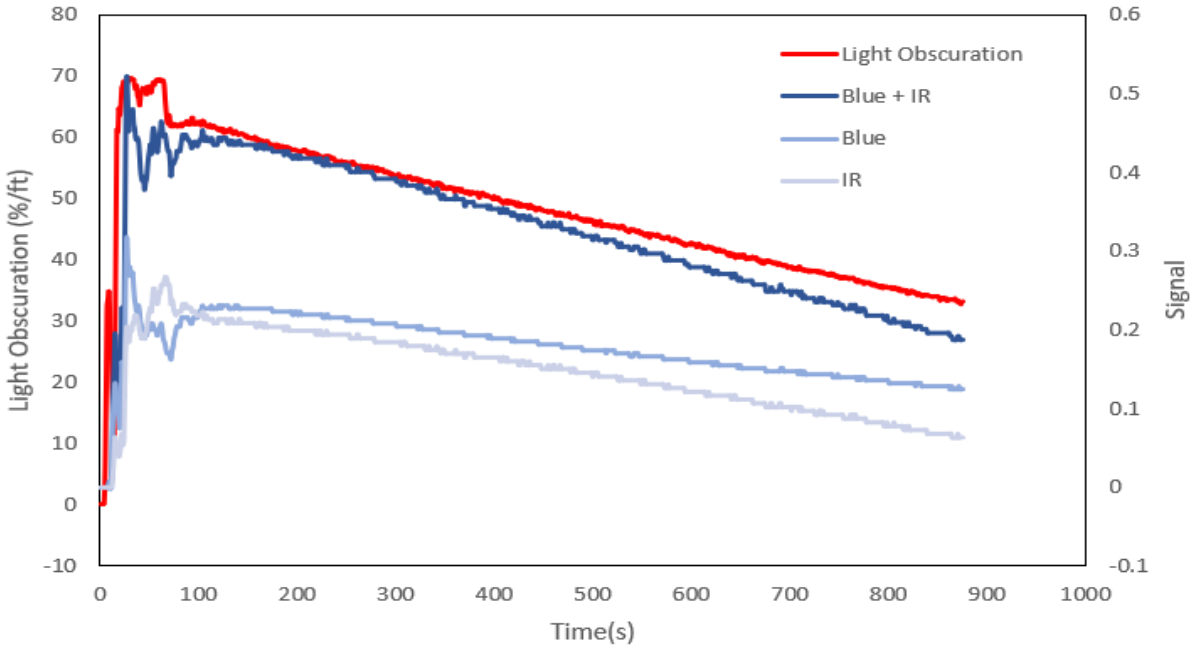

Figure A.37. Boeing Smoke Generator – MLRM - Light obscuration inside ULD and Blue, IR, and Blue + IR Signal

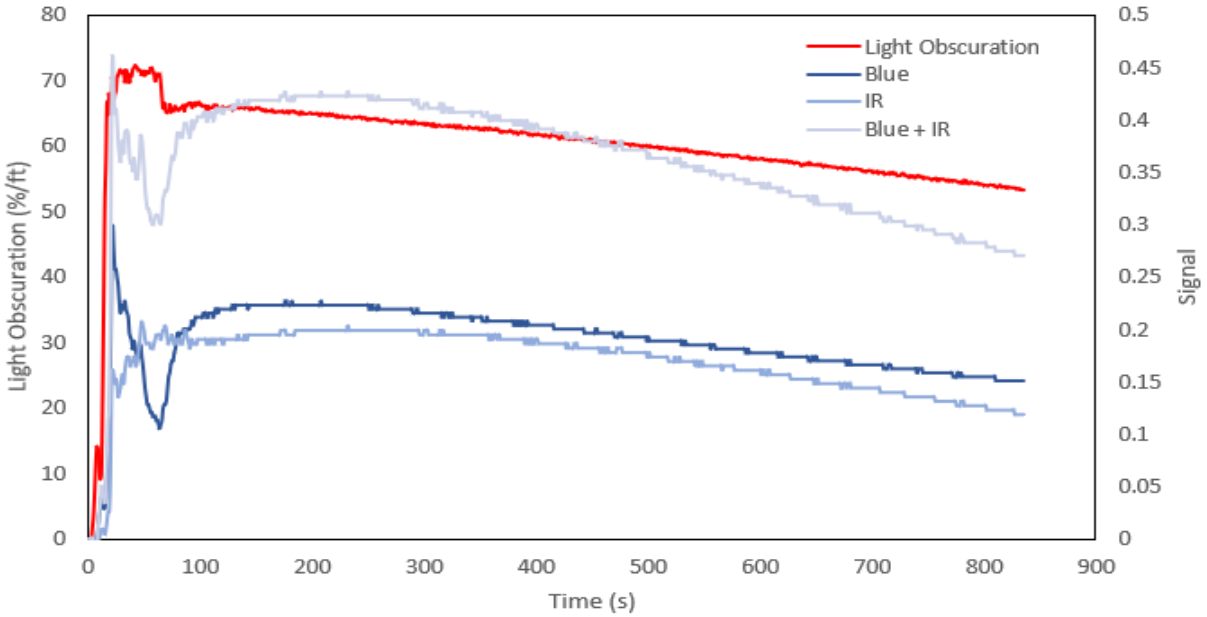

Figure A.38. Boeing Smoke Generator – SLRM - Light obscuration inside ULD and Blue, IR, and Blue + IR Signal

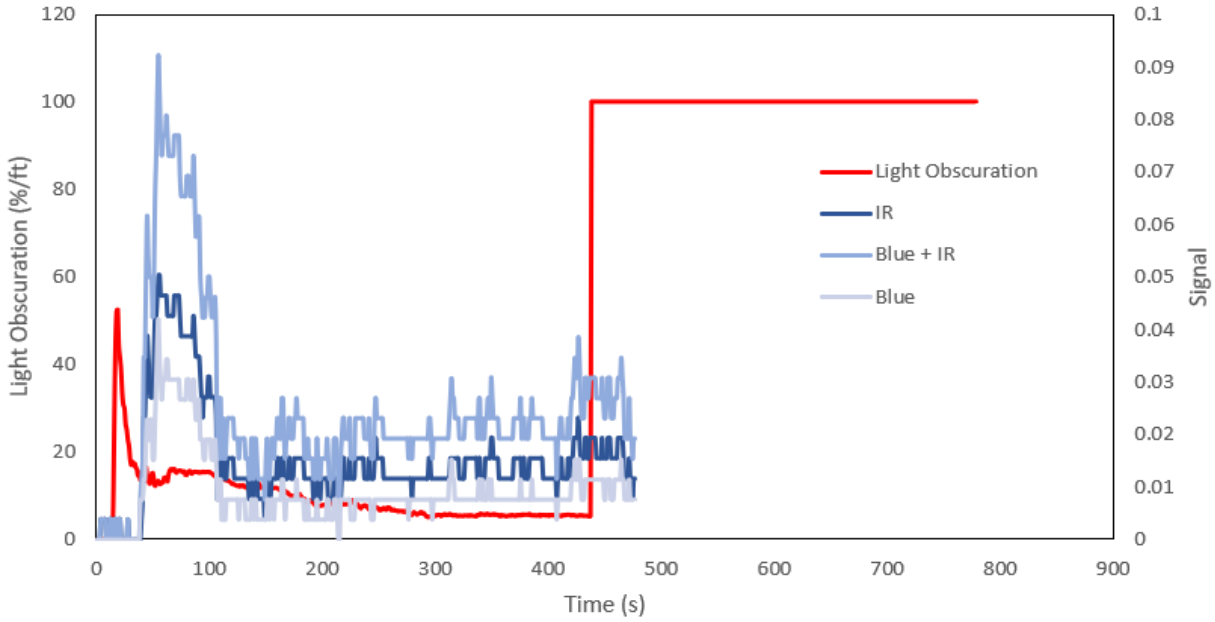

Figure A.39. Wires – SLRM - Light obscuration inside ULD and Blue, IR, and Blue + IR Signal

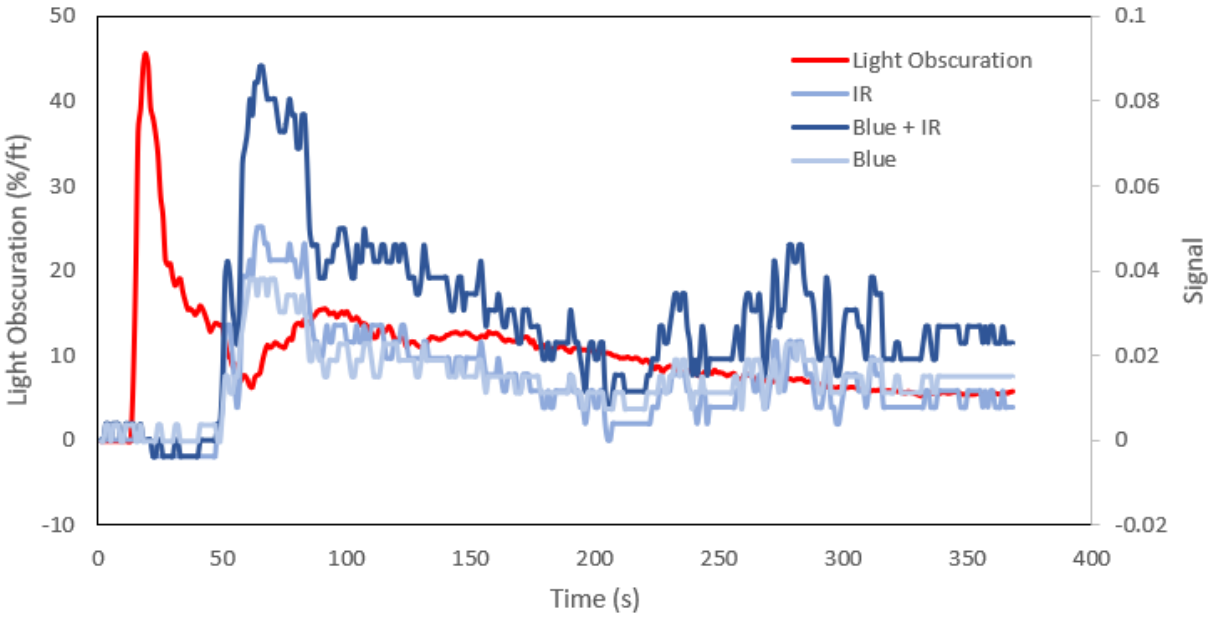

Figure A.40. Wires – MLRM - Light obscuration inside ULD and Blue, IR, and Blue + IR Signal

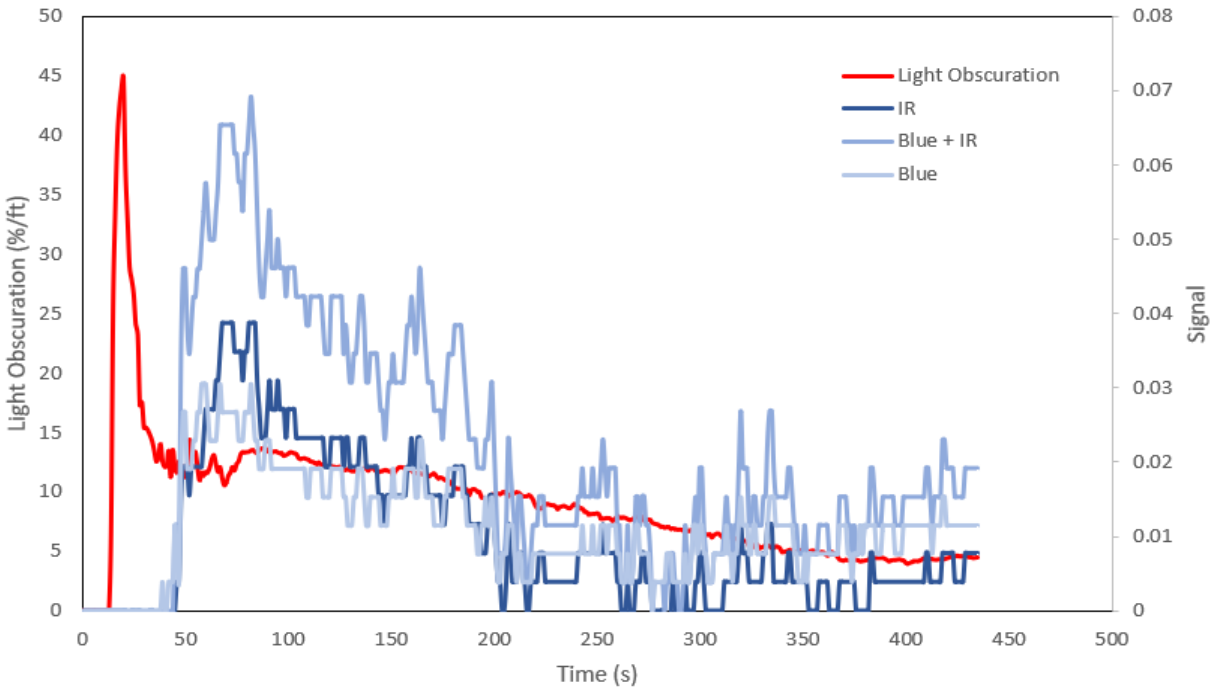

Figure A.41. Wires – SLRM - Light obscuration inside ULD and Blue, IR, and Blue + IR Signal

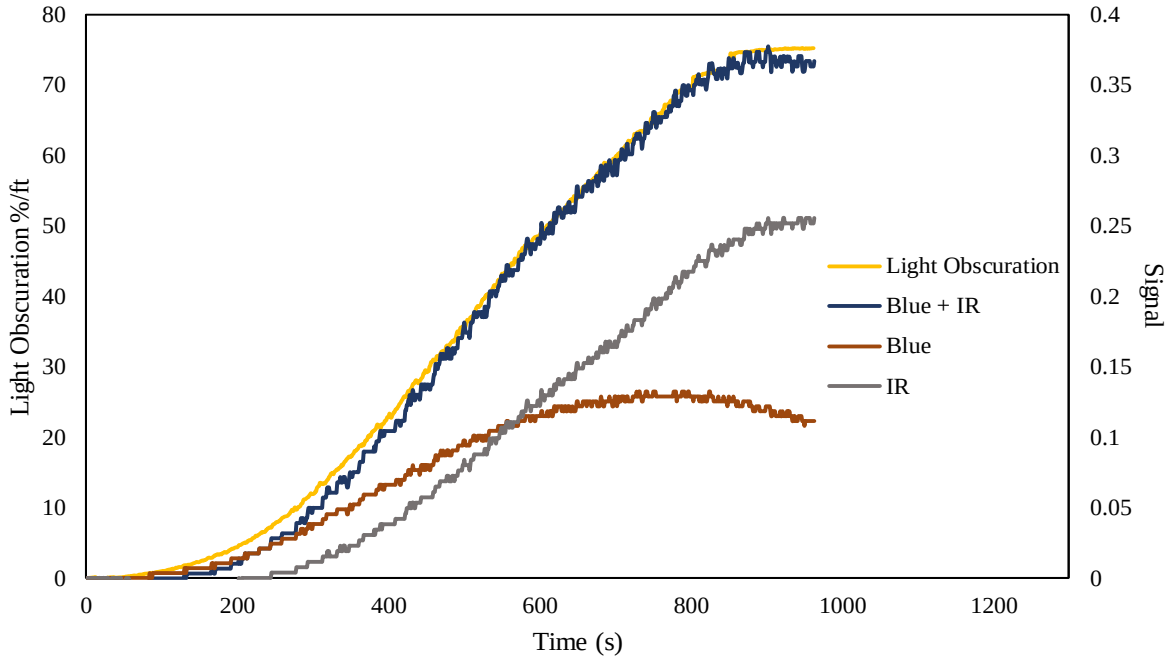

Figure A.42. Wood – LLRM - Light obscuration inside ULD and Blue, IR, and Blue + IR Signal

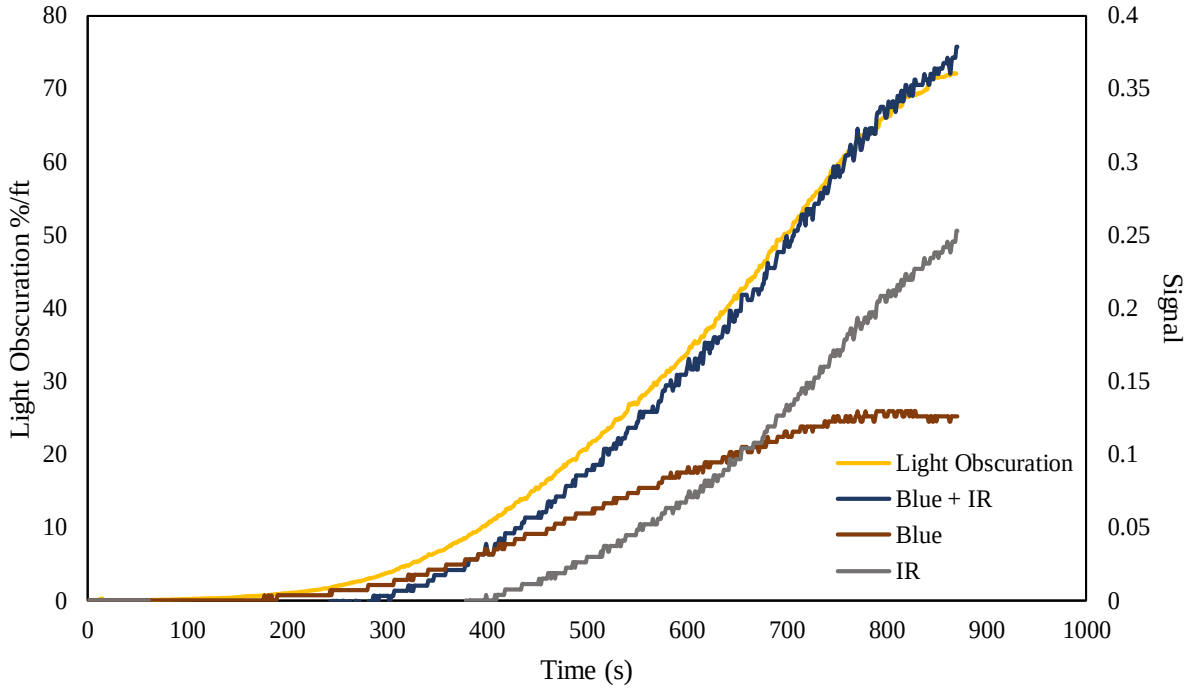

Figure A.43. Wood – MLRM - Light obscuration inside ULD and Blue, IR, and Blue + IR Signal

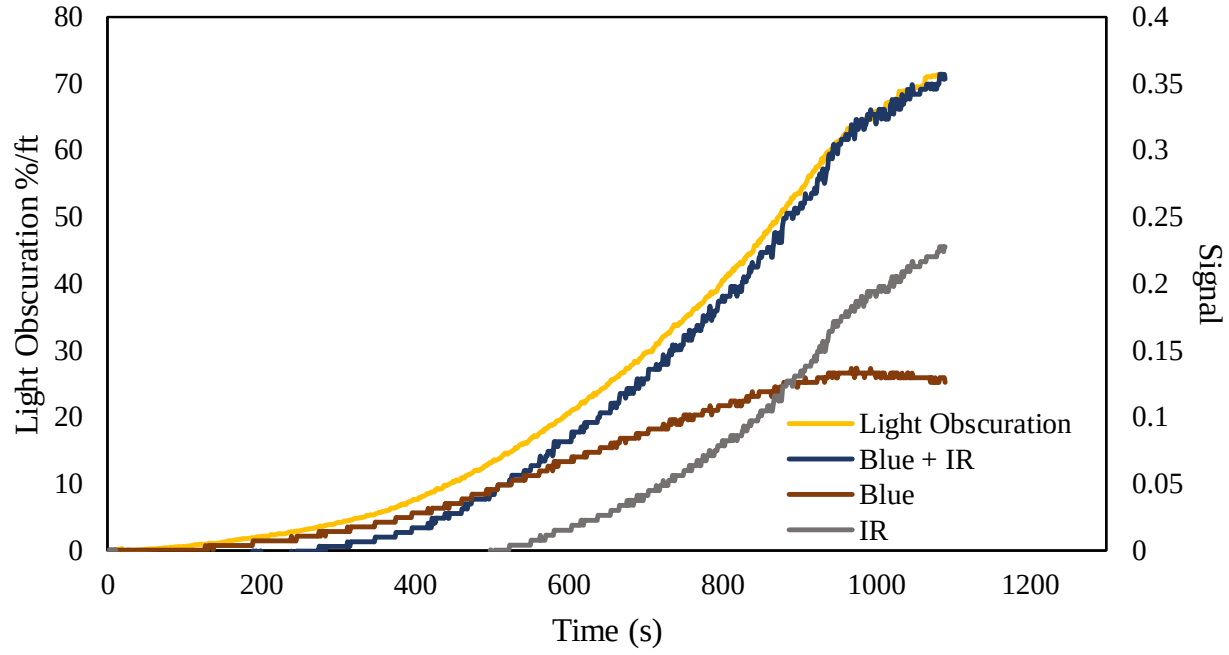

Figure A.44. Wood – SLRM - Light obscuration inside ULD and Blue, IR, and Blue + IR Signal

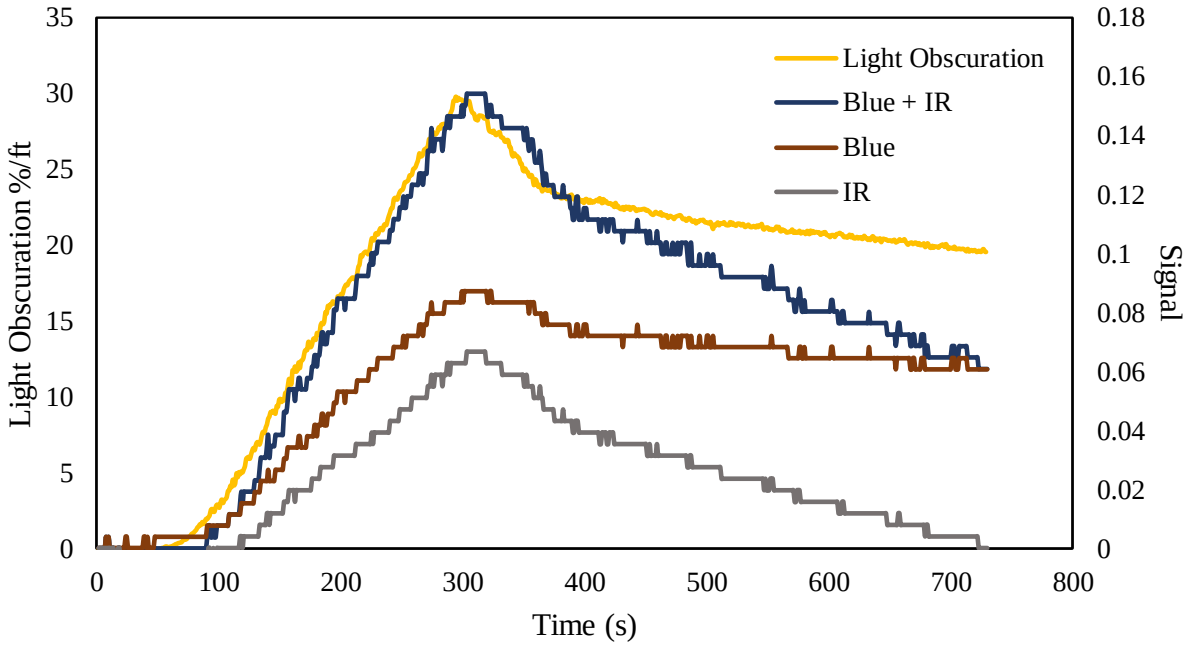

Figure A.45. Cotton – LLRM - Light obscuration inside ULD and Blue, IR, and Blue + IR Signal

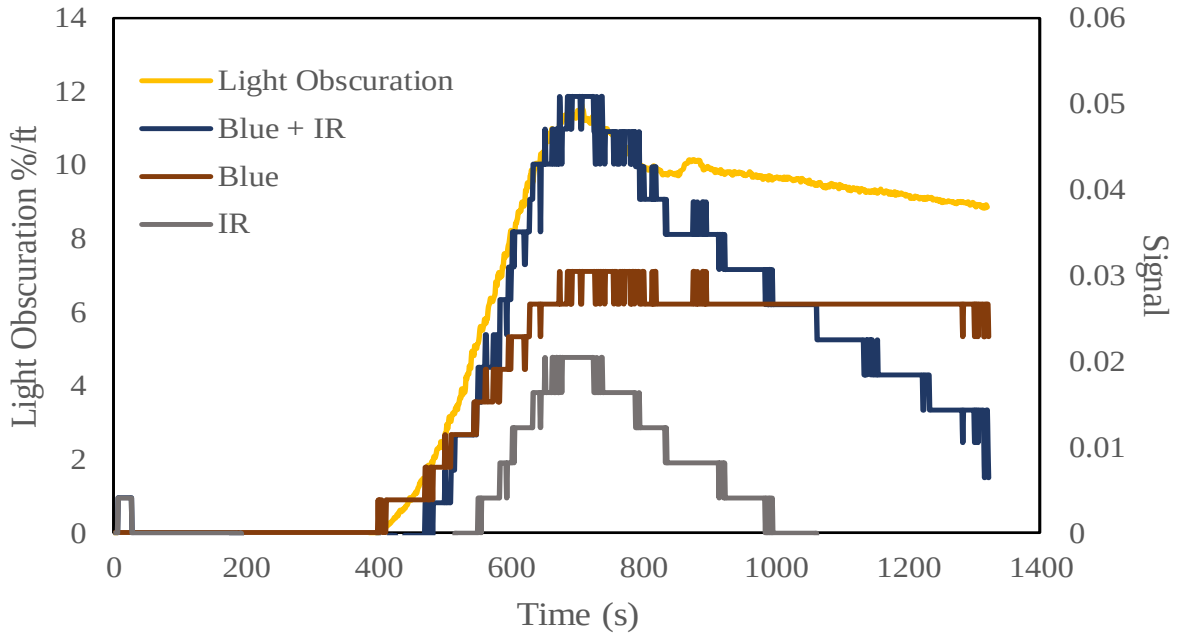

Figure A.46. Cotton – MLRM - Light obscuration inside ULD and Blue, IR, and Blue + IR Signal

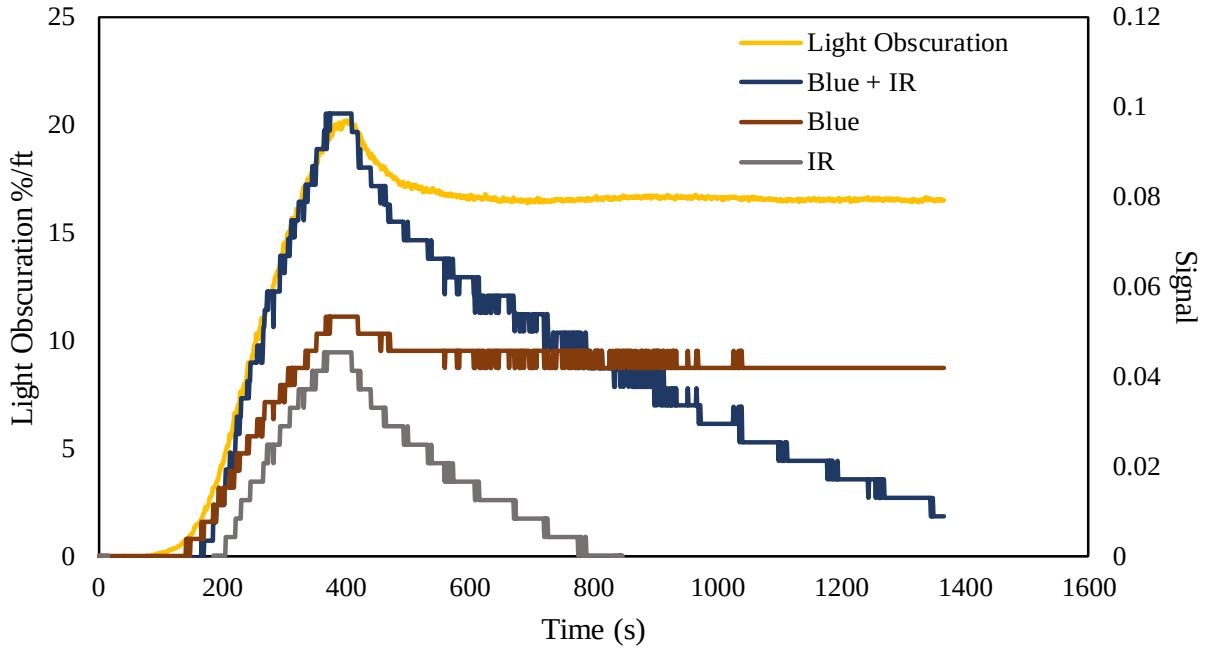

Figure A.47. Cotton – SLRM - Light obscuration inside ULD and Blue, IR, and Blue + IR Signal

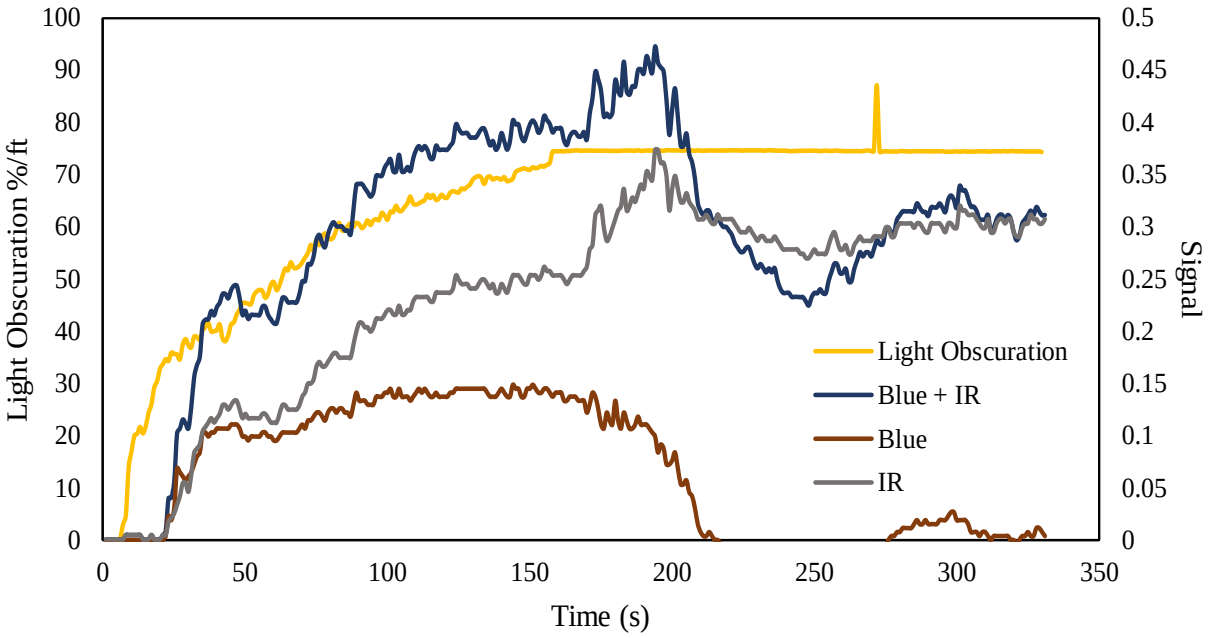

Figure A.48. Paper – LLRM - Light obscuration inside ULD and Blue, IR, and Blue + IR Signal

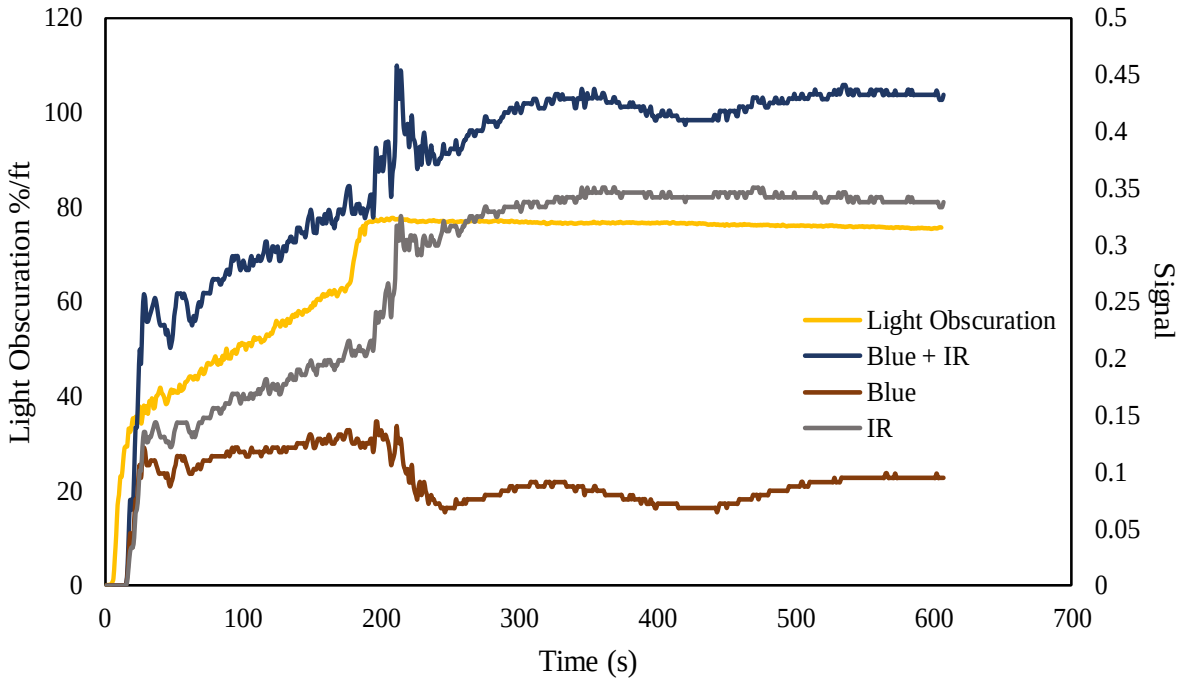

Figure A.49. Paper – MLRM - Light obscuration inside ULD and Blue, IR, and Blue + IR Signal

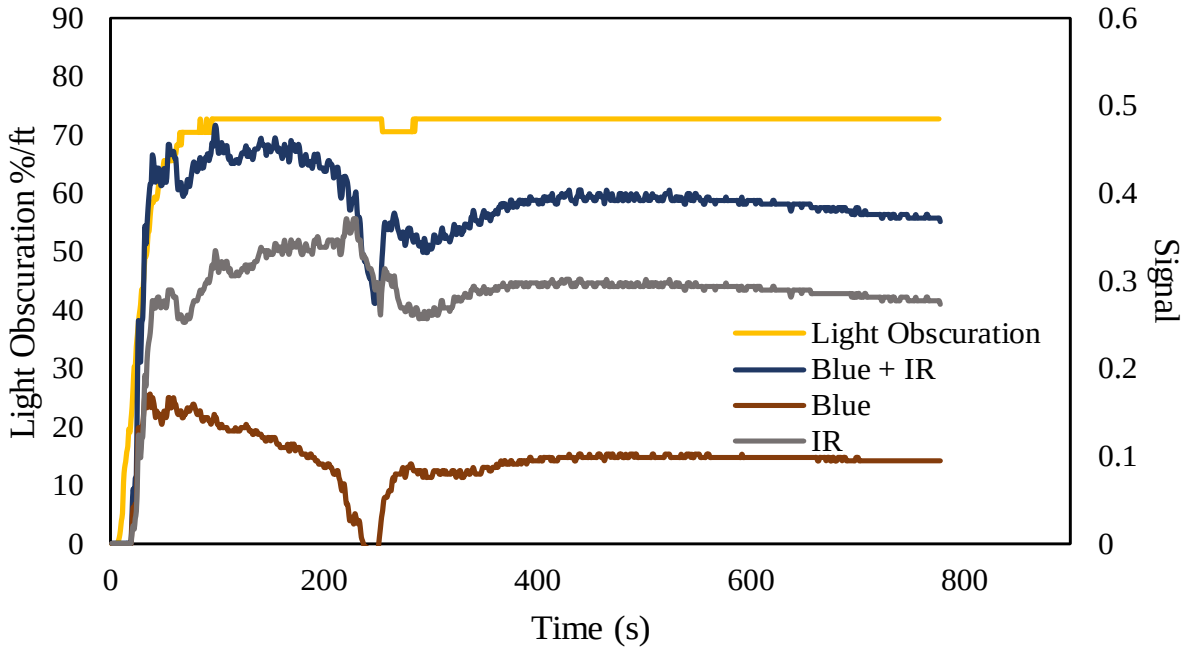

Figure A.50. Paper – SLRM - Light obscuration inside ULD and Blue, IR, and Blue + IR Signal

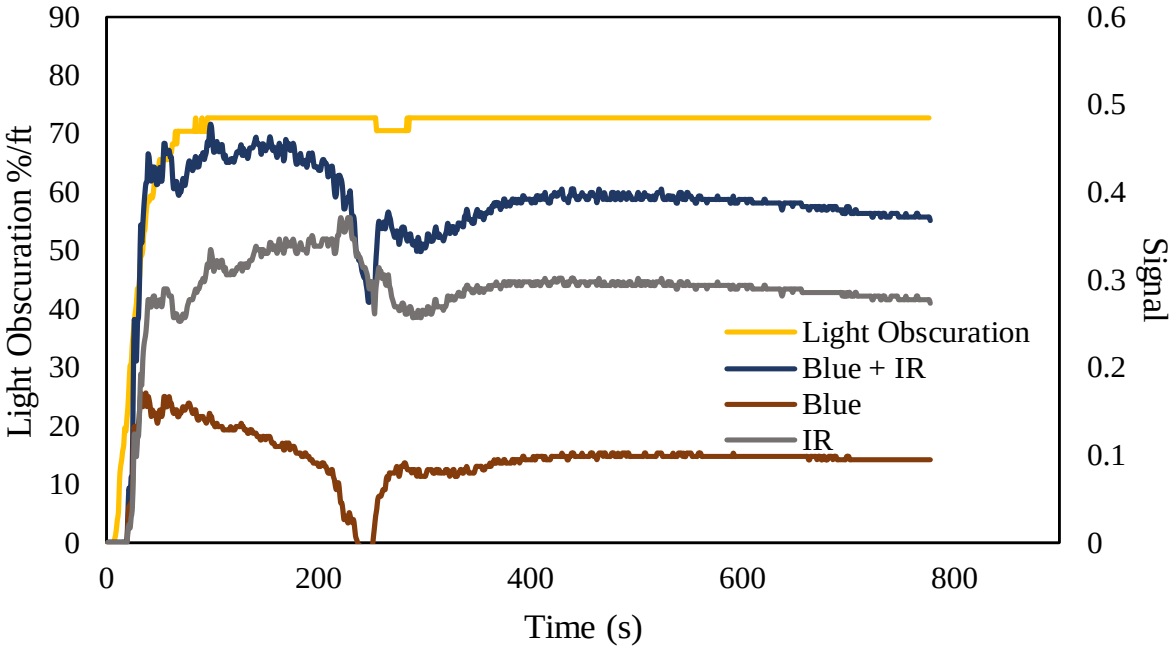

Figure A.51. Paper – SLRM - Light obscuration inside ULD and Blue, IR, and Blue + IR Signal

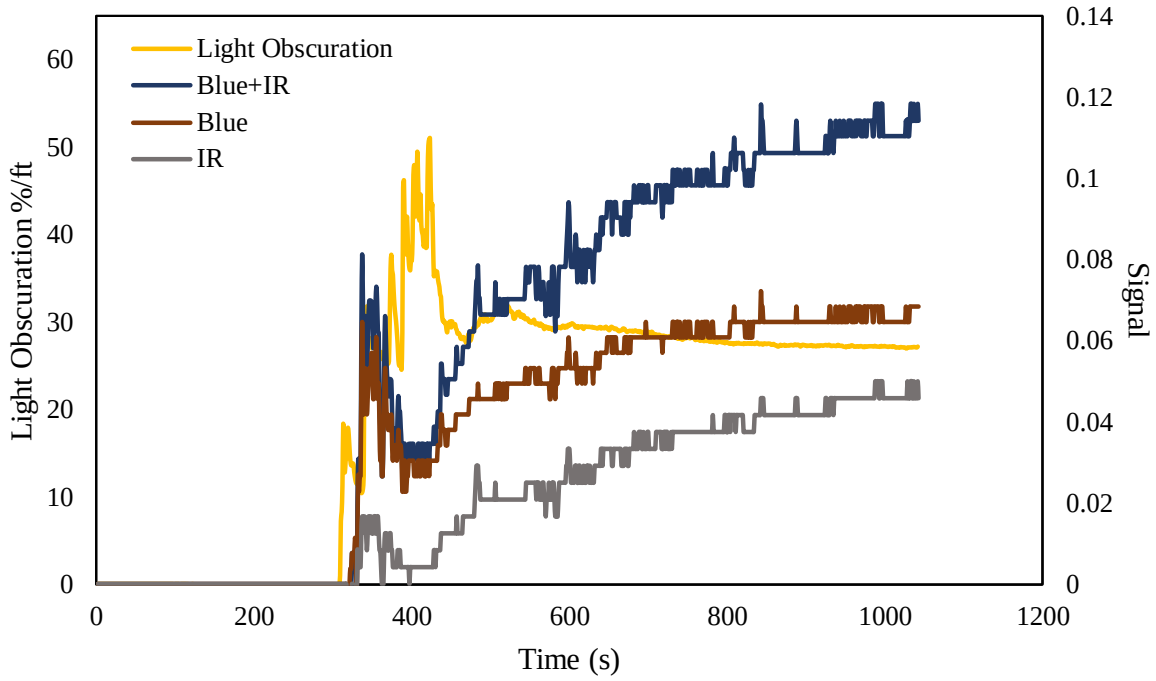

Figure A.52. Batteries – LLRM - Light obscuration inside ULD and Blue, IR, and Blue + IR Signal

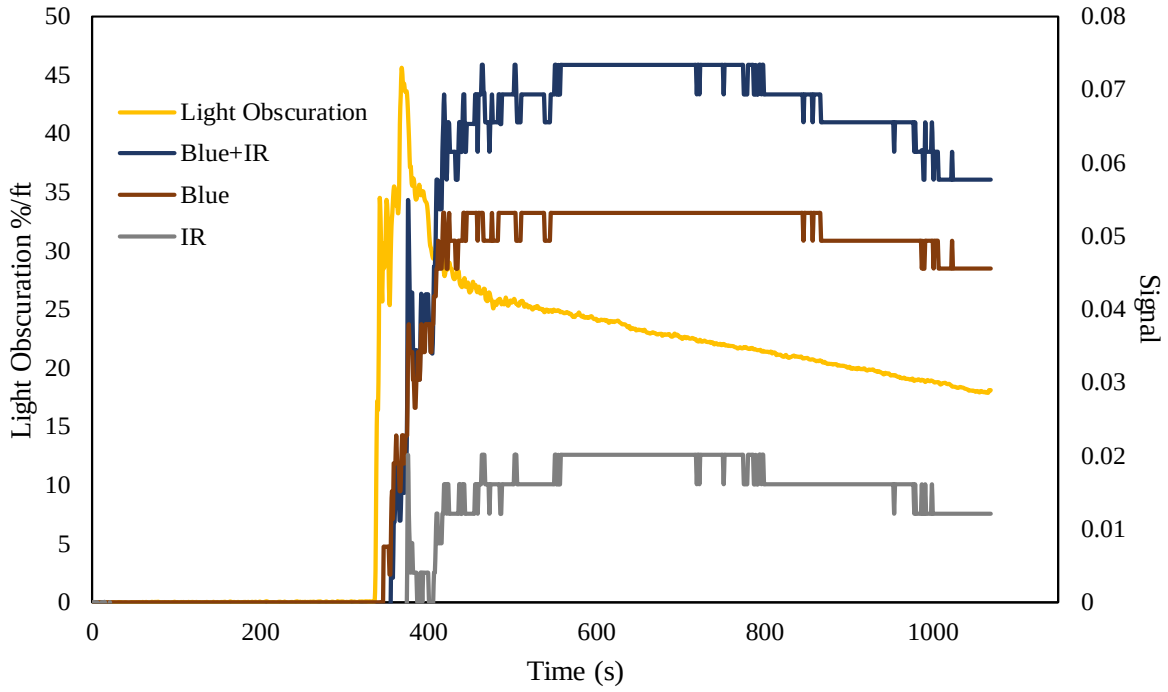

Figure A.53. Batteries – MLRM - Light obscuration inside ULD and Blue, IR, and Blue + IR Signal

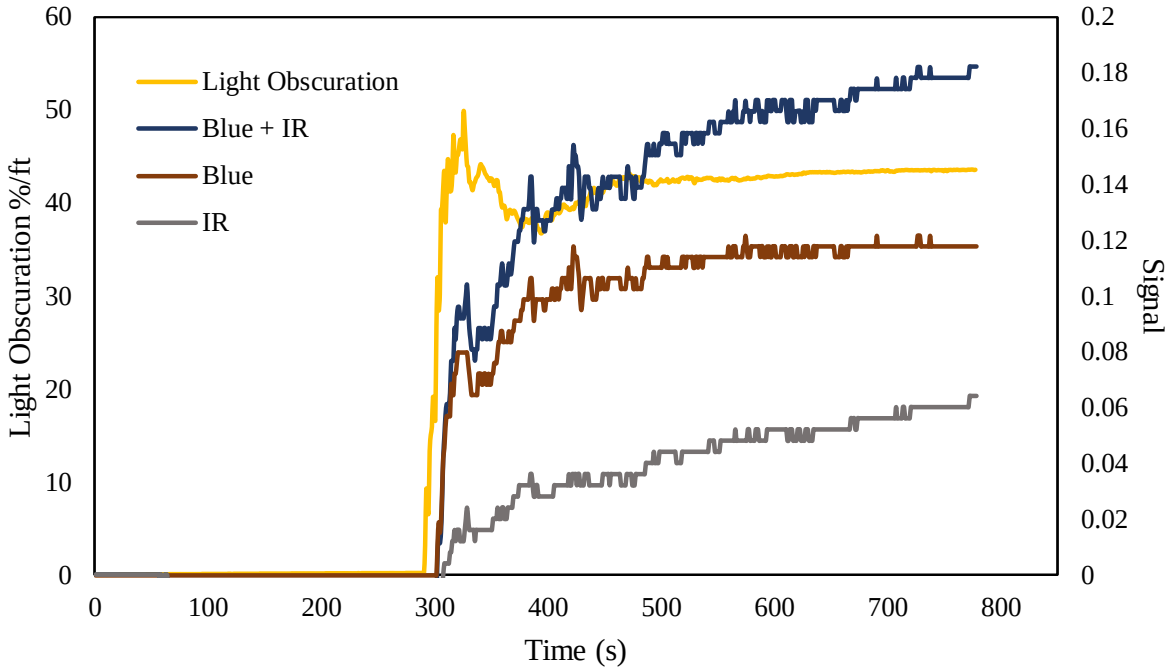

Figure A.54. Batteries – SLRM - Light obscuration inside ULD and Blue, IR, and Blue + IR Signal

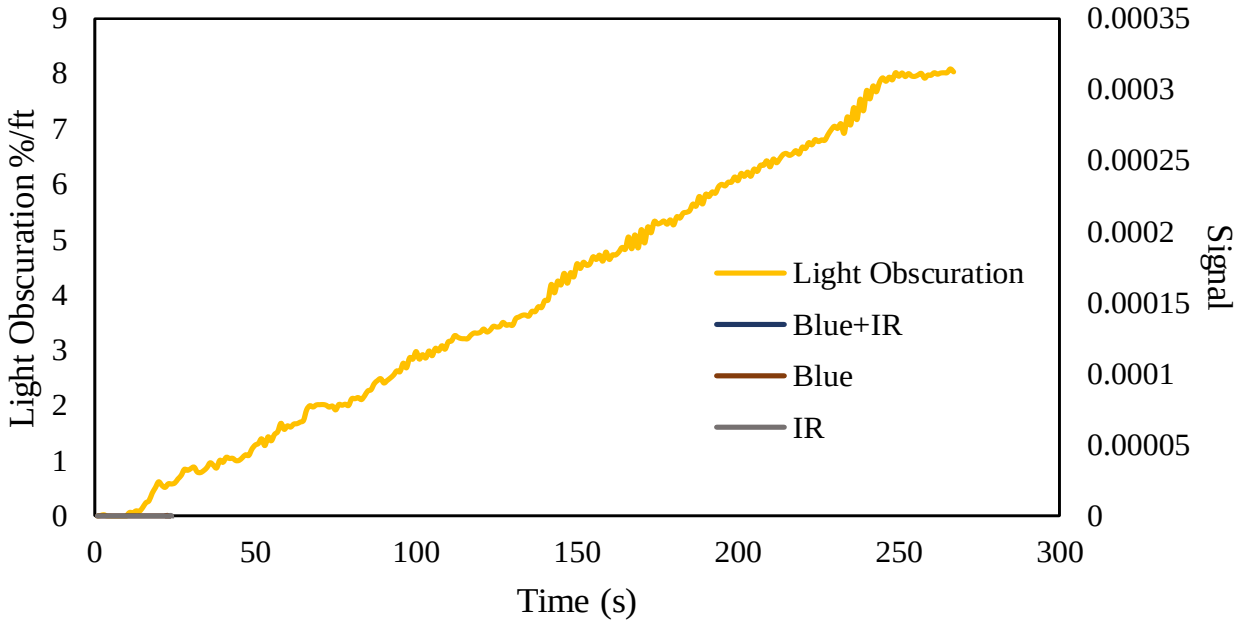

Figure A.55. Heptane – LLRM - Light obscuration inside ULD and Blue, IR, and Blue + IR Signal

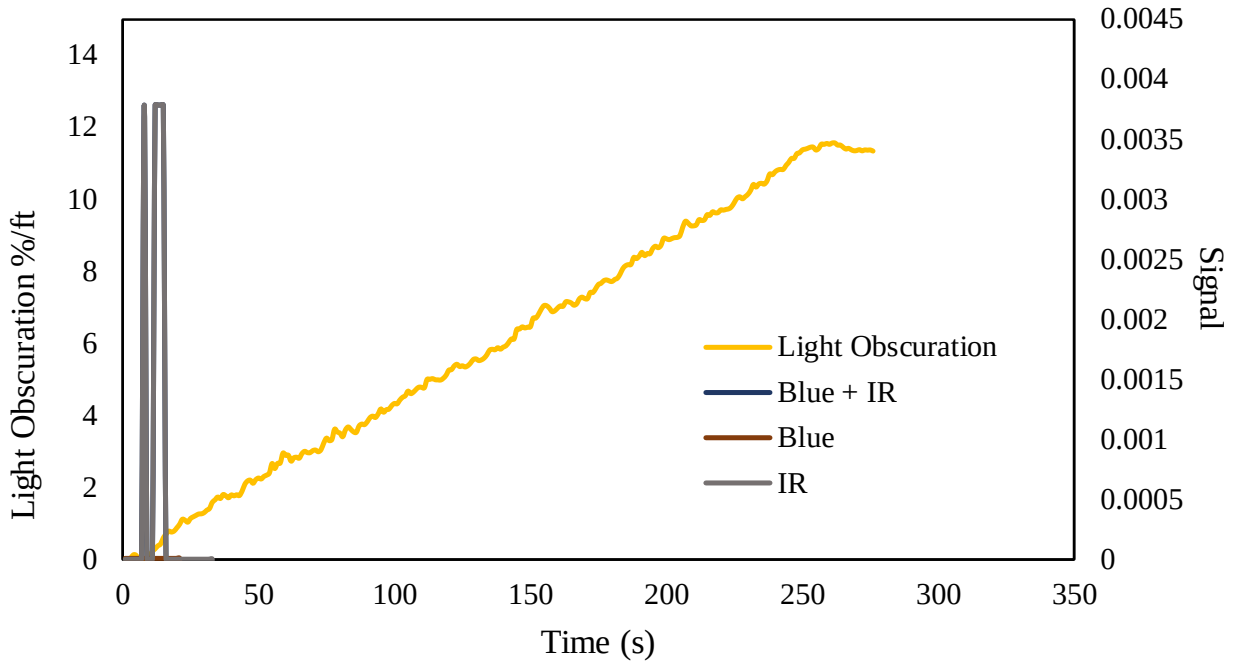

Figure A.56. Heptane – MLRM - Light obscuration inside ULD and Blue, IR, and Blue + IR Signal

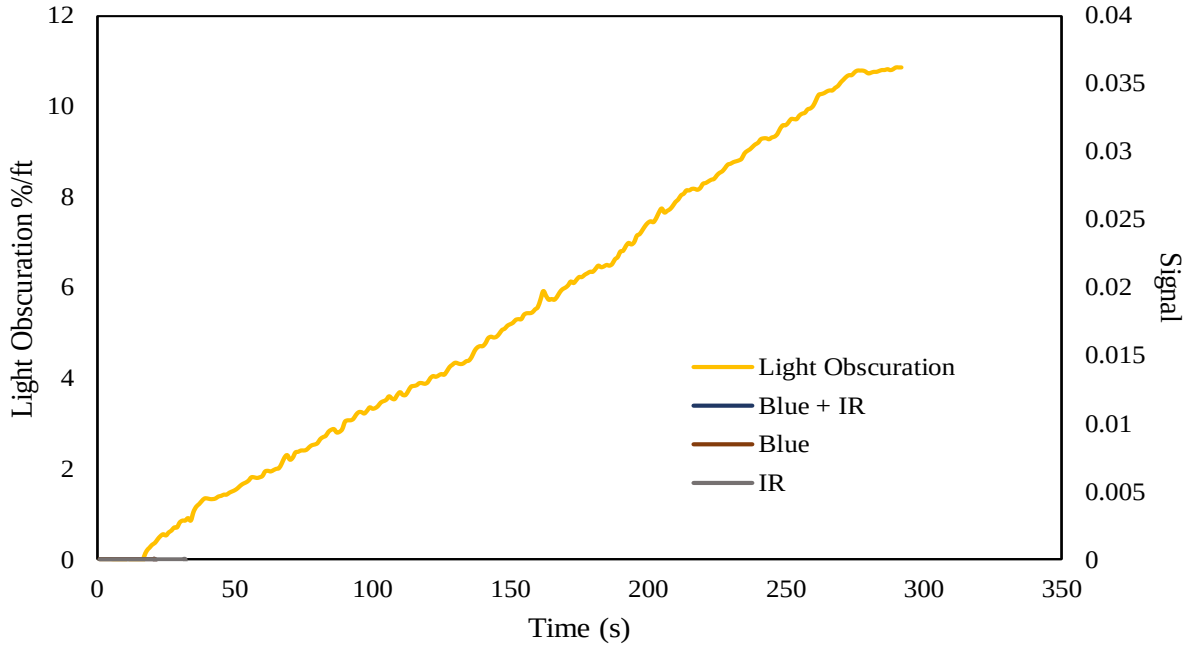

Figure A.57. Heptane – SLRM - Light obscuration inside ULD and Blue, IR, and Blue + IR Signal

Light Obscurations and CO_2 Concentration

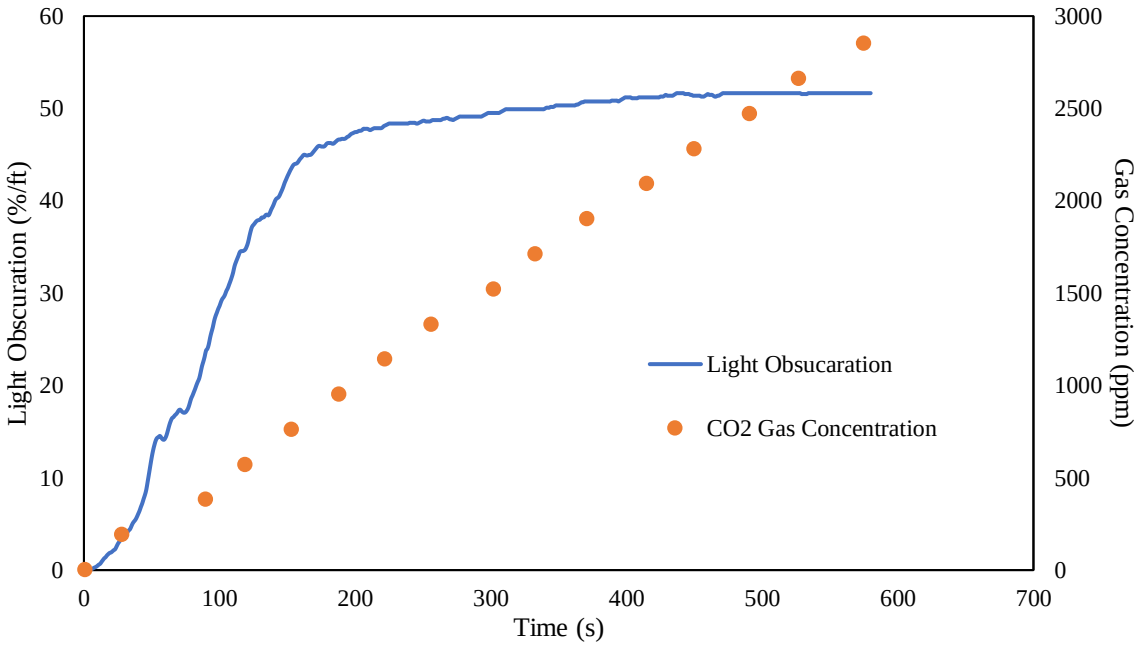

Figure A.58. Smoldering PU foam – MLRM - Light obscuration inside ULD and CO_2 Concentration

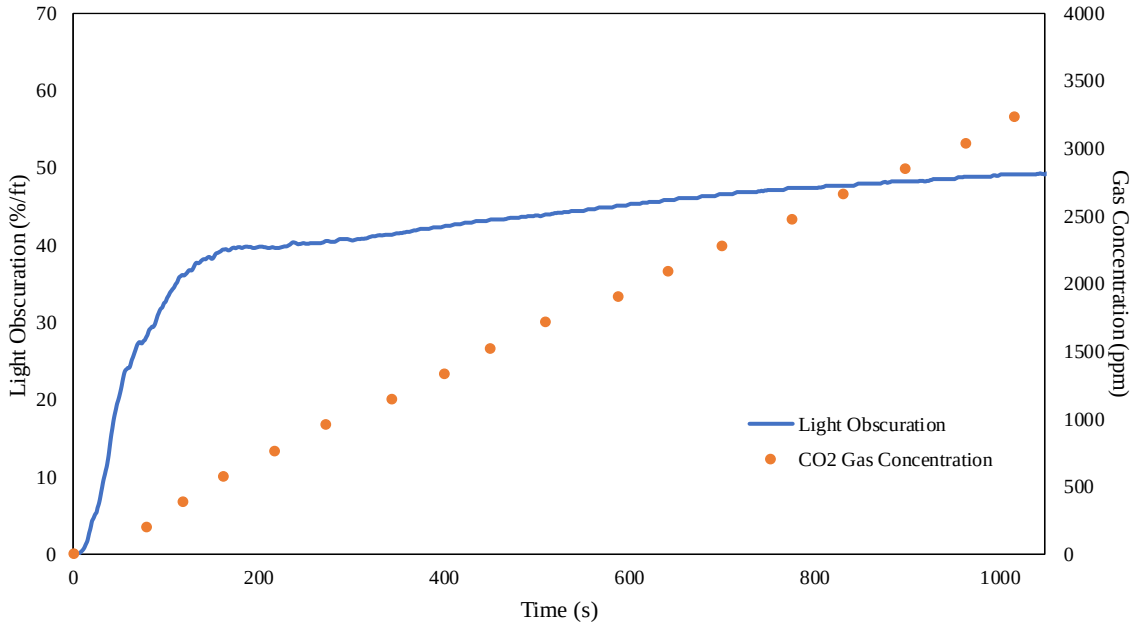

Figure A.59. Smoldering PU foam – SLRM - Light obscuration inside ULD and CO_2 Concentration

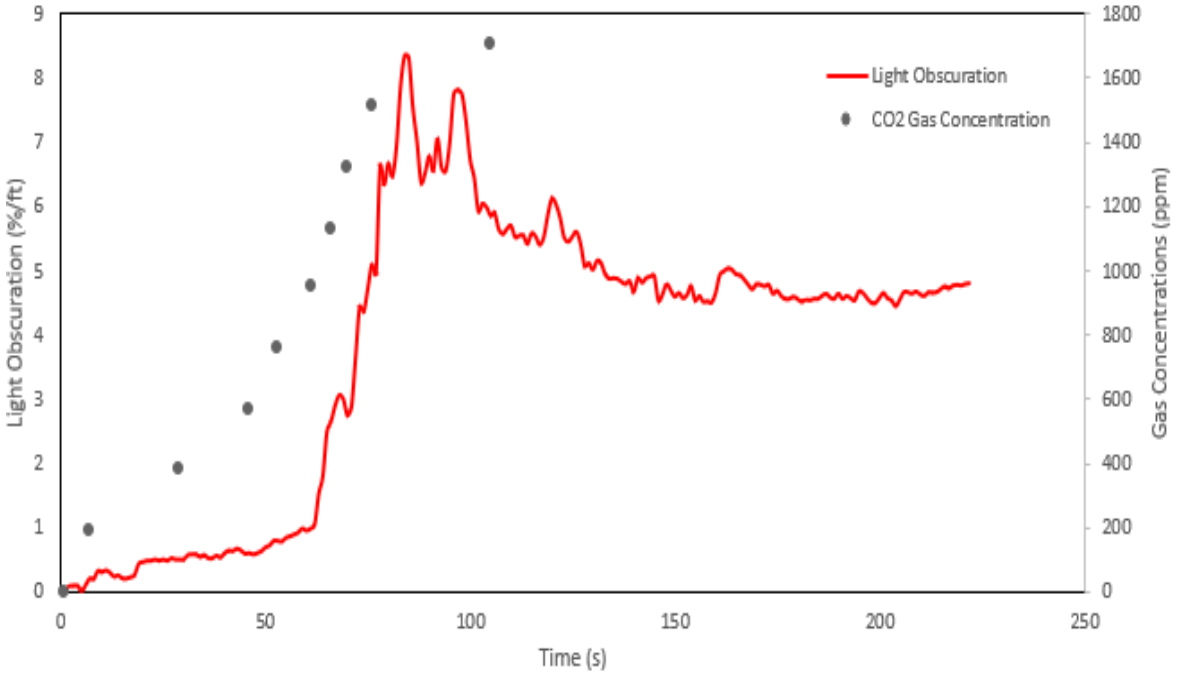

Figure A.60. Flame PU – LLRM - Light obscuration inside ULD and CO_2 Concentration

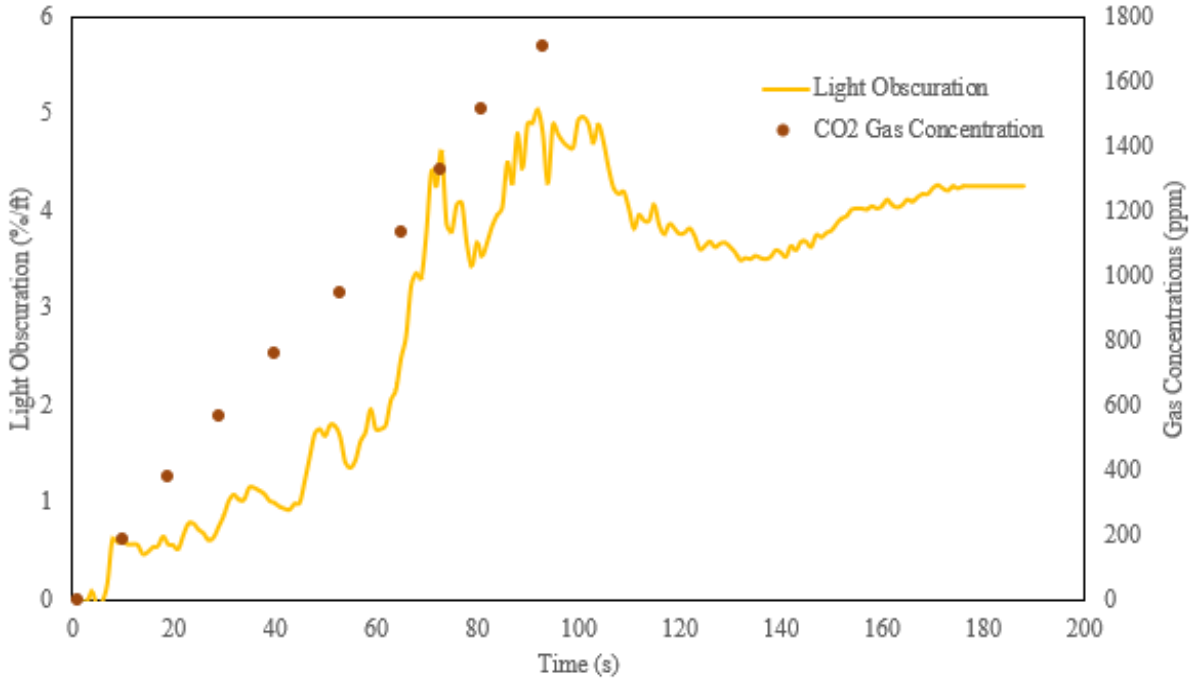

Figure A.61. Flame PU – MLRM - Light obscuration inside ULD and CO_2 Concentration

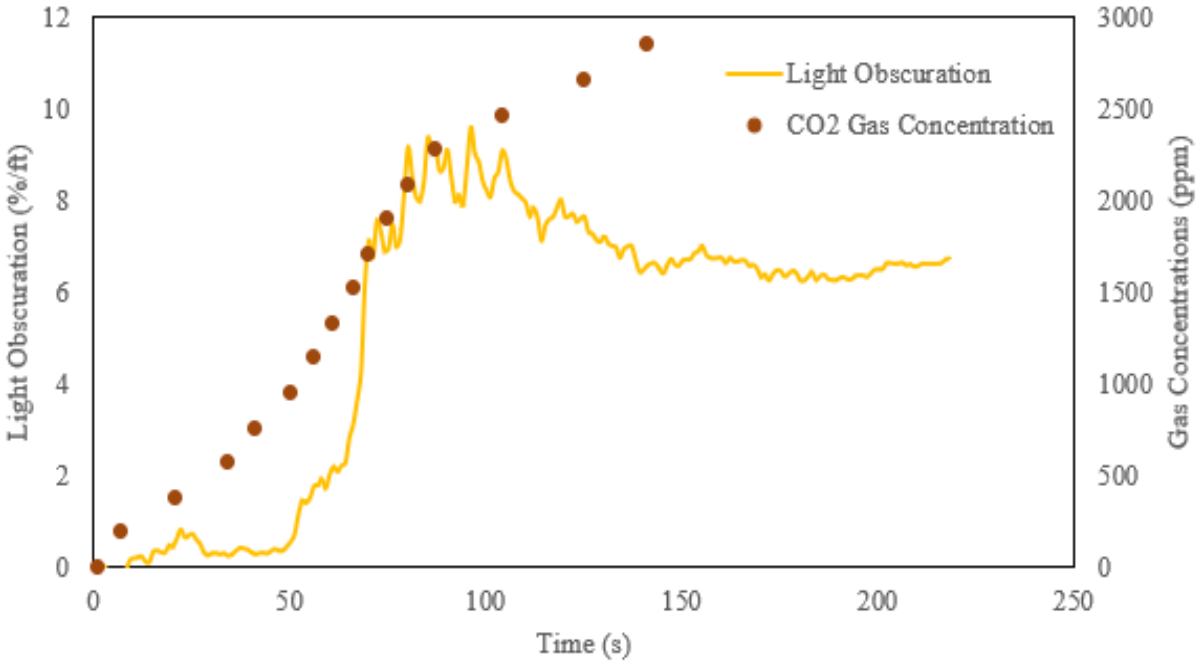

Figure A.62. Flame PU – SLRM - Light obscuration inside ULD and CO_2 Concentration

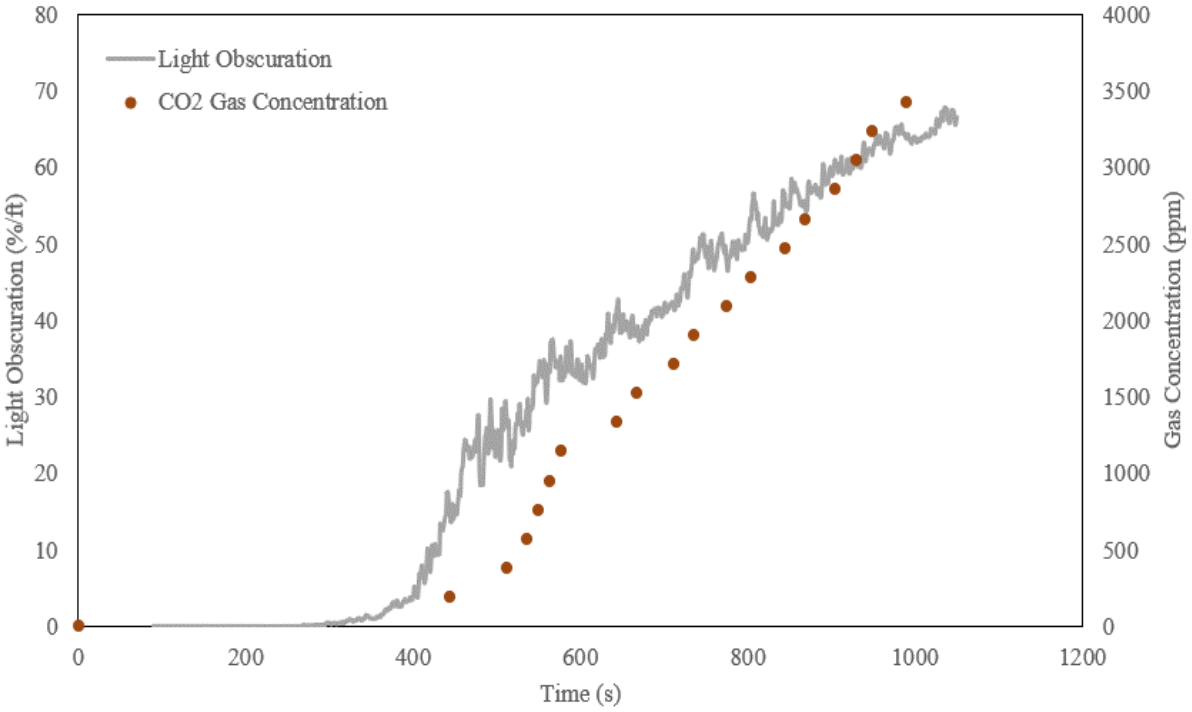

Figure A.63. Suitcase – MLRM - Light obscuration inside ULD and CO_2 Concentration

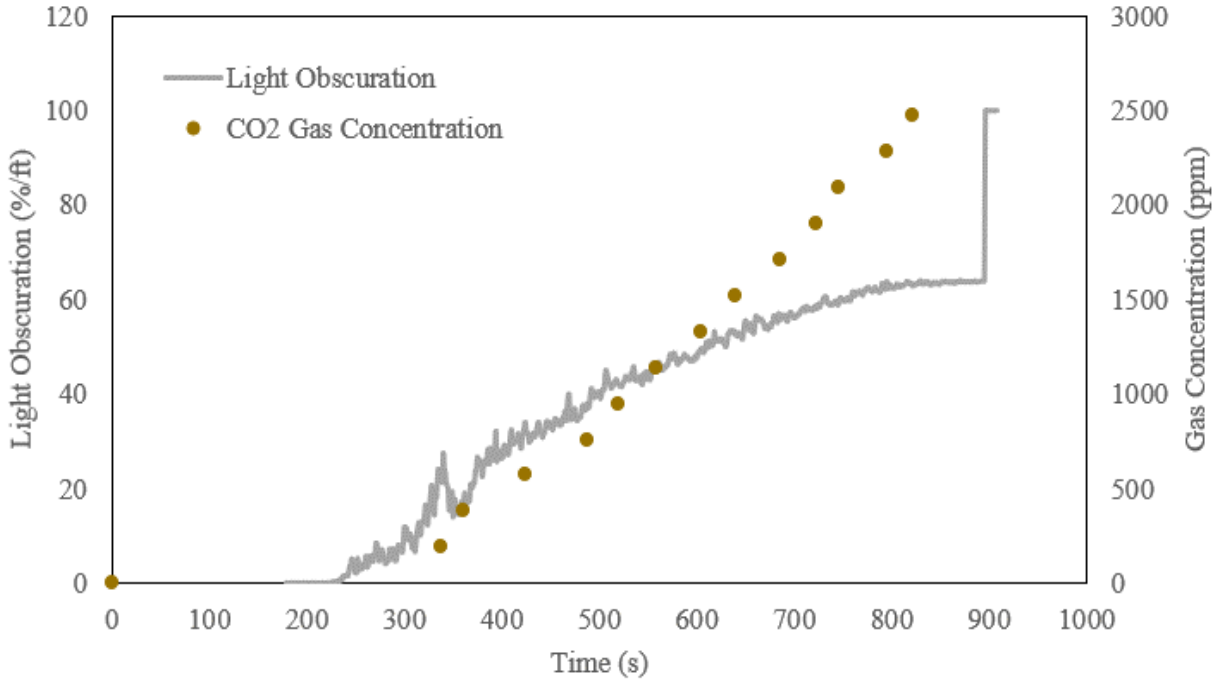

Figure A.64. Suitcase – SLRM - Light obscuration inside ULD and CO_2 Concentration

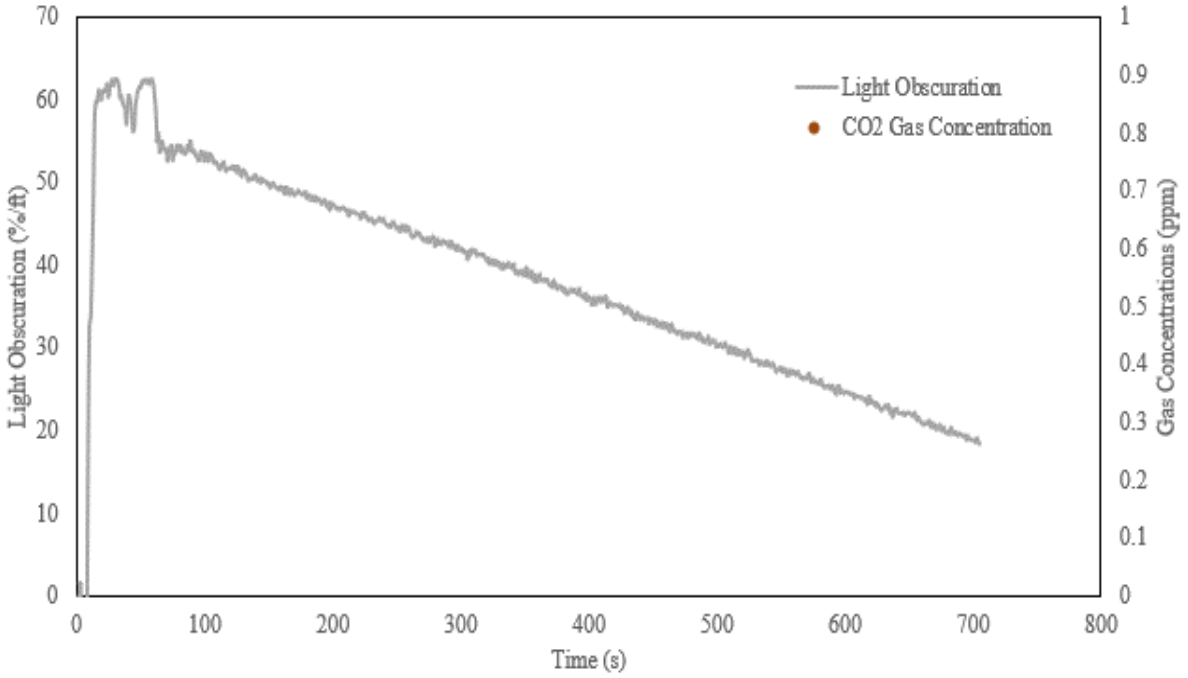

Figure A.65. Boeing Smoke Generator – LLRM - Light obscuration inside ULD and CO_2 Concentration

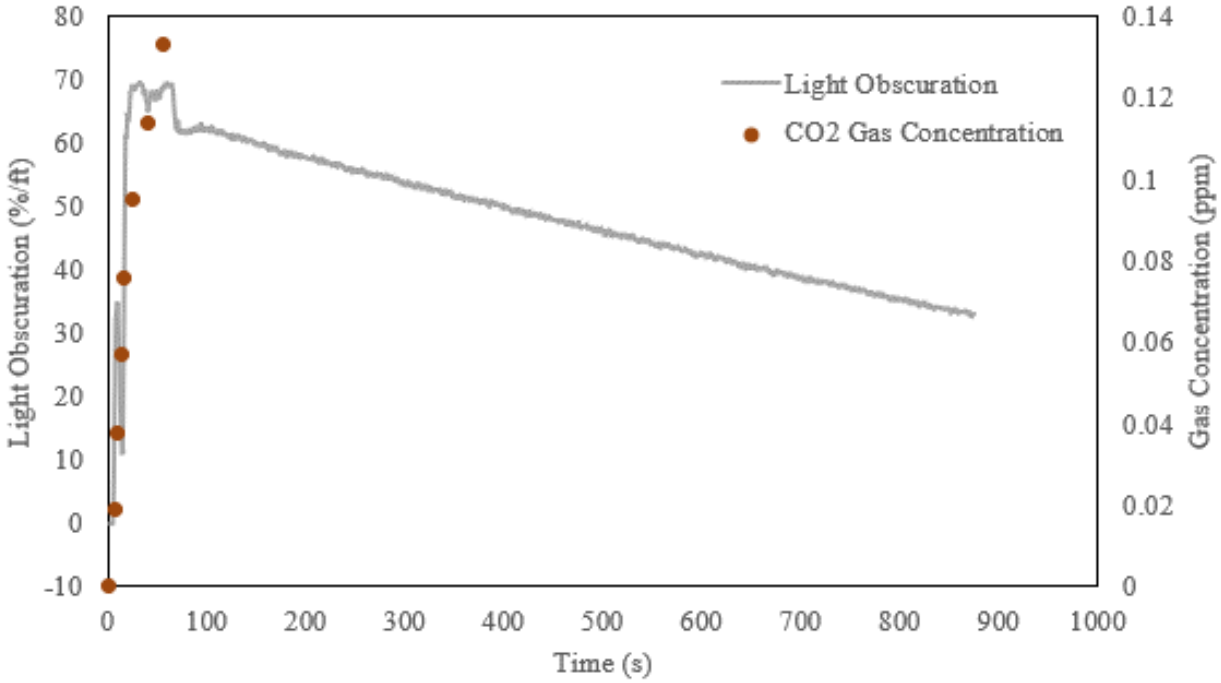

Figure A.66#. Boeing Smoke Generator – MLRM - Light obscuration inside ULD and CO_2 Concentration

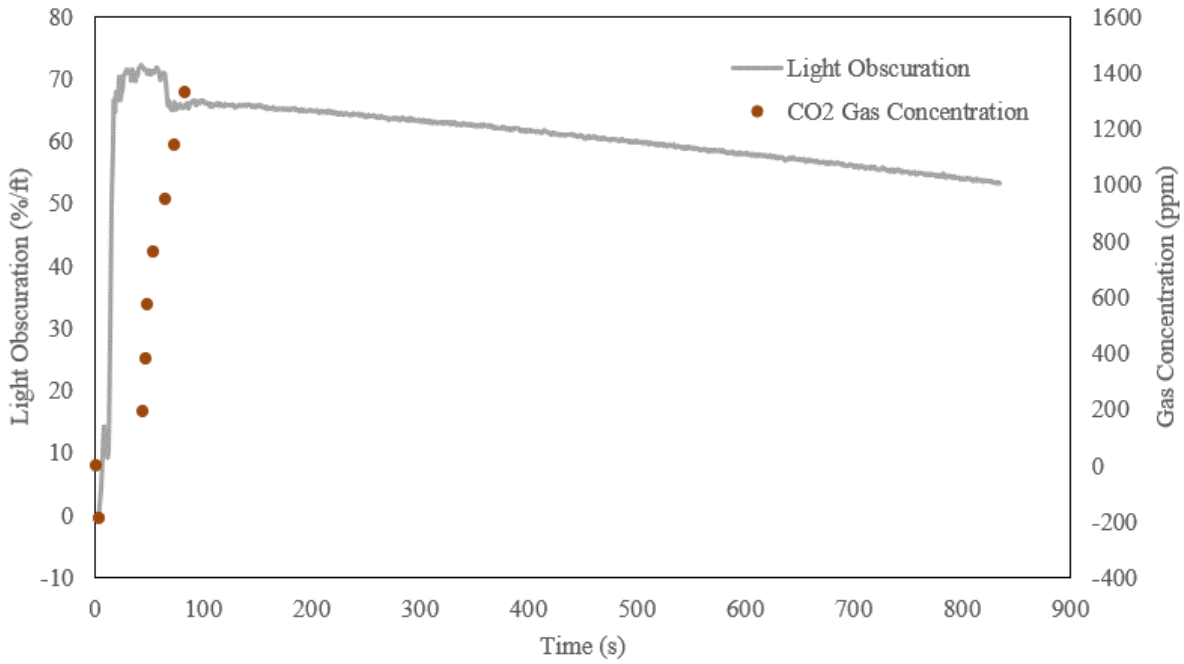

Figure A.67. Boeing Smoke Generator – SLRM - Light obscuration inside ULD and CO_2 Concentration

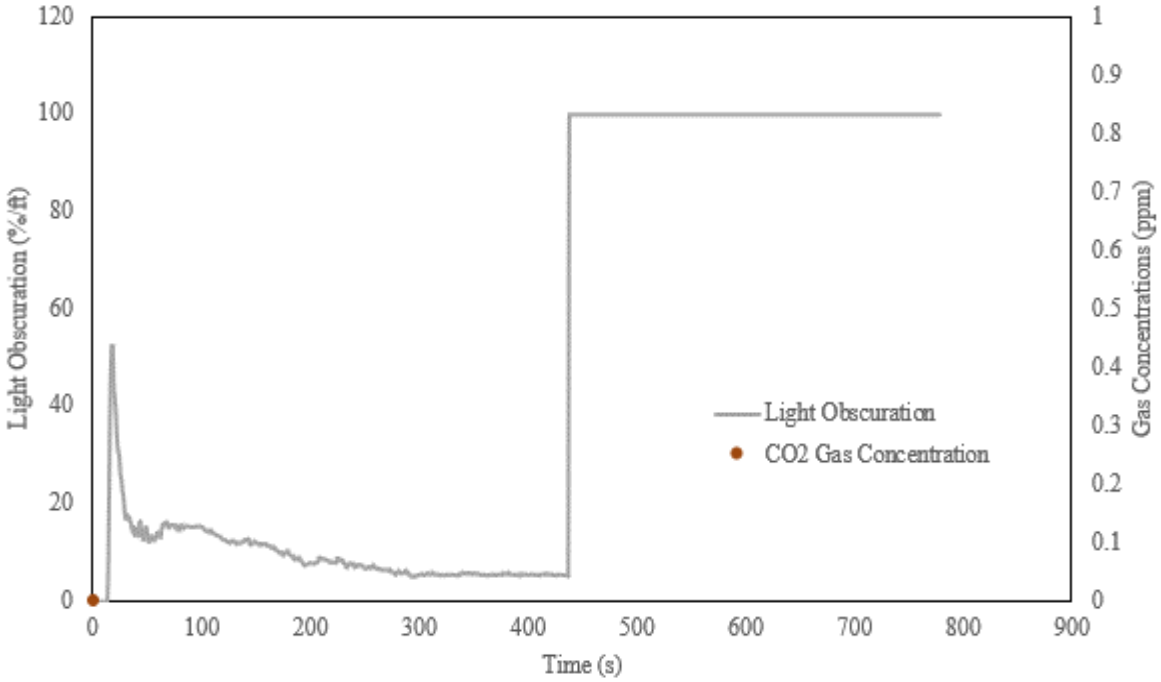

Figure A.68. Wires – LLRM - Light obscuration inside ULD and CO_2 Concentration

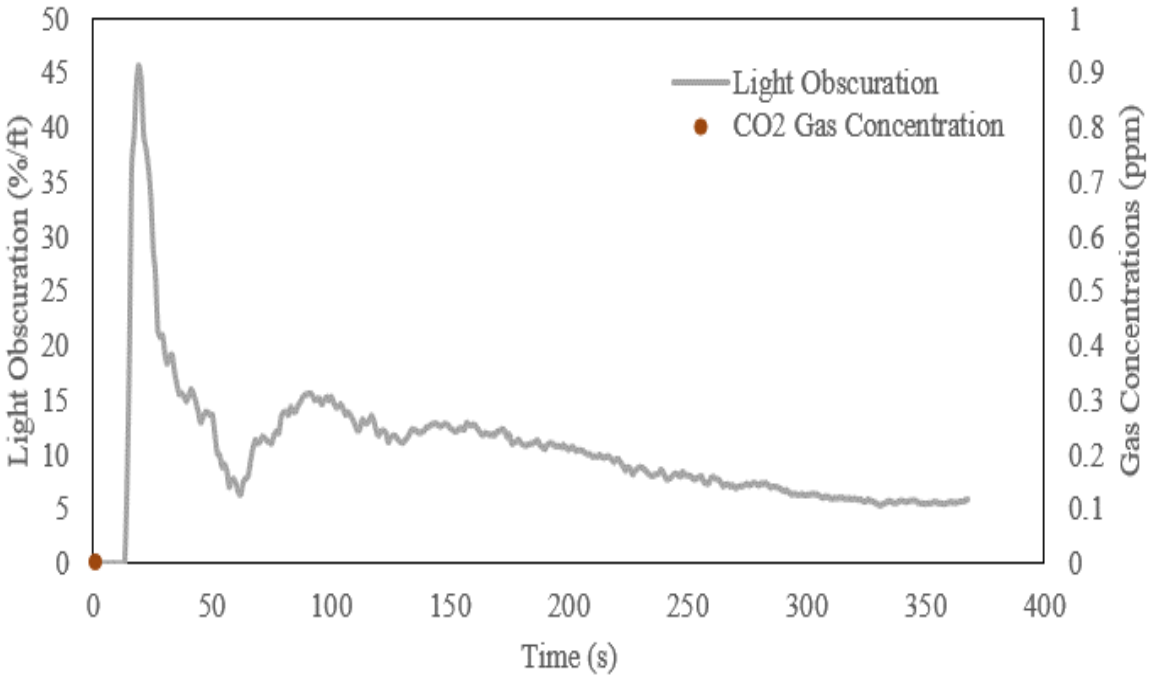

Figure A.69. Wires – MLRM - Light obscuration inside ULD and CO_2 Concentration

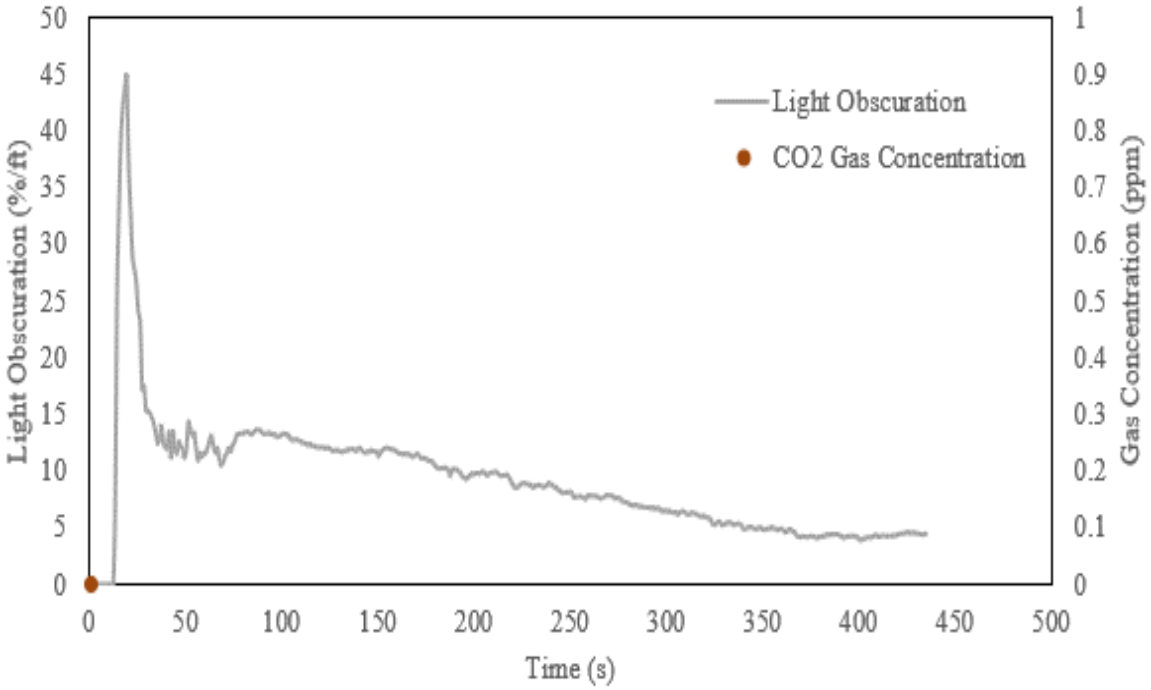

Figure A.70. Wires – SLRM - Light obscuration inside ULD and CO_2 Concentration

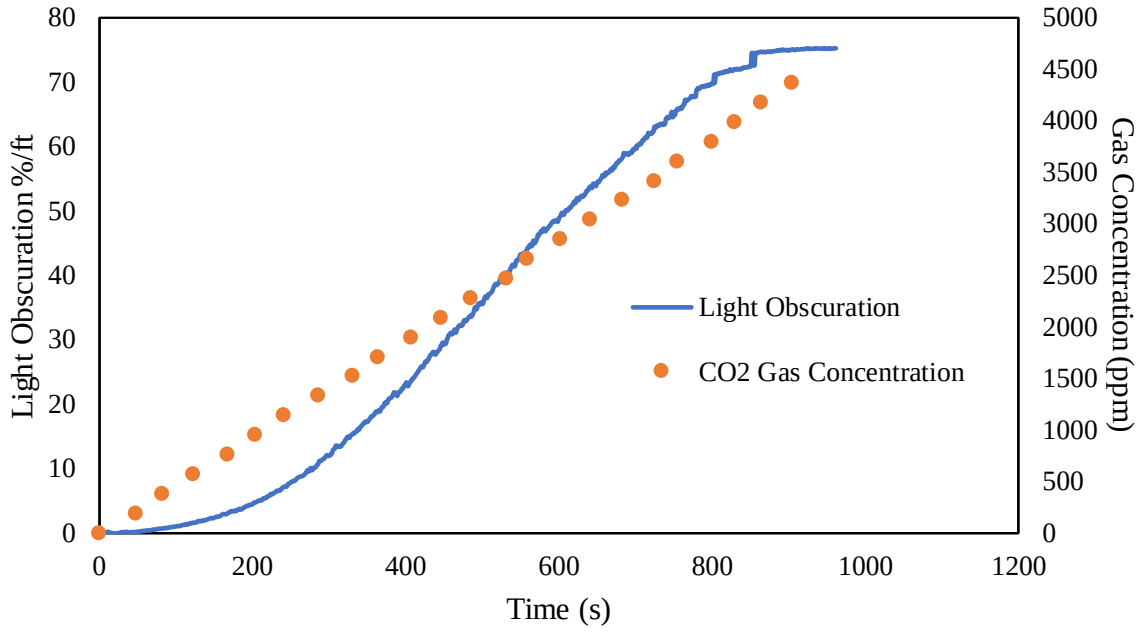

Figure A.71. Wood – LLRM - Light obscuration inside ULD and CO_2 Concentration

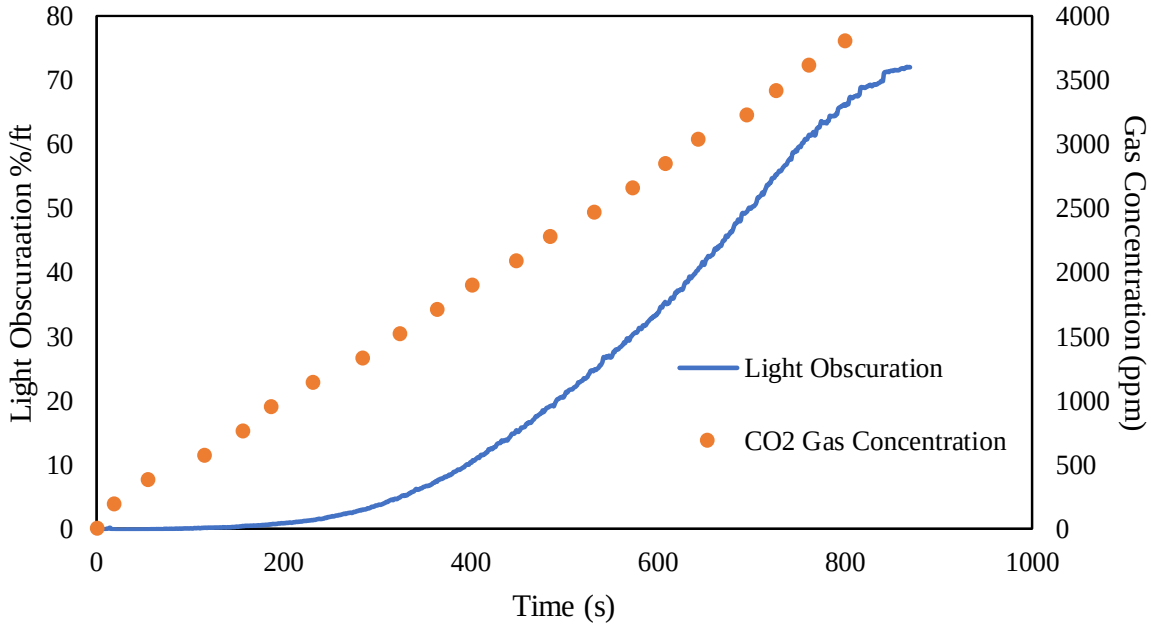

Figure A.72. Wood – MLRM - Light obscuration inside ULD and CO_2 Concentration

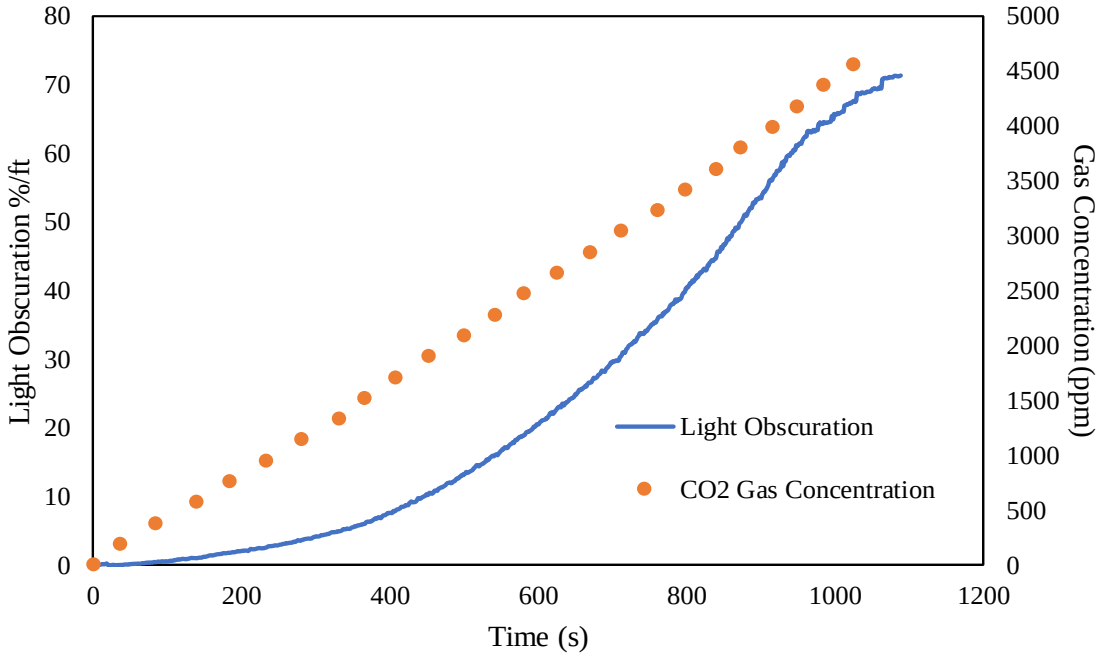

Figure A.73. Wood – SLRM - Light obscuration inside ULD and CO_2 Concentration

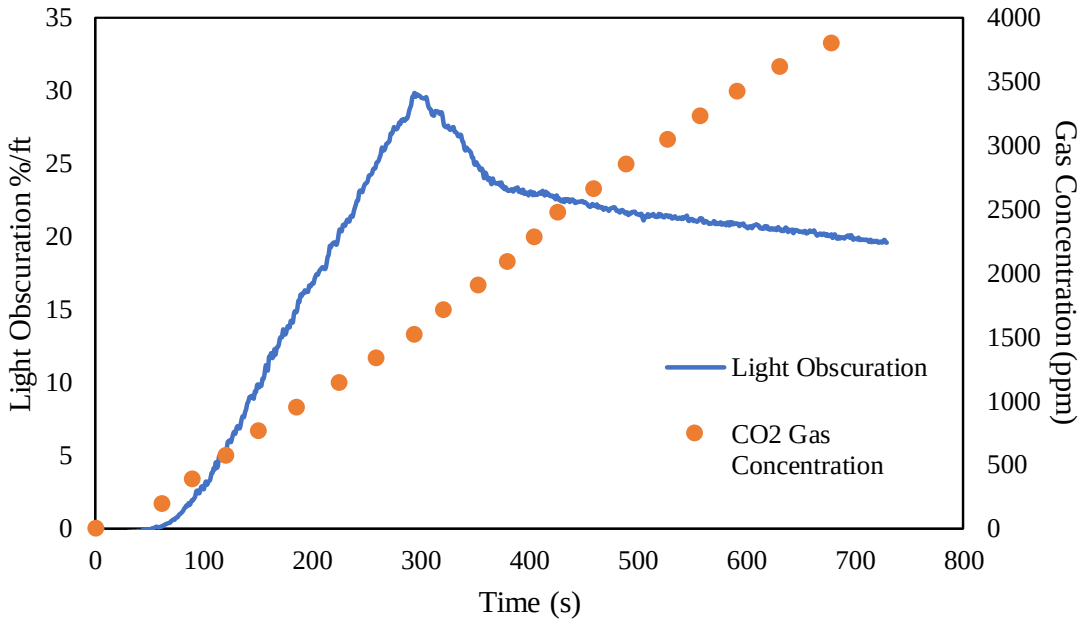

Figure A.74. Cotton – LLRM - Light obscuration inside ULD and CO_2 Concentration

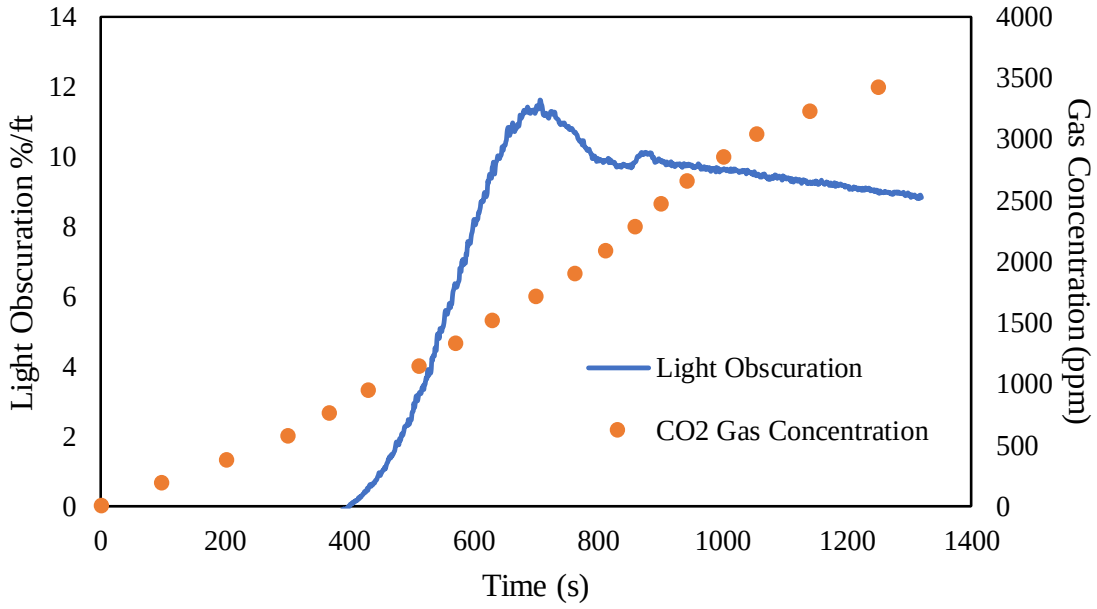

Figure A.75. Cotton – MLRM - Light obscuration inside ULD and CO_2 Concentration

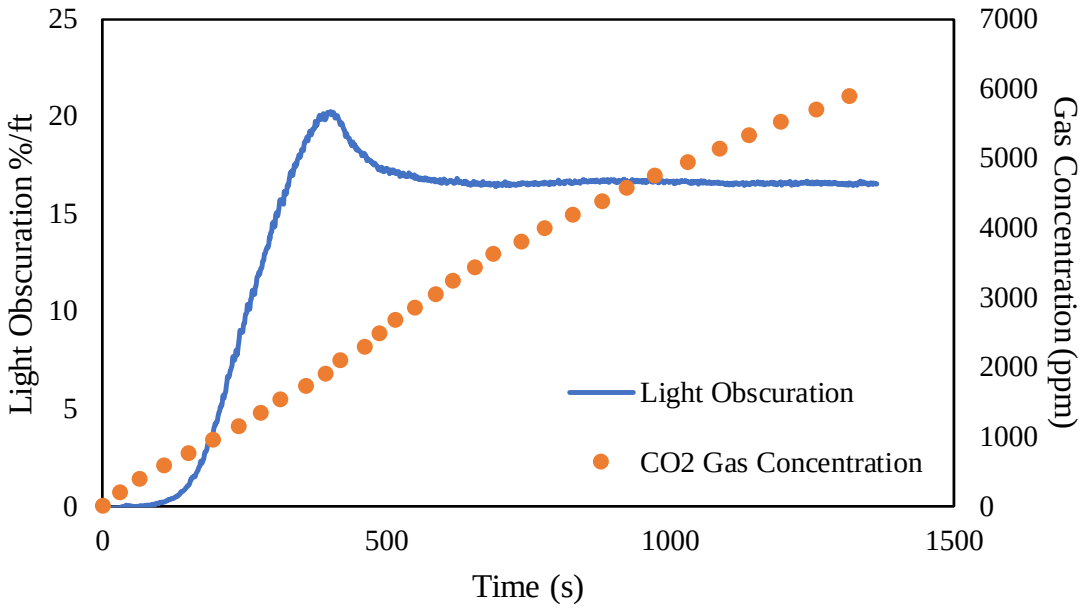

Figure A.76. Cotton – SLRM - Light obscuration inside ULD and CO_2 Concentration

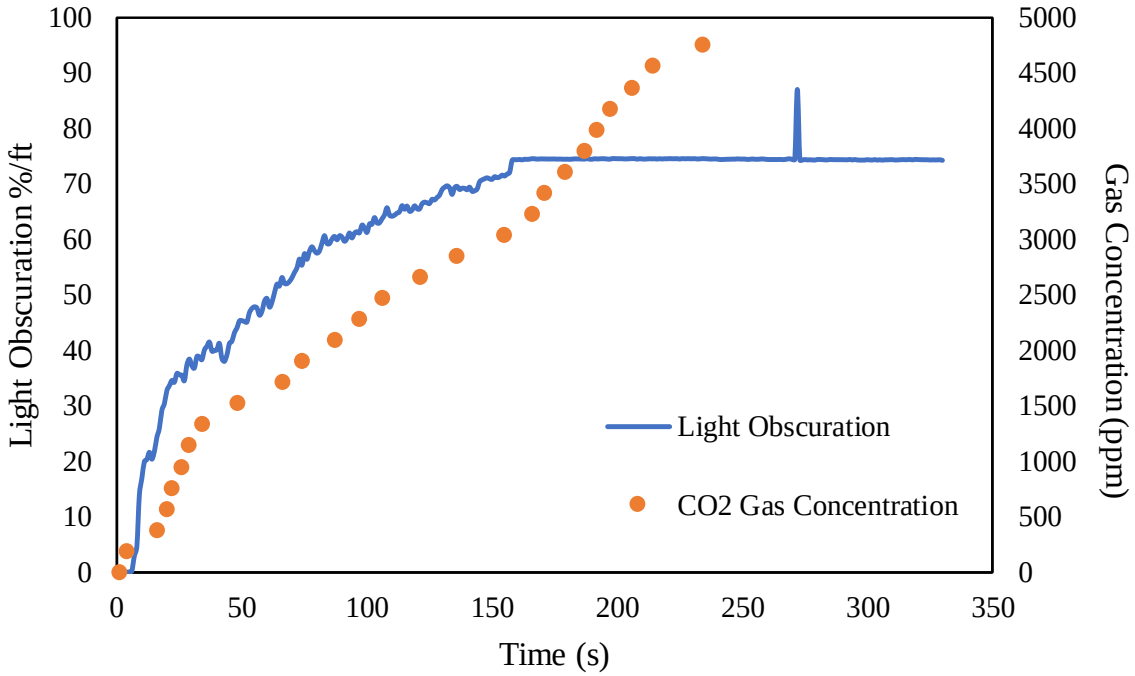

Figure A.77. Paper – LLRM - Light obscuration inside ULD and CO_2 Concentration

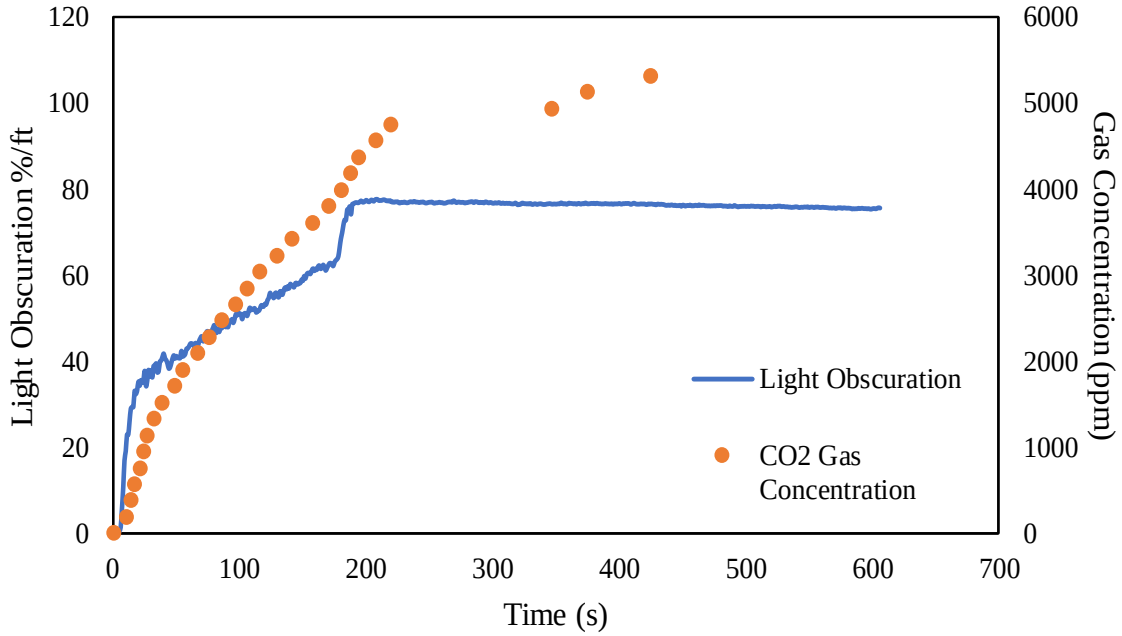

Figure A.78. Paper – MLRM - Light obscuration inside ULD and CO_2 Concentration

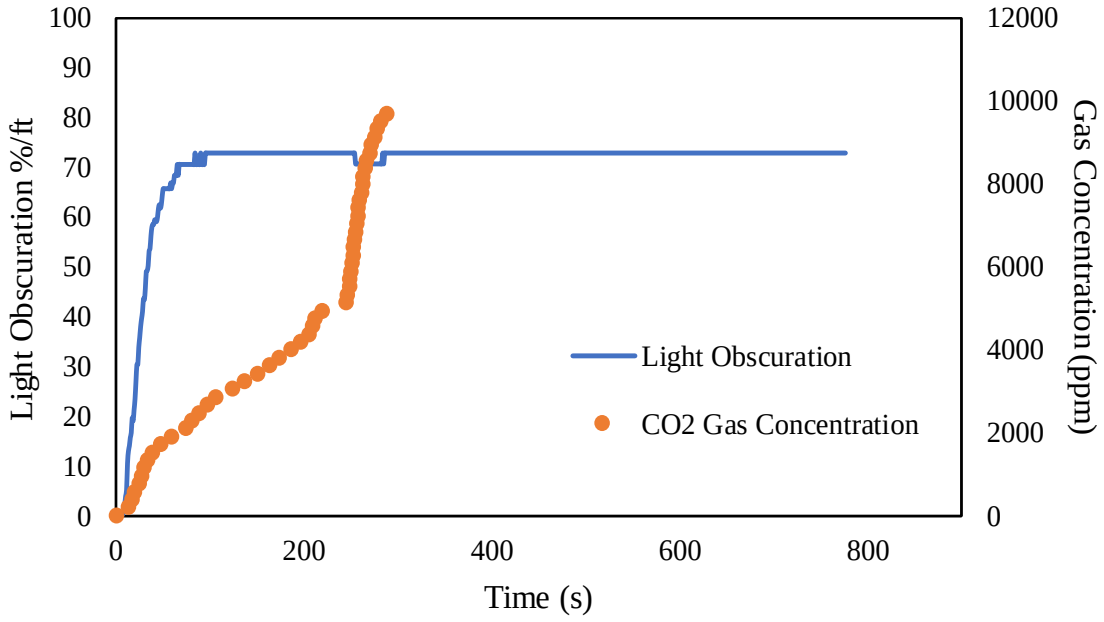

Figure A.79. Paper – SLRM - Light obscuration inside ULD and CO_2 Concentration

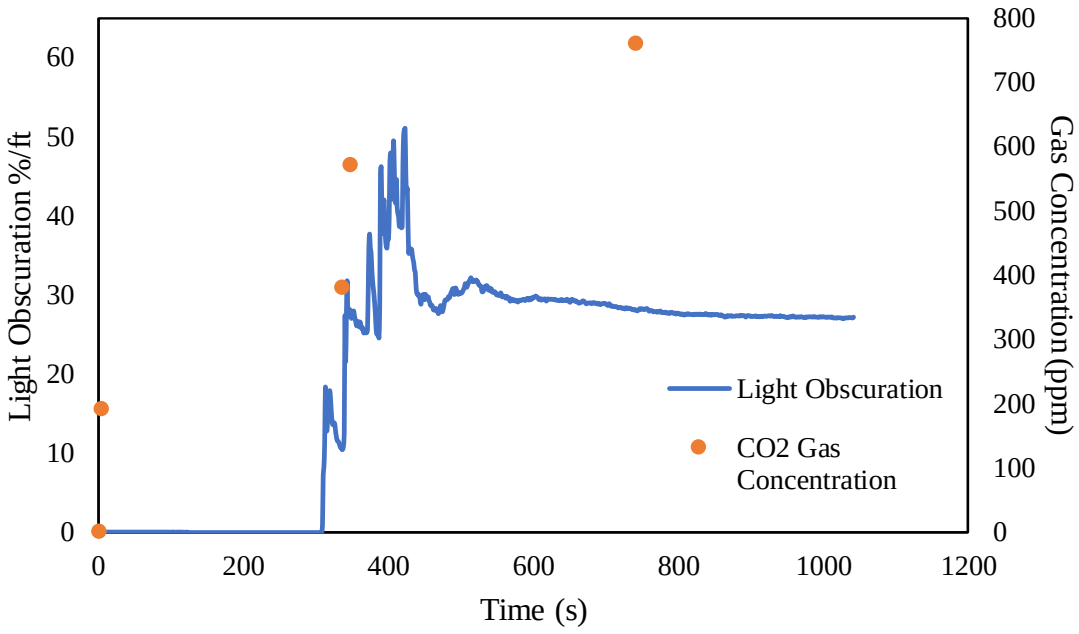

Figure A.80. Batteries – LLRM - Light obscuration inside ULD and CO_2 Concentration

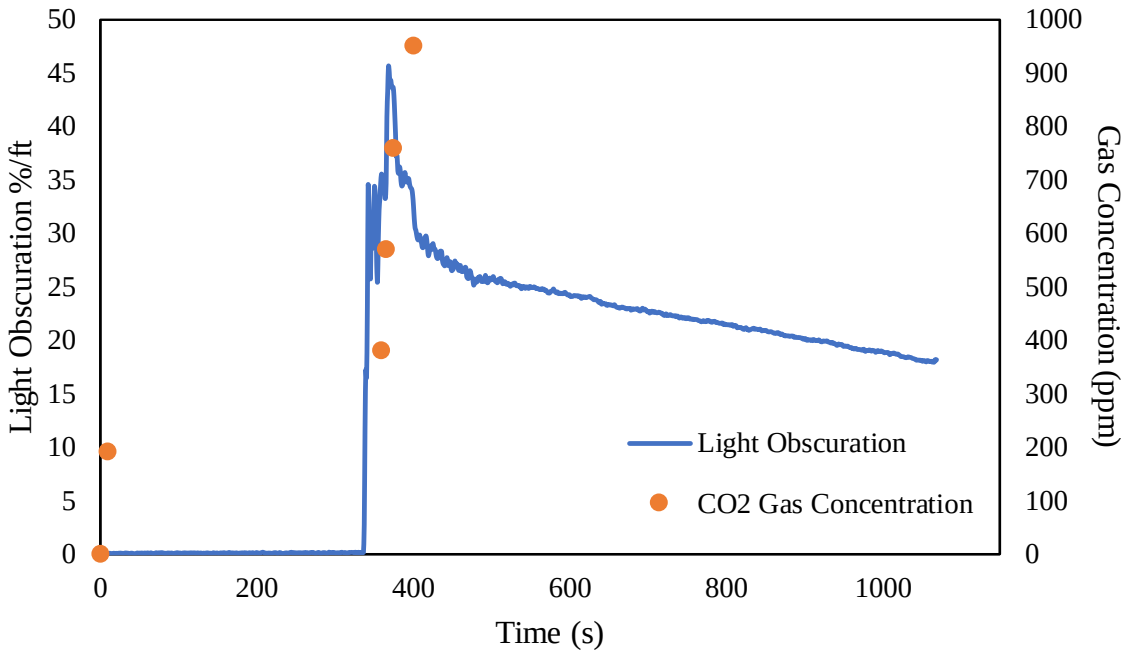

Figure A.81. Batteries – MLRM - Light obscuration inside ULD and CO_2 Concentration

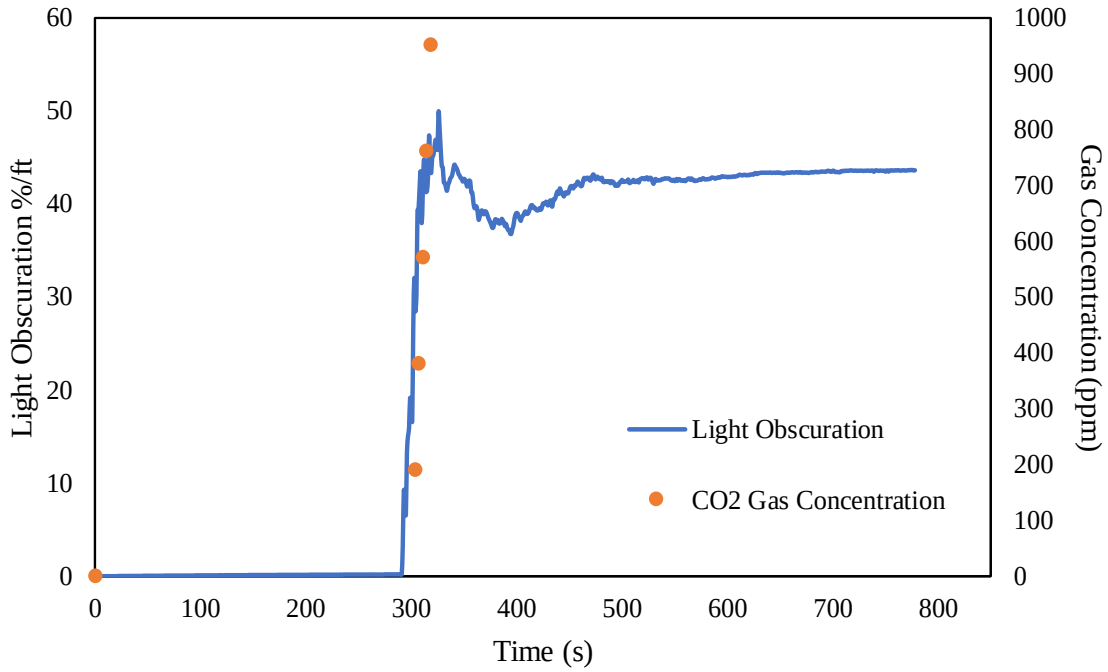

Figure A.82. Batteries – SLRM - Light obscuration inside ULD and CO_2 Concentration

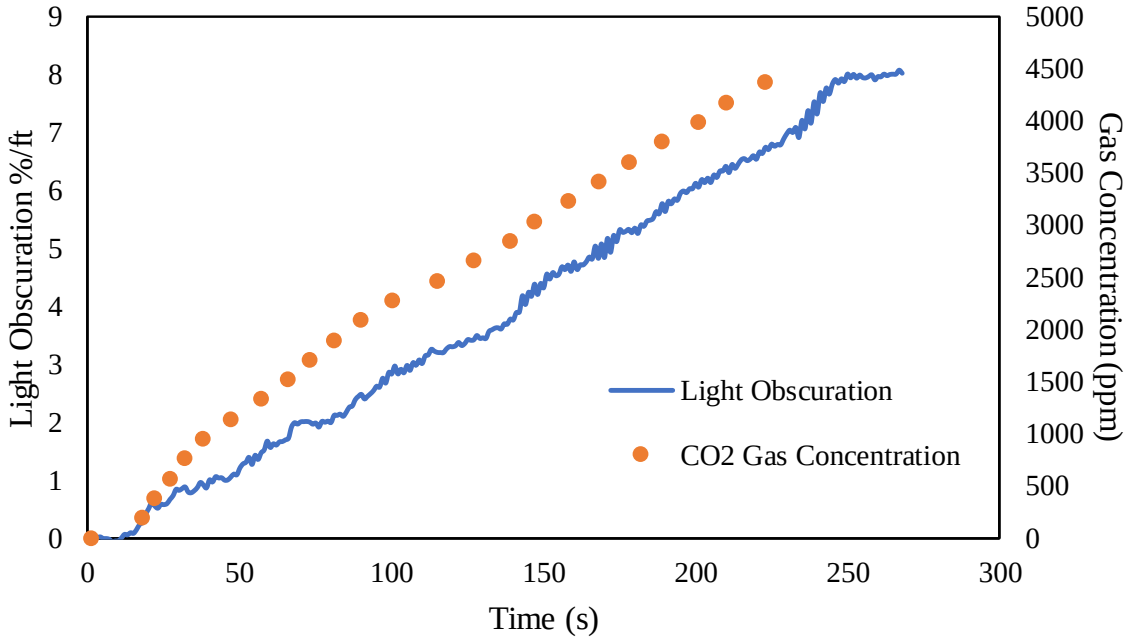

Figure A.83. Heptane – LLRM - Light obscuration inside ULD and CO_2 Concentration

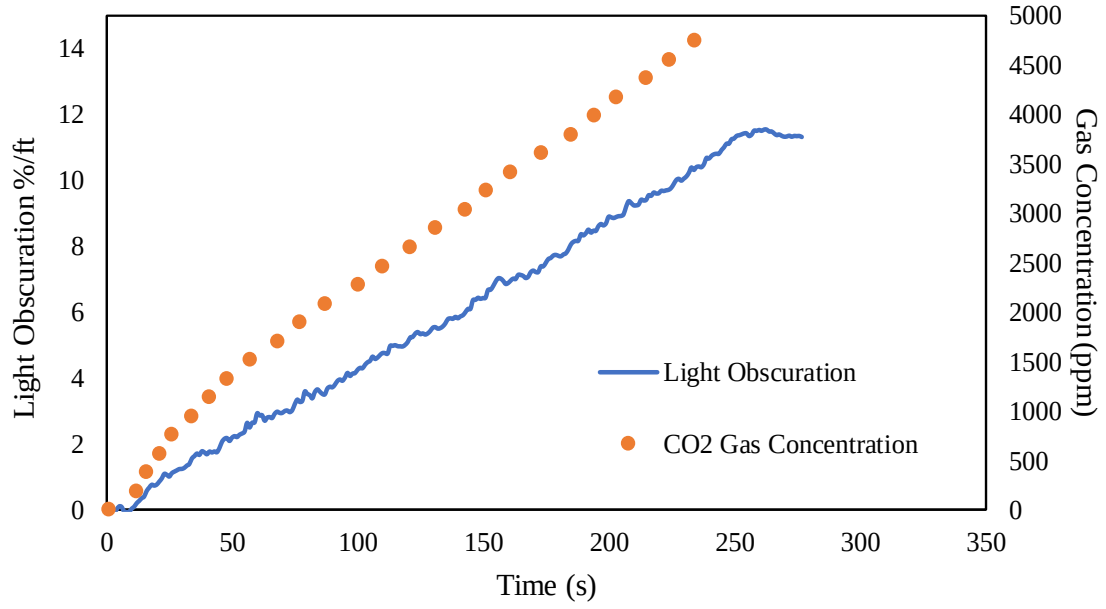

Figure A.84. Heptane – MLRM - Light obscuration inside ULD and CO_2 Concentration

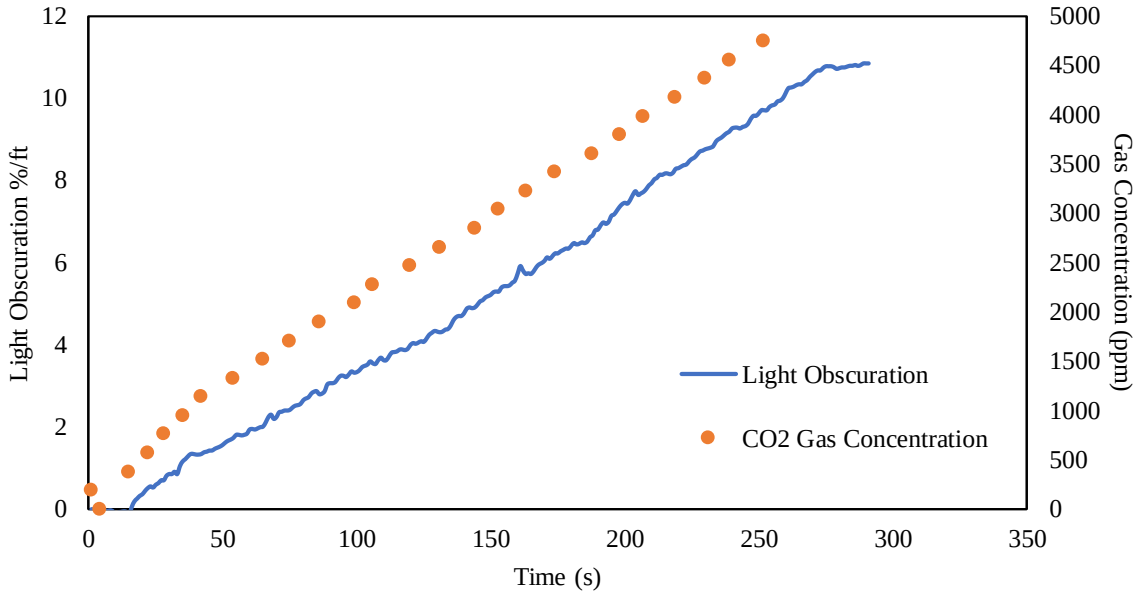

Figure A.85. Heptane – SLRM - Light obscuration inside ULD and CO_2 Concentration

Appendix D

FDS Code generated using PyroSim:

```
&MESH ID='Mesh3Bottom', FYI='bottom', IJK=30,25,5, XB=2.0,8.0,-2.5,2.5,0.0,1.0/
&MESH ID='Mesh2Top', FYI='top', IJK=60,50,10, XB=2.0,8.0,-2.5,2.5,1.0,2.0/
&MESH ID='Mesh01', IJK=24,50,20, XB=-0.6,2.0,-2.5,2.5,0.0,2.0/
&TRNX CC=1.566667, PC=1.6, MESH_NUMBER=3/ Mesh01


&REAC ID='HEPTANE',
    FYI='NIST NRC FDS5 Validation',
    FUEL='REAC_FUEL',
    FORMULA='C7H16',
    CO_YIELD=6.0E-3,
    SOOT_YIELD=0.015,
    RADIATIVE_FRACTION=0.35/

&PROP ID='THCP_uld_ceiling1 props', BEAD_DIAMETER=3.3E-3, BEAD_DENSITY=8700.0/
&PROP ID='THCP_uld_ceiling2 props', BEAD_DIAMETER=3.3E-3, BEAD_DENSITY=8700.0/
&PROP ID='THCP_uld_ceiling3 props', BEAD_DIAMETER=3.3E-3, BEAD_DENSITY=8700.0/
&PROP ID='THCP_uld_ceiling4 props', BEAD_DIAMETER=3.3E-3, BEAD_DENSITY=8700.0/
&PROP ID='THCP_uld_tree01 props', BEAD_DIAMETER=3.3E-3, BEAD_DENSITY=8700.0/
&PROP ID='THCP_uld_tree02 props', BEAD_DIAMETER=3.3E-3, BEAD_DENSITY=8700.0/
&PROP ID='THCP_uld_tree03 props', BEAD_DIAMETER=3.3E-3, BEAD_DENSITY=8700.0/
&PROP ID='THCP_uld_tree04 props', BEAD_DIAMETER=3.3E-3, BEAD_DENSITY=8700.0/
&PROP ID='THCP_uld_tree05 props', BEAD_DIAMETER=3.3E-3, BEAD_DENSITY=8700.0/
&PROP ID='THCP_uld_tree06 props', BEAD_DIAMETER=3.3E-3, BEAD_DENSITY=8700.0/
&PROP ID='THCP_uld_tree07 props', BEAD_DIAMETER=3.3E-3, BEAD_DENSITY=8700.0/
&PROP ID='Cleary Photoelectric P1',
    QUANTITY='CHAMBER OBSCURATION',
    ACTIVATION_OBSCURATION=0.0294,
    SPEC_ID='SOOT',
    ALPHA_E=1.8,
    BETA_E=-1.0,
    ALPHA_C=1.0,
    BETA_C=-0.8/
&PROP ID='THCP_cc_tree01 props', BEAD_DIAMETER=3.3E-3, BEAD_DENSITY=8700.0/
&PROP ID='THCP_cc_tree02 props', BEAD_DIAMETER=3.3E-3, BEAD_DENSITY=8700.0/
&PROP ID='THCP_cc_tree03 props', BEAD_DIAMETER=3.3E-3, BEAD_DENSITY=8700.0/
&PROP ID='THCP_cc_tree04 props', BEAD_DIAMETER=3.3E-3, BEAD_DENSITY=8700.0/
&PROP ID='THCP_cc_tree05 props', BEAD_DIAMETER=3.3E-3, BEAD_DENSITY=8700.0/
&PROP ID='THCP_cc_tree06 props', BEAD_DIAMETER=3.3E-3, BEAD_DENSITY=8700.0/
&PROP ID='THCP_cc_tree07 props', BEAD_DIAMETER=3.3E-3, BEAD_DENSITY=8700.0/
&PROP ID='THCP_cc_ceiling1 props', BEAD_DIAMETER=3.3E-3, BEAD_DENSITY=8700.0/
&PROP ID='THCP_cc_ceiling2 props', BEAD_DIAMETER=3.3E-3, BEAD_DENSITY=8700.0/
```

```
&PROP ID='THCP_cc_ceiling3 props', BEAD_DIAMETER=3.3E-3, BEAD_DENSITY=8700.0/
&PROP ID='THCP_cc_ceiling4 props', BEAD_DIAMETER=3.3E-3, BEAD_DENSITY=8700.0/
&PROP ID='THCP_cc_ceiling5 props', BEAD_DIAMETER=3.3E-3, BEAD_DENSITY=8700.0/
&PROP ID='THCP_cc_ceiling01 props', BEAD_DIAMETER=3.3E-3, BEAD_DENSITY=8700.0/
&PROP ID='THCP_cc_ceiling02 props', BEAD_DIAMETER=3.3E-3, BEAD_DENSITY=8700.0/
&PROP ID='THCP_cc_ceiling03 props', BEAD_DIAMETER=3.3E-3, BEAD_DENSITY=8700.0/
&PROP ID='THCP_cc_ceiling04 props', BEAD_DIAMETER=3.3E-3, BEAD_DENSITY=8700.0/
&PROP ID='THCP_cc_ceiling05 props', BEAD_DIAMETER=3.3E-3, BEAD_DENSITY=8700.0/
&PROP ID='THCP_cc_ceiling06 props', BEAD_DIAMETER=3.3E-3, BEAD_DENSITY=8700.0/
&PROP ID='THCP_cc_ceiling07 props', BEAD_DIAMETER=3.3E-3, BEAD_DENSITY=8700.0/
&PROP ID='THCP_cc_ceiling08 props', BEAD_DIAMETER=3.3E-3, BEAD_DENSITY=8700.0/
&PROP ID='THCP_cc_ceiling09 props', BEAD_DIAMETER=3.3E-3, BEAD_DENSITY=8700.0/
&PROP ID='THCP_cc_ceiling10 props', BEAD_DIAMETER=3.3E-3, BEAD_DENSITY=8700.0/
&PROP ID='THCP_cc_ceiling11 props', BEAD_DIAMETER=3.3E-3, BEAD_DENSITY=8700.0/
&PROP ID='THCP_cc_ceiling12 props', BEAD_DIAMETER=3.3E-3, BEAD_DENSITY=8700.0/
&PROP ID='THCP_cc_ceiling13 props', BEAD_DIAMETER=3.3E-3, BEAD_DENSITY=8700.0/
&PROP ID='THCP_cc_ceiling14 props', BEAD_DIAMETER=3.3E-3, BEAD_DENSITY=8700.0/
&PROP ID='THCP_cc_ceiling15 props', BEAD_DIAMETER=3.3E-3, BEAD_DENSITY=8700.0/

&DEVC ID='ASSDsampULD', QUANTITY='DENSITY', SPEC_ID='SOOT', XYZ=0.71,1.9,1.4, SETPOINT=0.01,
DEVC_ID='ASSDuld', FLOWRATE=7.1458E-6, DELAY=40.0/
&DEVC ID='ASSDsampCC', QUANTITY='DENSITY', SPEC_ID='SOOT', XYZ=3.0,0.71,1.4, DEVC_ID='ASSDcc',
FLOWRATE=1.223E-3, DELAY=27.0/
&DEVC ID='ASSDuld', QUANTITY='ASPIRATION', XYZ=0.71,1.9,1.4, BYPASS_FLOWRATE=0.0,
SETPOINT=0.0625/
&DEVC ID='ASSDcc', QUANTITY='ASPIRATION', XYZ=3.0,0.71,1.4, BYPASS_FLOWRATE=0.0,
SETPOINT=0.0625/
&DEVC ID='THCP_uld_ceiling1', PROP_ID='THCP_uld_ceiling1 props', QUANTITY='THERMOCOUPLE',
XYZ=0.381,0.381,1.57/
&DEVC ID='THCP_uld_ceiling2', PROP_ID='THCP_uld_ceiling2 props', QUANTITY='THERMOCOUPLE',
XYZ=1.143,0.381,1.57/
&DEVC ID='THCP_uld_ceiling3', PROP_ID='THCP_uld_ceiling3 props', QUANTITY='THERMOCOUPLE',
XYZ=0.381,0.8763,1.57/
&DEVC ID='THCP_uld_ceiling4', PROP_ID='THCP_uld_ceiling4 props', QUANTITY='THERMOCOUPLE',
XYZ=1.143,0.8763,1.57/
&DEVC ID='THCP_uld_tree01', PROP_ID='THCP_uld_tree01 props', QUANTITY='THERMOCOUPLE',
XYZ=0.75,1.397,1.57/
&DEVC ID='THCP_uld_tree02', PROP_ID='THCP_uld_tree02 props', QUANTITY='THERMOCOUPLE',
XYZ=0.75,1.397,1.48/
&DEVC ID='THCP_uld_tree03', PROP_ID='THCP_uld_tree03 props', QUANTITY='THERMOCOUPLE',
XYZ=0.75,1.397,1.39/
&DEVC ID='THCP_uld_tree04', PROP_ID='THCP_uld_tree04 props', QUANTITY='THERMOCOUPLE',
XYZ=0.75,1.397,1.3/
&DEVC ID='THCP_uld_tree05', PROP_ID='THCP_uld_tree05 props', QUANTITY='THERMOCOUPLE',
XYZ=0.75,1.397,1.21/
&DEVC ID='THCP_uld_tree06', PROP_ID='THCP_uld_tree06 props', QUANTITY='THERMOCOUPLE',
XYZ=0.75,1.397,1.12/
```

&DEVC ID='THCP_uld_tree07', PROP_ID='THCP_uld_tree07 props', QUANTITY='THERMOCOUPLE',
XYZ=0.75,1.397,1.03/
&DEVC ID='SmokeDetectorULD', PROP_ID='Cleary Photoelectric P1', XYZ=0.71,1.69,1.57/
&DEVC ID='SmokeDetectorCC', PROP_ID='Cleary Photoelectric P1', XYZ=3.0,0.8,1.4/
&DEVC ID='THCP_cc_tree01', PROP_ID='THCP_cc_tree01 props', QUANTITY='THERMOCOUPLE',
XYZ=3.0,1.397,1.57/
&DEVC ID='THCP_cc_tree02', PROP_ID='THCP_cc_tree02 props', QUANTITY='THERMOCOUPLE',
XYZ=3.0,1.397,1.48/
&DEVC ID='THCP_cc_tree03', PROP_ID='THCP_cc_tree03 props', QUANTITY='THERMOCOUPLE',
XYZ=3.0,1.397,1.39/
&DEVC ID='THCP_cc_tree04', PROP_ID='THCP_cc_tree04 props', QUANTITY='THERMOCOUPLE',
XYZ=3.0,1.397,1.3/
&DEVC ID='THCP_cc_tree05', PROP_ID='THCP_cc_tree05 props', QUANTITY='THERMOCOUPLE',
XYZ=3.0,1.397,1.12/
&DEVC ID='THCP_cc_tree06', PROP_ID='THCP_cc_tree06 props', QUANTITY='THERMOCOUPLE',
XYZ=3.0,1.397,1.21/
&DEVC ID='THCP_cc_tree07', PROP_ID='THCP_cc_tree07 props', QUANTITY='THERMOCOUPLE',
XYZ=3.0,1.397,1.03/
&DEVC ID='THCP_cc_ceiling1', PROP_ID='THCP_cc_ceiling1 props', QUANTITY='THERMOCOUPLE',
XYZ=0.45,-1.32,1.65/
&DEVC ID='THCP_cc_ceiling2', PROP_ID='THCP_cc_ceiling2 props', QUANTITY='THERMOCOUPLE',
XYZ=0.45,-0.66,1.65/
&DEVC ID='THCP_cc_ceiling3', PROP_ID='THCP_cc_ceiling3 props', QUANTITY='THERMOCOUPLE',
XYZ=0.45,0.0,1.65/
&DEVC ID='THCP_cc_ceiling4', PROP_ID='THCP_cc_ceiling4 props', QUANTITY='THERMOCOUPLE',
XYZ=0.45,0.66,1.65/
&DEVC ID='THCP_cc_ceiling5', PROP_ID='THCP_cc_ceiling5 props', QUANTITY='THERMOCOUPLE',
XYZ=0.45,1.32,1.65/
&DEVC ID='THCP_cc_ceiling01', PROP_ID='THCP_cc_ceiling01 props', QUANTITY='THERMOCOUPLE',
XYZ=1.15,-1.32,1.65/
&DEVC ID='THCP_cc_ceiling02', PROP_ID='THCP_cc_ceiling02 props', QUANTITY='THERMOCOUPLE',
XYZ=1.15,-0.66,1.65/
&DEVC ID='THCP_cc_ceiling03', PROP_ID='THCP_cc_ceiling03 props', QUANTITY='THERMOCOUPLE',
XYZ=1.15,0.0,1.65/
&DEVC ID='THCP_cc_ceiling04', PROP_ID='THCP_cc_ceiling04 props', QUANTITY='THERMOCOUPLE',
XYZ=1.15,0.66,1.65/
&DEVC ID='THCP_cc_ceiling05', PROP_ID='THCP_cc_ceiling05 props', QUANTITY='THERMOCOUPLE',
XYZ=1.15,1.32,1.65/
&DEVC ID='THCP_cc_ceiling06', PROP_ID='THCP_cc_ceiling06 props', QUANTITY='THERMOCOUPLE',
XYZ=1.85,-1.32,1.65/
&DEVC ID='THCP_cc_ceiling07', PROP_ID='THCP_cc_ceiling07 props', QUANTITY='THERMOCOUPLE',
XYZ=1.85,-0.66,1.65/
&DEVC ID='THCP_cc_ceiling08', PROP_ID='THCP_cc_ceiling08 props', QUANTITY='THERMOCOUPLE',
XYZ=1.85,0.0,1.65/
&DEVC ID='THCP_cc_ceiling09', PROP_ID='THCP_cc_ceiling09 props', QUANTITY='THERMOCOUPLE',
XYZ=1.85,0.66,1.65/
&DEVC ID='THCP_cc_ceiling10', PROP_ID='THCP_cc_ceiling10 props', QUANTITY='THERMOCOUPLE',
XYZ=1.85,1.32,1.65/

```
&DEVC ID='THCP_cc_ceiling11', PROP_ID='THCP_cc_ceiling11 props', QUANTITY='THERMOCOUPLE',
XYZ=2.55,-1.32,1.65/
&DEVC ID='THCP_cc_ceiling12', PROP_ID='THCP_cc_ceiling12 props', QUANTITY='THERMOCOUPLE',
XYZ=2.55,-0.66,1.65/
&DEVC ID='THCP_cc_ceiling13', PROP_ID='THCP_cc_ceiling13 props', QUANTITY='THERMOCOUPLE',
XYZ=2.55,0.0,1.65/
&DEVC ID='THCP_cc_ceiling14', PROP_ID='THCP_cc_ceiling14 props', QUANTITY='THERMOCOUPLE',
XYZ=2.55,0.66,1.65/
&DEVC ID='THCP_cc_ceiling15', PROP_ID='THCP_cc_ceiling15 props', QUANTITY='THERMOCOUPLE',
XYZ=2.55,1.32,1.65/
&DEVC ID='OD', QUANTITY='OPTICAL DENSITY', XYZ=0.71,1.69,1.57, SETPOINT=1.2195/
&DEVC ID='CO2 Detector_ULD', QUANTITY='VOLUME FRACTION', SPEC_ID='CARBON DIOXIDE',
XYZ=0.71,1.9,1.57/
&DEVC ID='CO Detector_ULD', QUANTITY='VOLUME FRACTION', SPEC_ID='CARBON MONOXIDE',
XYZ=0.71,1.9,1.57/
&DEVC ID='CO Detector_CC', QUANTITY='VOLUME FRACTION', SPEC_ID='CARBON MONOXIDE',
XYZ=3.0,0.71,1.4/
&DEVC ID='CO2 Detector_CC', QUANTITY='VOLUME FRACTION', SPEC_ID='CARBON DIOXIDE',
XYZ=3.0,0.71,1.4/
&DEVC ID='OD_ULD', QUANTITY='OPTICAL DENSITY', XYZ=0.71,1.9,1.4/
&DEVC ID='OD_CC', QUANTITY='OPTICAL DENSITY', XYZ=2.31,0.7,1.4/
&DEVC ID='FLOW 2a', QUANTITY='VOLUME FLOW', XB=1.6,1.6,0.05,0.15,1.1,1.3/
&DEVC ID='FLOW 3a', QUANTITY='VOLUME FLOW', XB=1.6,1.6,0.05,0.15,0.8,1.0/
&DEVC ID='FLOW 4a', QUANTITY='VOLUME FLOW', XB=1.6,1.6,0.05,0.15,0.5,0.7/
&DEVC ID='FLOW3', QUANTITY='VOLUME FLOW', XB=0.1,0.2,0.0,0.0,1.1,1.2/
&DEVC ID='FLOW 2b', QUANTITY='VOLUME FLOW', XB=1.6,1.6,1.25,1.35,1.1,1.3/
&DEVC ID='FLOW 3b', QUANTITY='VOLUME FLOW', XB=1.6,1.6,1.25,1.35,0.8,1.0/
&DEVC ID='FLOW 4b', QUANTITY='VOLUME FLOW', XB=1.6,1.6,1.25,1.35,0.5,0.7/

&MATL ID='Aluminum',
    SPECIFIC_HEAT=0.9,
    CONDUCTIVITY=235.0,
    DENSITY=2710.0,
    ABSORPTION_COEFFICIENT=7.5,
    EMISSIVITY=0.1/
&MATL ID='Plexiglass',
    SPECIFIC_HEAT=1.47,
    CONDUCTIVITY=0.17,
    DENSITY=1051.1,
    ABSORPTION_COEFFICIENT=1.0,
    EMISSIVITY=0.86/
&MATL ID='AL/Boron',
    SPECIFIC_HEAT=0.9,
    CONDUCTIVITY=235.0,
    DENSITY=2710.0,
    ABSORPTION_COEFFICIENT=7.5,
    EMISSIVITY=0.1/
```

```
&SURF ID='AL',
    FYI='Aluminum Material',
    RGB=92,233,213,
    BACKING='VOID',
    MATL_ID(1,1)='Aluminum',
    MATL_MASS_FRACTION(1,1)=1.0,
    THICKNESS(1)=0.02/
&SURF ID='Plexiglass',
    FYI='Plexiglass material for door of ULD',
    BACKING='VOID',
    MATL_ID(1,1)='Plexiglass',
    MATL_MASS_FRACTION(1,1)=1.0,
    THICKNESS(1)=0.02/
&SURF ID='Burner',
    TEXTURE_MAP='psm_fire.jpg',
    MLRPUA=4.44E-3,
    RAMP_Q='Burner_RAMP_Q'/
&RAMP ID='Burner_RAMP_Q', T=0.0, F=0.0/
&RAMP ID='Burner_RAMP_Q', T=10.0, F=1.0/
&RAMP ID='Burner_RAMP_Q', T=281.0, F=1.0/
&RAMP ID='Burner_RAMP_Q', T=291.0, F=0.0/
&SURF ID='AL/Boron',
    RGB=146,202,166,
    BACKING='VOID',
    MATL_ID(1,1)='AL/Boron',
    MATL_MASS_FRACTION(1,1)=1.0,
    THICKNESS(1)=0.02/

&OBST ID='ULDwall1', XB=0.06,1.58,0.0,0.02,0.09,1.61, RGB=204,132,227, TRANSPARENCY=0.4,
SURF_ID='AL'/ Wall
&OBST ID='ULDwall2', XB=0.06,1.58,1.98,2.0,0.6488,1.61, RGB=204,132,227, TRANSPARENCY=0.4,
SURF_ID='AL'/ Wall
&OBST ID='ULD Floor', XB=0.06,1.58,5.0E-3,1.52,0.07,0.09, RGB=204,132,227, TRANSPARENCY=0.4,
SURF_ID='AL'/
&OBST ID='ULD Ceiling', XB=0.06,1.58,5.0E-3,2.0,1.61,1.63, RGB=204,132,227, TRANSPARENCY=0.4,
SURF_ID='AL'/
&OBST ID='burner box', XB=0.75,0.85,0.63,0.73,0.07,0.17, SURF_IDS='Burner','INERT','INERT'/
&OBST ID='ULDwall3', XB=0.06,1.6,1.7,1.8,0.3,0.4, RGB=204,132,227, TRANSPARENCY=0.4,
SURF_ID='AL'/
&OBST ID='ULDwall3', XB=0.06,1.6,1.5,1.6,0.1,0.1, RGB=204,132,227, TRANSPARENCY=0.4,
SURF_ID='AL'/
&OBST ID='ULDwall3', XB=0.06,1.6,1.6,1.7,0.2,0.2, RGB=204,132,227, TRANSPARENCY=0.4,
SURF_ID='AL'/
&OBST ID='ULDwall3', XB=0.06,1.6,1.8,1.9,0.5,0.5, RGB=204,132,227, TRANSPARENCY=0.4,
SURF_ID='AL'/
&OBST ID='ULDwall3', XB=0.06,1.6,1.9,2.0,0.6,0.6, RGB=204,132,227, TRANSPARENCY=0.4,
SURF_ID='AL'/
```

&OBST ID='ULDwall3', XB=0.06,1.6,1.6,1.6,0.1,0.2, RGB=204,132,227, TRANSPARENCY=0.4,
SURF_ID='AL'/
&OBST ID='ULDwall3', XB=0.06,1.6,1.7,1.7,0.2,0.3, RGB=204,132,227, TRANSPARENCY=0.4,
SURF_ID='AL'/
&OBST ID='ULDwall3', XB=0.06,1.6,1.8,1.8,0.4,0.5, RGB=204,132,227, TRANSPARENCY=0.4,
SURF_ID='AL'/
&OBST ID='ULDwall3', XB=0.06,1.6,1.9,1.9,0.5,0.6, RGB=204,132,227, TRANSPARENCY=0.4,
SURF_ID='AL'/
&OBST ID='ULDwall4', XB=0.06,0.06,1.082467E-15,1.6,0.1,1.6, RGB=204,132,227, TRANSPARENCY=0.4,
SURF_ID='AL'/
&OBST ID='ULDwall4', XB=0.06,0.06,1.6,1.7,0.2,1.6, RGB=204,132,227, TRANSPARENCY=0.4,
SURF_ID='AL'/
&OBST ID='ULDwall4', XB=0.06,0.06,1.7,1.8,0.3,1.6, RGB=204,132,227, TRANSPARENCY=0.4,
SURF_ID='AL'/
&OBST ID='ULDwall4', XB=0.06,0.06,1.8,1.9,0.5,1.6, RGB=204,132,227, TRANSPARENCY=0.4,
SURF_ID='AL'/
&OBST ID='ULDwall4', XB=0.06,0.06,1.9,2.0,0.6,1.6, RGB=204,132,227, TRANSPARENCY=0.4,
SURF_ID='AL'/
&OBST ID='ULDwall5', XB=1.6,1.6,1.5,1.6,0.1,1.6, RGB=204,132,227, TRANSPARENCY=0.4, SURF_ID='AL'/
&OBST ID='ULDwall5', XB=1.6,1.6,1.6,1.7,0.2,1.6, RGB=204,132,227, TRANSPARENCY=0.4, SURF_ID='AL'/
&OBST ID='ULDwall5', XB=1.6,1.6,1.7,1.8,0.3,1.6, RGB=204,132,227, TRANSPARENCY=0.4, SURF_ID='AL'/
&OBST ID='ULDwall5', XB=1.6,1.6,1.8,1.9,0.5,1.6, RGB=204,132,227, TRANSPARENCY=0.4, SURF_ID='AL'/
&OBST ID='ULDwall5', XB=1.6,1.6,1.9,2.0,0.6,1.6, RGB=204,132,227, TRANSPARENCY=0.4, SURF_ID='AL'/
&OBST ID='ULDdoor', XB=1.6,1.6,1.082467E-15,1.5,0.1,1.6, RGB=51,164,239, TRANSPARENCY=0.498039,
SURF_ID='Plexiglass'/
&OBST ID='CCwall1', XB=-0.27,-0.27,-0.1,1.5,0.0,1.7, RGB=204,132,227, TRANSPARENCY=0.4,
SURF_ID='AL/Boron'/
&OBST ID='CCwall1', XB=-0.27,-0.27,1.5,1.6,0.1,1.7, RGB=204,132,227, TRANSPARENCY=0.4,
SURF_ID='AL/Boron'/
&OBST ID='CCwall1', XB=-0.27,-0.27,1.6,1.7,0.2,1.7, RGB=204,132,227, TRANSPARENCY=0.4,
SURF_ID='AL/Boron'/
&OBST ID='CCwall1', XB=-0.27,-0.27,1.7,1.8,0.3,1.7, RGB=204,132,227, TRANSPARENCY=0.4,
SURF_ID='AL/Boron'/
&OBST ID='CCwall1', XB=-0.27,-0.27,1.8,1.9,0.4,1.7, RGB=204,132,227, TRANSPARENCY=0.4,
SURF_ID='AL/Boron'/
&OBST ID='CCwall1', XB=-0.27,-0.27,1.9,2.0,0.6,1.7, RGB=204,132,227, TRANSPARENCY=0.4,
SURF_ID='AL/Boron'/
&OBST ID='CCwall1', XB=6.6,6.8,-0.1,1.5,0.0,1.0, RGB=204,132,227, TRANSPARENCY=0.4,
SURF_ID='AL/Boron'/
&OBST ID='CCwall1', XB=6.6,6.8,1.5,1.7,0.2,1.0, RGB=204,132,227, TRANSPARENCY=0.4,
SURF_ID='AL/Boron'/
&OBST ID='CCwall1', XB=6.6,6.8,1.7,1.9,0.4,1.0, RGB=204,132,227, TRANSPARENCY=0.4,
SURF_ID='AL/Boron'/
&OBST ID='CCwall1', XB=6.6,6.8,1.9,2.1,0.6,1.0, RGB=204,132,227, TRANSPARENCY=0.4,
SURF_ID='AL/Boron'/
&OBST ID='CCwall1', XB=6.7,6.7,-0.1,2.0,1.0,1.7, RGB=204,132,227, TRANSPARENCY=0.4,
SURF_ID='AL/Boron'/

&OBST ID='CCwall2', XB=-0.27,-0.27,-1.5,-0.1,0.0,1.7, RGB=204,132,227, TRANSPARENCY=0.4,
PERMIT_HOLE=.FALSE., SURF_ID='AL/Boron'/
&OBST ID='CCwall2', XB=-0.27,-0.27,-1.6,-1.5,0.1,1.7, RGB=204,132,227, TRANSPARENCY=0.4,
PERMIT_HOLE=.FALSE., SURF_ID='AL/Boron'/
&OBST ID='CCwall2', XB=-0.27,-0.27,-1.7,-1.6,0.2,1.7, RGB=204,132,227, TRANSPARENCY=0.4,
PERMIT_HOLE=.FALSE., SURF_ID='AL/Boron'/
&OBST ID='CCwall2', XB=-0.27,-0.27,-1.8,-1.7,0.3,1.7, RGB=204,132,227, TRANSPARENCY=0.4,
PERMIT_HOLE=.FALSE., SURF_ID='AL/Boron'/
&OBST ID='CCwall2', XB=-0.27,-0.27,-1.9,-1.8,0.4,1.7, RGB=204,132,227, TRANSPARENCY=0.4,
PERMIT_HOLE=.FALSE., SURF_ID='AL/Boron'/
&OBST ID='CCwall2', XB=-0.27,-0.27,-2.0,-1.9,0.6,1.7, RGB=204,132,227, TRANSPARENCY=0.4,
PERMIT_HOLE=.FALSE., SURF_ID='AL/Boron'/
&OBST ID='CCwall2', XB=6.6,6.8,-1.5,-0.1,0.0,1.0, RGB=204,132,227, TRANSPARENCY=0.4,
PERMIT_HOLE=.FALSE., SURF_ID='AL/Boron'/
&OBST ID='CCwall2', XB=6.6,6.8,-1.7,-1.5,0.2,1.0, RGB=204,132,227, TRANSPARENCY=0.4,
PERMIT_HOLE=.FALSE., SURF_ID='AL/Boron'/
&OBST ID='CCwall2', XB=6.6,6.8,-1.9,-1.7,0.4,1.0, RGB=204,132,227, TRANSPARENCY=0.4,
PERMIT_HOLE=.FALSE., SURF_ID='AL/Boron'/
&OBST ID='CCwall2', XB=6.6,6.8,-2.1,-1.9,0.6,1.0, RGB=204,132,227, TRANSPARENCY=0.4,
PERMIT_HOLE=.FALSE., SURF_ID='AL/Boron'/
&OBST ID='CCwall2', XB=6.7,6.7,-2.0,-0.1,1.0,1.7, RGB=204,132,227, TRANSPARENCY=0.4,
PERMIT_HOLE=.FALSE., SURF_ID='AL/Boron'/
&OBST ID='CCwall3', XB=2.0,6.8,-2.1,-2.1,0.6,1.0, RGB=204,132,227, TRANSPARENCY=0.4,
SURF_ID='AL/Boron'/
&OBST ID='CCwall3', XB=2.0,6.7,-2.1,-2.0,1.0,1.7, RGB=204,132,227, TRANSPARENCY=0.4,
SURF_ID='AL/Boron'/
&OBST ID='CCwall3', XB=-0.27,2.0,-2.1,-2.0,0.6,1.7, RGB=204,132,227, TRANSPARENCY=0.4,
SURF_ID='AL/Boron'/
&OBST ID='CCwall4', XB=2.0,6.8,2.1,2.1,0.6,1.0, RGB=204,132,227, TRANSPARENCY=0.4,
SURF_ID='AL/Boron'/
&OBST ID='CCwall4', XB=2.0,6.7,2.0,2.1,1.0,1.7, RGB=204,132,227, TRANSPARENCY=0.4,
SURF_ID='AL/Boron'/
&OBST ID='CCwall4', XB=-0.27,2.0,2.0,2.1,0.6,1.7, RGB=204,132,227, TRANSPARENCY=0.4,
SURF_ID='AL/Boron'/
&OBST ID='CCwall5', XB=2.0,6.8,1.5,1.7,0.0,0.2, RGB=204,132,227, TRANSPARENCY=0.4,
SURF_ID='AL/Boron'/
&OBST ID='CCwall5', XB=2.0,6.8,1.7,1.9,0.4,0.4, RGB=204,132,227, TRANSPARENCY=0.4,
SURF_ID='AL/Boron'/
&OBST ID='CCwall5', XB=2.0,6.8,1.9,2.1,0.6,0.6, RGB=204,132,227, TRANSPARENCY=0.4,
SURF_ID='AL/Boron'/
&OBST ID='CCwall5', XB=2.0,6.8,1.7,1.7,0.2,0.4, RGB=204,132,227, TRANSPARENCY=0.4,
SURF_ID='AL/Boron'/
&OBST ID='CCwall5', XB=2.0,6.8,1.9,1.9,0.4,0.6, RGB=204,132,227, TRANSPARENCY=0.4,
SURF_ID='AL/Boron'/
&OBST ID='CCwall5', XB=-0.27,2.0,1.5,1.6,0.0,0.1, RGB=204,132,227, TRANSPARENCY=0.4,
SURF_ID='AL/Boron'/
&OBST ID='CCwall5', XB=-0.27,2.0,1.6,1.7,0.1,0.2, RGB=204,132,227, TRANSPARENCY=0.4,
SURF_ID='AL/Boron'/

&OBST ID='CCwall5', XB=-0.27,2.0,1.9,2.0,0.5,0.6, RGB=204,132,227, TRANSPARENCY=0.4,
SURF_ID='AL/Boron'/
&OBST ID='CCwall5', XB=-0.27,2.0,1.7,1.8,0.3,0.3, RGB=204,132,227, TRANSPARENCY=0.4,
SURF_ID='AL/Boron'/
&OBST ID='CCwall5', XB=-0.27,2.0,1.8,1.9,0.4,0.4, RGB=204,132,227, TRANSPARENCY=0.4,
SURF_ID='AL/Boron'/
&OBST ID='CCwall5', XB=-0.27,2.0,2.0,2.1,0.6,0.6, RGB=204,132,227, TRANSPARENCY=0.4,
SURF_ID='AL/Boron'/
&OBST ID='CCwall5', XB=-0.27,2.0,1.7,1.7,0.2,0.3, RGB=204,132,227, TRANSPARENCY=0.4,
SURF_ID='AL/Boron'/
&OBST ID='CCwall5', XB=-0.27,2.0,1.8,1.8,0.3,0.4, RGB=204,132,227, TRANSPARENCY=0.4,
SURF_ID='AL/Boron'/
&OBST ID='CCwall5', XB=-0.27,2.0,1.9,1.9,0.4,0.5, RGB=204,132,227, TRANSPARENCY=0.4,
SURF_ID='AL/Boron'/
&OBST ID='CCwall6', XB=2.0,6.8,-1.7,-1.5,0.0,0.2, RGB=204,132,227, TRANSPARENCY=0.4,
SURF_ID='AL/Boron'/
&OBST ID='CCwall6', XB=2.0,6.8,-1.9,-1.7,0.4,0.4, RGB=204,132,227, TRANSPARENCY=0.4,
SURF_ID='AL/Boron'/
&OBST ID='CCwall6', XB=2.0,6.8,-2.1,-1.9,0.6,0.6, RGB=204,132,227, TRANSPARENCY=0.4,
SURF_ID='AL/Boron'/
&OBST ID='CCwall6', XB=2.0,6.8,-1.7,-1.7,0.2,0.4, RGB=204,132,227, TRANSPARENCY=0.4,
SURF_ID='AL/Boron'/
&OBST ID='CCwall6', XB=2.0,6.8,-1.9,-1.9,0.4,0.6, RGB=204,132,227, TRANSPARENCY=0.4,
SURF_ID='AL/Boron'/
&OBST ID='CCwall6', XB=-0.27,2.0,-1.6,-1.5,0.0,0.1, RGB=204,132,227, TRANSPARENCY=0.4,
SURF_ID='AL/Boron'/
&OBST ID='CCwall6', XB=-0.27,2.0,-1.7,-1.6,0.1,0.2, RGB=204,132,227, TRANSPARENCY=0.4,
SURF_ID='AL/Boron'/
&OBST ID='CCwall6', XB=-0.27,2.0,-2.0,-1.9,0.5,0.6, RGB=204,132,227, TRANSPARENCY=0.4,
SURF_ID='AL/Boron'/
&OBST ID='CCwall6', XB=-0.27,2.0,-1.8,-1.7,0.3,0.3, RGB=204,132,227, TRANSPARENCY=0.4,
SURF_ID='AL/Boron'/
&OBST ID='CCwall6', XB=-0.27,2.0,-1.9,-1.8,0.4,0.4, RGB=204,132,227, TRANSPARENCY=0.4,
SURF_ID='AL/Boron'/
&OBST ID='CCwall6', XB=-0.27,2.0,-2.1,-2.0,0.6,0.6, RGB=204,132,227, TRANSPARENCY=0.4,
SURF_ID='AL/Boron'/
&OBST ID='CCwall6', XB=-0.27,2.0,-1.7,-1.7,0.2,0.3, RGB=204,132,227, TRANSPARENCY=0.4,
SURF_ID='AL/Boron'/
&OBST ID='CCwall6', XB=-0.27,2.0,-1.8,-1.8,0.3,0.4, RGB=204,132,227, TRANSPARENCY=0.4,
SURF_ID='AL/Boron'/
&OBST ID='CCwall6', XB=-0.27,2.0,-1.9,-1.9,0.4,0.5, RGB=204,132,227, TRANSPARENCY=0.4,
SURF_ID='AL/Boron'/
&OBST ID='CCfloor', XB=2.0,6.8,-1.5,1.5,0.0,0.0, RGB=204,132,227, TRANSPARENCY=0.4,
SURF_ID='AL/Boron'/
&OBST ID='CCfloor', XB=-0.27,2.0,-1.5,1.6,0.0,0.0, RGB=204,132,227, TRANSPARENCY=0.4,
SURF_ID='AL/Boron'/
&OBST ID='CCceiling', XB=2.0,6.7,-2.1,2.1,1.7,1.7, RGB=204,132,227, TRANSPARENCY=0.4,
SURF_ID='AL/Boron'/

```
&OBST ID='CCceiling', XB=-0.27,2.0,-2.1,2.1,1.7,1.7, RGB=204,132,227, TRANSPARENCY=0.4,
SURF_ID='AL/Boron'/

&HOLE ID='Hole 2a', XB=1.49,1.6,1.082467E-15,0.1,1.1,1.3/
&HOLE ID='Hole 3a', XB=1.49,1.6,1.082467E-15,0.1,0.8,1.0/
&HOLE ID='Hole 4a', XB=1.49,1.6,1.082467E-15,0.1,0.5,0.7/
&HOLE ID='Hole3', XB=0.06,0.17,1.082467E-15,0.1,1.1,1.2/
&HOLE ID='Hole 2b', XB=1.49,1.6,1.2,1.3,1.1,1.3/
&HOLE ID='Hole 3b', XB=1.49,1.6,1.2,1.3,0.8,1.0/
&HOLE ID='Hole 4b', XB=1.49,1.6,1.2,1.3,0.5,0.7/
```

Bibliography

Advisory Circular, AC 25-9A, “Smoke Detection, Penetration, and Evacuation Tests and Related Flight Manual Emergency Procedures,” 1994.

Aircraft and Aerospace Applications: Part One. (2004, March). Retrieved March 25, 2020, from http://www.totalmateria.com/Article95.htm

Avaiation Safety Network. (2020). Retirevied from: https://aviationsafety.net/database/record.php?id=20060208-0

ANSI/UL 217-2011: Standard for Safety Smoke Alarms, Underwriters Laboratories Inc., Northbrook, IL, 2011.

Blake, D. (2009). Effects of Cargo Loading and Active Containers on Aircraft Cargo Compartment Smoke Detection Times. FAA.

Blake, D. (2006). Development of a Standardized Fire Source for Aircraft Cargo Compartment Fire Detection Systems. FAA.

Blake, D. (2000). Aircraft Cargo Compartment Smoke Detector Alarm Incidents on U.S.-Registered Aircraft, 1974-1999. FAA.

Button, Vera Lucia da Silveira Nantes. (2015). Principles of measurement and transduction of biomedical variables. Amsterdam: Elsevier.

Cleary, T., Grosshandler, W. (1999). Survey of Fire Detection Technologies and System Evaluation/Certification Methodologies and Their Suitability for Aircraft Cargo Compartments. FAA.

Chin, S. (2018). Scalability of Smoke Density and the Viability of New Detection Methods in Aircrafts. College Park, MD. University of Maryland.

Emami, T. (2018). “CHARACTERIZATION OF SMOKE MACHINES IN TESTING AIRCRAFT SMOKE DETECTORS” FAA, Atlantic City International Airport.DOT/FAA/TC-TT18/9

FAA Lessons Learned (1987). Federal Aviation Administration. (n.d.). South African Airways Flight 295, Boeing 747-244B Combi, Serial Number 22171. Retrieved from https://lessonslearned.faa.gov/ll_main.cfm?TabID=1&LLID=33

FAA Lessons Learned. (1996). Federal Aviation Administration. (n.d.). ValuJet Airlines Flight 592, McDonnell Douglas Model DC-9-32, N904VJ. Retrieved from https://lessonslearned.faa.gov/ll_main.cfm?TabID=1&LLID=10

FAA Office of Security and Hazardous Materials Safety. (2020). Events With Smoke, Fire, Extreme Heat Or Explosion Involving Lithium Batteries.

Fabian, T. Z., & Gandhi, P. D. (2007). Smoke Characterization Project. Quincy, MA: Underwriters Laboratories Inc.

Girfhari, A. (2008). Aircraft Cargo Compartment Multisensor Smoke Detection Algorithm Development. Washington, DC: Federal Aviation Administration.

Hill, R. (2017). The History of Cargo Administration Compartment Fire Protection in Transport Aircraft. FAA. Retrieved from: https://www.fire.tc.faa.gov/pdf/systems/May17Meeting/Hill-0517-cargofireprotectionhistory.pdf

Justin, G., & Gottuk, D. (n.d.). Alarm Thresholds for Smoke Detector Modeling. Baltimore, MD: Hughes Associates.

Karp, Matthew. False Alarm Resistant Smoke Detection and Smoke Generator Standardization. International Aircraft Systems Fire Protection Working Group Meeting. Atlantic City, NJ. 8 May 2018. PowerPoint presentation.

Kevin, M. G., Hostikka, S., Floyd, J., McDermott, R., & Vanella, M. (2020). Fire Dynamics Simulator User's Guide (6th ed.). NIST. doi: file:///C:/Users/owner/Downloads/FDS_User_Guide (5).pdf

LLC, S. R. (n.d.). ULD Container Types: LD-3. Retrieved from https://www.searates.com/reference/ld3/

Moody, M. "Re: Fire On-Board Aircraft – Safe Land Time". March 30, 2020. Email.

Nordisk AAY (AAA). (n.d.). Retrieved from http://www.nordisk-aviation.com/en/md-containers/aay-aaa/

NTSB. (2006). Inflight Cargo Fire United Parcel Service Company Flight 1307. Philadelphia, Pennsylvania.

Pongratz, P. (2014). Methods to Increase Velocity of Makeup Air for Atrium Smoke Control – A CFD Study. College Park, MD. University of Maryland.

Suo-Anttila, J., Gill, W., Luketa-Hanlin, A., & Gallegos, C. (2007). Cargo Compartment Smoke Transport Computational Fluid Dynamics Code Validation. FAA.

Smoke Detectors for Protective Signaling Systems., UL 268, Underwriters Laboratories. 2016.

Smoke Detectors for Protective Signaling Systems., UL 268, Underwriters Laboratories. 2016.

Teledyne Gas. (2020, January 13). A Guide to the Applications of Flame Detectors. Retrieved from https://www.azosensors.com/article.aspx?ArticleID=335

Title 14 Code of Federal Regulations (CFR) Part 25.858, 2/10/1998

Wilk, T. (2014). Smoke Detection Delay for Fire in a Cargo Container. FAA.

Workley, F. (1998). Fire Suppression In Cargo Compartments. FAA.

World Air Cargo Forcast. (2017). Retrieved 2020, from https://www.boeing.com/commercial/market/cargo-forecast/importance-of-freighters/

Xtralis. (n.d.). VESDA-E VEU Aspirating Smoke Detector (Highest Sensitivity ASD). Retrieved from https://xtralis.com/product/107/vesda-e-veu-aspirating-smoke-detector

Xtralis 864. (n.d.). Vesda-E Vea. Retrieved from: https://xtralis.com/file/864

Xtralis 922. (n.d.). New Approach for Point Addressable Smoke Detection.